Journal of Research of the National Institute of Standards and Technology

Volume 99 Number 6 November–December 1994

U.S. Department of Commerce—**Ronald H. Brown,** Secretary
Technology Administration—**Mary L. Good,** Under Secretary for Technology
National Institute of Standards and Technology—**Arati Prabhakar,** Director

The Journal of Research of the National Institute of Standards and Technology features advances in measurement methodology and analyses consistent with the NIST responsibility as the nation's measurement science laboratory. It includes reports on instrumentation for making accurate and precise measurements in fields of physical science and engineering, as well as the mathematical models of phenomena which enable the predictive determination of information in regions where measurements may be absent. Papers on critical data, calibration techniques, quality assurance programs, and well-characterized reference materials reflect NIST programs in these areas. Special issues of the Journal are devoted to invited papers in a particular field of measurement science. Occasional survey articles and conference reports appear on topics related to the Institute's technical and scientific programs.

ISSN 1044-677X **Coden: JRITEF** **Library of Congress Catalog Card No.: 89-656121**

United States Government Printing Office, Washington: 1994

Volume 99, Number 6, November–December 1994
Journal of Research of the National Institute of Standards and Technology

Contents

Articles

Conference Reports

Indexes to Volume 98

Volume 99, Number 6, November–December 1994
Journal of Research of the National Institute of Standards and Technology

News Briefs

Volume 99, Number 6, November–December 1994
Journal of Research of the National Institute of Standards and Technology

Volume 99, Number 6, November–December 1994
Journal of Research of the National Institute of Standards and Technology

[J. Res. Natl. Inst. Stand. Technol. 99, 725 (1994)]

An Intercomparison Between NPL (India) and NIST (USA) Pressure Standards in the Hydraulic Pressure Region up to 26 MPa

Volume 99 Number 6 November–December 1994

J. K. N. Sharma and Kamlesh K. Jain

National Physical laboratory, New Delhi, India

and

C. D. Ehrlich, J. C. Houck, and D. B. Ward

National Institute of Standards and Technology, Gaithersburg, MD 20899-0001

Results are presented of an intercomparison of pressure measurements between the National Physical Laboratory (NPL), India, and the National Institute of Standards and Technology (NIST), USA, using piston gauge pressure standards over the range 6 MPa to 26 MPa. The intercomparison, using the NPL piston gauge pressure standard, with a nominal effective area of 8.4×10^{-5} m^2, and the NIST piston gauge pressure standard, with a nominal effective area of 2.0×10^{-5} m^2, was carried out at the NPL.

The intercomparison data obtained show a relative difference of 1×10^{-6} in the zero-pressure effective area (A_0) of the NPL standard as obtained by the NIST standard. At 6 MPa the relative difference in effective areas is 3.5×10^{-6}; at the full scale pressure of 26 MPa, the relative difference is 12×10^{-6}. These differences are in excellent agreement with the statements of uncertainty of the respective standards as obtained from the primary standards of these two laboratories.

Key words: hydraulic pressure, piston gauge; pressure.

Accepted: July 14, 1994

1. Introduction

Piston gauges [1] and liquid column manometers [2] are widely used instruments for the most accurate measurement of pneumatic pressure in the near-atmospheric pressure region (10 kPa to 1 MPa). Piston gauges are also used to measure pneumatic pressures to over 100 MPa, and hydraulic pressures from as low as 1 MPa to over 1 GPa. In a typical piston gauge, a cylindrical piston rotates in a closely-fitted cylinder. The pressure is derived from the known downward gravitational force on the piston and weights that is balanced by an upward force generated by the action of the system pressure on a known area when the piston is floating at its reference position. The uncertainty with which a pressure measurement can be made using a piston gauge then depends on the uncertainties with which measurements of both the downward force and the effective area of the piston-cylinder assembly can be made.

The elastic deformation of the piston-cylinder assembly is usually negligible in the atmospheric pressure range. The uncertainty in the evaluation of the effective area at low pressure [3] is mainly limited by the uncertainty with which absolute dimensional measurements can be made of the piston and cylinder. Recent studies [4] have shown that the effective areas of large-diameter (35 mm), atmospheric-pressure range piston-cylinder assemblies may have significant distortion coefficients, at the 6 parts in 10^6 level. Even so, effective areas of these gauges obtained by dimensional measurements and incorporating theoretical distortion coefficients based on simple elastic theory are found to agree to within 10 parts in 10^6 with values obtained by crossfloat against either manometers or standard gauges having known pressure dependence of the effective area.

At higher pressures, besides the dimensional uncertainty, there is additional uncertainty in determining the effective area of a piston gauge due to the distortion of the piston and cylinder assembly. Compounding the problem, higher-pressure pistons and cylinders typically have relatively small diameters, so that a given dimensional uncertainty results in a relatively larger uncertainty in both the low-pressure effective area (A_0) and the distortion coefficient (b) of the gauge [5].

Close agreement of experimentally-determined pressure-dependent effective areas, using different techniques within a metrological laboratory, creates confidence in the measurements. To add further confidence in pressure measurement, international intercomparisons are often performed. Such intercomparisons can establish uniformity of measurements and mutual compatibility of standards, and reveal possible systematic errors or reaffirm the uncertainty within which the laboratory can make relative pressure measurements.

While the results of international intercomparisons of piston gauges in the pneumatic pressure region [6, 7] up to 10 MPa, and at hydraulic pressures [8–12] up to 500 MPa, are reported in the literature, there is relatively little such intercomparison in the lower hydraulic pressure region. With this in mind, a series of pressure comparison measurements in the hydraulic hydrostatic pressure region up to 26 MPa was carried out between NPL (India) and NIST (USA). Direct piston gauge crossfloats used to accomplish the comparison were performed at NPL, and the results are reported here.

2. Description and Metrological Characteristics of the Standards

2.1 The NPL Transfer Standard

The NPL transfer standard piston gauge that was used for these measurements, denoted NPL-28, is equipped with a reentrant type piston-cylinder system capable of measuring a full-scale pressure of 28 MPa. A schematic representation of the NPL piston gauge is shown in Fig. 1. The piston is rotated to relieve friction by a pulley coupled to a dc motor. To minimize thermal problems the motor is mounted at a distance of 300 mm from the piston-cylinder assembly. The effective area of NPL-28 was determined by dimensional measurements and also by crossfloating over the range 5 MPa to 26 MPa against another NPL piston gauge of 100 MPa full scale pressure, denoted NPL-100. NPL-100 in turn was calibrated against the NPL controlled clearance primary pressure standard. The other parameters associated with NPL-28 are given in Table 1. Figure 2 shows the residuals from the best linear fit of the effective area A_e of NPL-28 as a function of the nominal applied pressure, as obtained using NPL-100 as the standard. The best linear fit of the model $A_e=A_0(1+bp)$ is obtained when $A_0=8.400\,423\times10^{-5}$ m^2 and $b=-1.62\times10^{-12}$ Pa^{-1}.

The 3σ standard deviation of the A_0 coefficient is $(6\times10^{-6})A_0$. The 3σ overall uncertainty of A_e of NPL-28 as obtained during calibration by NPL-100 is $(88\times10^{-6})A_e$.

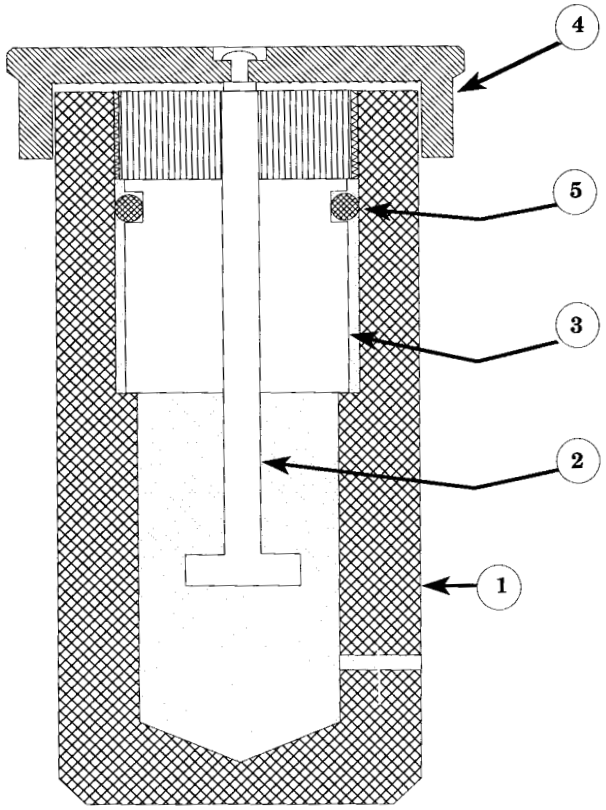

Fig. 1. A schematic cross-sectional view of the measuring system of the NPL piston gauge standard NPL-28: (1) pressure column, (2) piston, (3) cylinder assembly, (4) weight table (5) O-rings.

2.2 The NIST Transfer Standard

The NIST transfer standard piston gauge, denoted NIST-45, is equipped with a simple-type piston-cylinder assembly having a full pressure range of 50 MPa. The piston is rotated by an oval-shaped pulley coupled to a dc motor mounted at a distance from the piston-cylinder in order to minimize the heat transferred from the motor to the piston and cylinder during operation. The effective area and the pressure coefficient of the piston-cylinder assembly of NIST-45 were obtained at NIST [13] by calibrating NIST-45 against primary controlled clearance piston gauge NIST-27, which has a full pressure range of 28 MPa. Figure 3 shows the residuals of the effective area of NIST-45 from the best fit of the model $A_e=A_0(1+bp)$ where $A_0=1.961\,191\times10^{-5}$ m^2 and $b=9.85\times10^{-13}$ Pa^{-1}. The 3σ uncertainty of A_e of NIST-45 as obtained during calibration by NIST-27 is $(35\times10^{-6})A_e$.

Table 1. Description and metrological parameters of the piston-cylinder assemblies used in the pressure comparison measurements

Piston gauge designation	NPL-28	NIST-45
Piston-cylinder (type)	Reentrant	Simple
Full scale pressure (MPa)	28	50
Piston material	Tungsten carbide	Tungsten carbide
Cylinder material	Tungsten carbide	Tungsten carbide
Fluid	Spinesstic 22[a]	Spinesstic 22[a]
Coefficient of thermal expansion for piston ($°C^{-1}$)	4.5×10^{-6}	4.5×10^{-6}
Coefficient of thermal expansion for cylinder ($°C^{-1}$)	4.5×10^{-6}	4.5×10^{-6}
Effective area at atmospheric pressure and at 23 °C (m^2)	8.400 423×10^{-5}	1.961 191×10^{-5}
Distortion coefficient (Pa^{-1})	-1.62×10^{-12}	9.85×10^{-13}
Estimated total relative uncertainty (3σ) of the effective area, $\Delta A_e/A_e$	88×10^{-6}	35×10^{-6}

[a] Certain commercial equipment, instruments, or materials are identified in this paper to foster understanding. Such identification does not imply recommendation or endorsement by the National Institute of Standards and Technology, nor does it imply that the materials or equipment identified are necessarily the best available for the purpose.

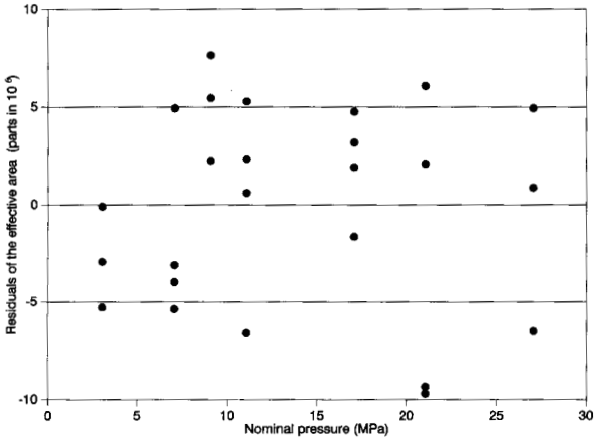

Fig. 2. Residuals of measured values of the effective area (A_e) of PL-28 from the best linear fit of the model $A_e=A_0(1+bp)$, where $A_0=8.400\ 423\times10^{-5}$ m^2 and $b=-1.62\times10^{-12}$ Pa^{-1}, obtained when calibrated by the NPL standard (NPL-100).

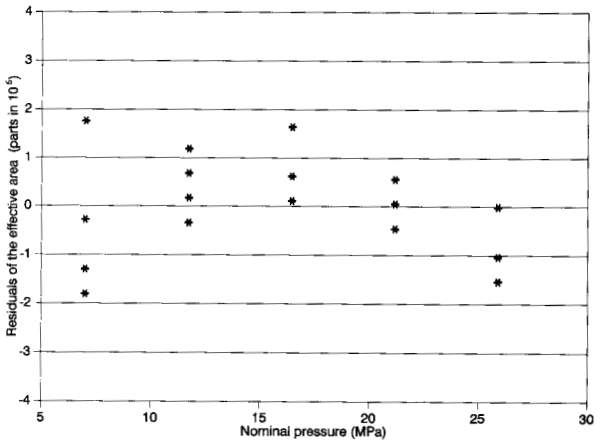

Fig. 3. Residuals of measured values of the effective area (A_e) of the NIST piston gauge standard NIST-45 from the best linear fit of the model $A_e=A_0(1+bp)$, where $A_0=1.961\ 191\times10^{-5}$ m^2 and $b=9.85\times10^{-13}$ Pa^{-1}, obtained when calibrated by the NIST primary standard (NIST-27) used in the controlled clearance gauge mode.

3. Experimental Procedure

The piston gauges used were kept on a heavy non-magnetic stainless steel base to minimize vibration and magnetic effects. All measurements were made in an environment which provided stable temperature conditions of (23±1) °C. The temperature of NPL-28 was measured within 0.1 °C by a mercury-in-glass thermometer placed near the pressure column. The temperature of the NIST transfer standard was measured with a platinum resistance thermometer (PRT) attached near the piston, and its output was read with an autoranging digital multimeter having a resolution of 2 mΩ corresponding to a temperature resolution of 0.005 °C.

The intercomparison between NPL-28 and NIST-45 was carried out using the well-established crossfloat method [1]. Before the crossfloat, both piston gauges were leveled to ensure the verticality of their axes, and the systems were checked for leaks to the full scale pressure of 28 MPa. The piston gauges were loaded with the weights calculated to generate the desired pressure, and were then pressurized to float at their reference levels. The gauges were then isolated from the rest of the pressurizing system, and subsequently from each other, by closing the isolation valves provided in the pressure line and between the gauges. The position and fall rate of both pistons were measured using the output of an electronic displacement transducer recorded on a strip chart recorder. By adjusting the fractional weights on NIST-45, which was generating comparatively lower pressures, crossfloat equilibrium was achieved, as determined when both gauges had the same respective fall

rates independent of whether the isolation valve between the gauges was closed or open. The pressure was then increased to the next higher step, as discussed later, and the procedure was repeated, up to the pressure of 26 MPa. A period of about 30 min between two successive pressures was found adequate to allow the system to return to equilibrium, and about 10 min was required to repeat the observation at any pressure point.

For an individual crossfloat balance, the effective area of the test gauge expressed in terms of the other experimental parameters is [13]:

$$A_{e(T)} = A_0(1+bp)\ [1+(\alpha_p+\alpha_c)(T-T_r)] \tag{1a}$$

$$= \frac{\sum_{i=1}^{n} [M_i \left(1-\frac{\rho_{air}}{\rho_{m_i}}\right)g]+\gamma_f \cdot C}{p_s+\Delta p} \tag{1b}$$

where

M_i is the true mass of the ith weight on the test gauge

ρ_{air} is the density of air in the vicinity of the weights

ρ_{m_i} is the density of the ith weight on the test gauge

g is the local acceleration due to gravity

A_0 is the effective area at the reference temperature and atmospheric pressure

b is the pressure distortion coefficient of the piston and cylinder combination

α_p is the linear thermal expansion coefficient of the piston

α_c is the linear thermal expansion coefficient of the cylinder

T is the temperature of the piston and cylinder

T_r is the reference temperature

γ_f is the surface tension of the operating liquid

C is the circumference of the piston

p_s is the pressure at the reference level of the standard gauge.

Δp is the head correction $(\rho_f-\rho_{air})gH$, where H is the height difference between the reference levels of the two gauges and ρ_f is the density of the pressure transmitting fluid. Δp can be positive or negative depending on whether the reference level of the standard is lower or higher than that of the test gauge.

As it was not possible to bring the reference levels of the individual piston gauges to the same operating level during crossfloat, a pressure head correction term (Δp) was applied. In this case, the reference level of NPL-28 was higher by 0.105 m than that of NIST-45.

A computer program developed and used at NIST [7] gives the effective area and the pressure coefficients of the test gauge based upon those of the standard. This program also provides the residuals and the standard deviation of the predicted value of the area, and the standard deviation of the coefficients.

4. Results and Discussion

Three test cycles, up to 26 MPa, were carried out during the intercomparison of NPL-28 and NIST-45. In one cycle, the pressure was increased to (6, 12, 16, 20 and 26) MPa, and then decreased from (20 to 6) MPa in similar steps. In the other two cycles, the measurement proceeded from the highest pressure to the lowest and back to the highest. A fourth set of observations was also taken where the pressure was increased from the lowest to the highest pressure only. A total of 32 independent observations were made, nine in each of the first three test cycles and five in the fourth test.

Figure 4 shows a plot of the residuals of the effective area of NPL-28, as a function of the nominal applied pressure, when NPL-28 is crossfloated against NIST-45. This figure gives the deviation of the measured values of the effective area, in parts in 10^6, for the individual measured pressures, from the fitted equation $A_e=A_0(1+bp)$ where $A_0=8.400\ 415\times10^{-5}$ m^2 and $b=-2.05\times10^{-13}$ Pa^{-1}. The distribution of the residuals of the effective area (A_e) of NPL-28 in Fig. 4 is taken to be random.

The value of A_0 of NPL-28 as obtained by crossfloat against NPL-100 exceeds by 1×10^{-6} the value obtained by crossfloat against NIST-45. This 1×10^{-6} difference is well below the 3σ standard deviation of the A_0 coefficient, and hence the agreement at low pressure is excellent. Further, the value of b for NPL-28 when it is crossfloated against NIST-45 differs from the value when it is crossfloated against NPL-100 (given in Table 1) by 0.43×10^{-12} Pa^{-1}. Considering the 3σ standard deviations of these measured values, i.e., 0.2×10^{-12} Pa^{-1} and 0.4×10^{-12} Pa^{-1}, respectively, the difference is not unreasonable. Additionally, these observed differences in A_0 and b cause a relative difference in the effective area of 3.5×10^{-6} at a measured pressure of 6 MPa, increasing to 12×10^{-6} at a full scale pressure of 26 MPa. These results are compatible with the measurement uncertainties associated with the individual piston gauges as given in Table 1.

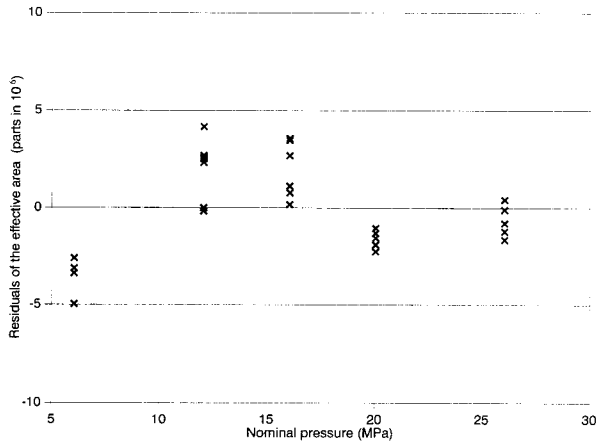

Fig. 4. Residuals of measured values of the effective area (A_e) of NPL-28 from the best linear fit of the model $A_e=A_0\ (1+bp)$, where $A_0=8.400\ 415\times10^{-5}$ m^2 and $b=-2.05\times10^{-12}$ Pa^{-1}, obtained when calibrated by NIST-45.

The uncertainty in the measurement of pressure using a piston gauge arises from two main sources: (1) inherent uncertainties associated with the gauge itself and (2) other uncertainties associated with the local experimental conditions. The former is mainly attributable to the determination of the effective area of the piston-cylinder assembly and uncertainties in the mass of the load and/or piston. However, the latter arises from the experimental procedures, the major components of which were (i) uncertainty associated with the measurement of temperature, (ii) correction due to any difference of reference levels and (iii) the resolution of the balancing criteria when the two systems are in equilibrium.

During the cross float of NPL-28 and NIST-45 the fractional mass was adjusted so as not to contribute more than $\pm1.2\times10^{-6}$ uncertainty (3σ) at the minimum pressure of 6 MPa, which decreases to less than 1×10^{-6} at the full scale pressure of 26 MPa. As the reference levels were measured with an uncertainty of 5.00×10^{-4} m (3σ) and temperature was read with an estimated accuracy of 0.1 °C (3σ), the contribution to the total estimated uncertainties in effective area due to temperature and difference in reference level is not significant compared to the total uncertainties associated with the standards NPL-28 and NIST-45

5. Conclusions

The comparison of the effective area of NPL-28 as determined by NIST-45 and NPL-100 show agreement between the two pressure standards (NPL-28 and NIST-45) that is significantly better than the estimated (3σ) uncertainty of either gauge. The low-pressure area of NPL-28 obtained from NPL-100 differs by only 1×10^{-6} from the area value obtained during comparison with NIST-45. The effective areas of NPL-28 determined by these same two paths differ by 3.5×10^{-6} at 6 MPa, increasing to 12×10^{-6} at 26 MPa. This study thus shows the agreement of measurements of effective area, and hence demonstrates the compatibility of the standards maintained by these two laboratories, for hydraulic pressures to 26 MPa.

6. References

[1] P. L. M. Heydemann and B. E. Welch, Experimental Thermodynamics, Volume II, B. LeNeindre and B. Vodar, eds., Butterworth & Co. Ltd., London (1975), p. 147.
[2] P. L. M. Heydemann, C. R. Tilford, C. R. and R. W. Hyland, J. Vac. Sci. Technol. **14**, 597 (1977).
[3] A. H. Bass, J. Phys. E: Sci. Instrum. **11**, 682 (1978).
[4] K. Jain, C. Ehrlich, J. Houck, and J. K. N. Sharma, Meas. Sci. Technol. **4**, 249 (1993).
[5] R. S. Dadson, S. L. Lewis, and G. N. Peggs, The Pressure Balance: Theory an Practice, National Physical Laboratory, Teddington, England, HMSO (1982).
[6] J. K. N. Sharma, K. K. Jain, A. K. Badyopadhyay, and J. Jäger, J. Phys. E: Sci. Instrum. **21**, 635 (1988).
[7] J. C. Houck, G. F. Molinar, and R. Maghenzani, J. Res. Natl. Bur. Stand. (U.S.) **88**, 253 (1983).
[8] J. C. Legras, G. F. Molinar, K. Schmalhofer, J. K. N. Sharma, M. Thane, and D. B. Walker, BIPM Int. Report 90/10 (1990).
[9] G. F. Molinar, L. Bianchi, J. K. N. Sharma, and K. K. Jain, High Temp. High Pressure **18**, 241 (1986).
[10] H. Bauer and J. Jäger, Metrologia **16**, 111 (1980).
[11] G. N. Peggs, S. L. Lewis, P. B. Clapham, J. Jäger, H. Bauer, G. Schopper, and N. Schultz, NPL Report No. M 32, (June 1978).
[12] G. N. Peggs, S. L. Lewis, and J. C. Legras, NPL Report No. M 39 (March 1980).
[13] K. Jain, C. Ehrlich, and J. Houck, Rev. Sci. Instrum. **63**, 3127 (1992).

About the authors: *Dr. J. K. N. Sharma is the recently retired Deputy Director and Head of Physico-Mechanical Standards at the National Physical Laboratory, New Delhi, India. Dr. Kamlesh Jain is a physicist in the Pressure Group at the National Physical Laboratory, New Delhi, India. Dr. Charles Ehrlich is the Leader of the Pressure Group in the Thermophysics Division of the National Institute of Standards and Technology. Mr. James Houck is a retired physicist from the Pressure Group in the Thermophysics Division of the National Institute of Standards and Technology. Mr. Donald Ward is a technician in the Pressure Group in the Thermophysics Division of the National Institute of Standards and Technology. The National Institute of Standards and Technology is an agency of the Technology Administration, U.S. Department of Commerce.*

Volume 99, Number 6, November–December 1994
Journal of Research of the National Institute of Standards and Technology

[J. Res. Natl. Inst. Stand. Technol. 99, 731 (1994)]

Intercomparison of the ITS-90 Radiance Temperature Scales of the National Physical Laboratory (U.K.) and the National Institute of Standards and Technology

Volume 99 | Number 6 | November–December 1994

G. Machin

The National Physical Laboratory,
Queens Road, Teddington,
Middlesex, TW11 OLW,
United Kingdom

B. Carol Johnson and C. Gibson

National Institute of Standards and Technology,
Gaithersburg, MD 20899-0001,
USA

and

R. L. Rusby

The National Physical Laboratory,
Queens Road, Teddington,
Middlesex, TW11 OLW,
United Kingdom

An intercomparison of radiance temperature scales has been performed by the National Physical Laboratory (NPL) and the National Institute of Standards and Technology (NIST) using a standard transfer pyrometer operating at a wavelength of approximately 1000 nm. It was found that the radiance temperature scales established by the two laboratories were in agreement to 0.1% or better of the temperature over the range 1000 °C to 2500 °C.

Key words: intercomparison; ITS-90; radiance temperature; temperature scales.

Accepted: July 29, 1994

1. Introduction

To maintain confidence in national standards it is essential to periodically inter-compare them to confirm their equivalence. The last intercomparison of radiance temperature scales between the National Physical Laboratory (NPL) and the National Bureau of Standards (NBS) (now NIST) was undertaken in the early 1970s [1] using high stability tungsten ribbon lamps calibrated, in turn, at the two laboratories. Subsequently, the results of this intercomparison were incorporated in a Memorandum of Understanding (MoU) between the two laboratories on the equivalence of their respective realizations of the International Practical Temperature Scale of 1968 (IPTS-68). According to the MoU the scales, established by NPL and NBS on the basis of the lamps at 660 nm, were in agreement at the 2 standard deviation level to within 0.6 °C from 1000 °C to 1500 °C and to within 2 °C

from 1500 °C to 2200 °C. Note that expanded uncertainties are used in this paper, corresponding to a 95% level of confidence assuming a normal distribution [2].

Since the early 1970s both NPL and NIST have made significant changes to the way they establish their radiance temperature scales. In particular, both laboratories have developed facilities to make radiance temperature intercomparisons in the infra-red using blackbody sources. Moreover, a new temperature scale, the ITS-90, has been introduced [3]. In view of these changes and because most commercial radiation thermometers now operate at infra-red wavelengths (rather than at 660 nm) it was decided to perform an entirely new intercomparison of radiance temperature scales at a longer wavelength.

2. Radiance Temperature Scales

2.1 The NPL Radiance Temperature Scale

The radiance temperature scale at NPL is maintained on the basis of two high stability evacuated tungsten ribbon lamps. These are described by Quinn [4] and Coates [5]. NPL realizes the ITS-90 using a blackbody cavity (with an emissivity of >0.99995) immersed in a substantial ingot (0.8 kg) of high purity gold. The radiance of the gold point (1337.33 K) is measured using the NPL primary pyrometer at 655 nm. This provides the fiducial point for the scale. The two lamps are calibrated using a "bootstrap" technique. The current through each lamp ribbon is adjusted until the radiance is about that of the gold point. One lamp (lamp 1) is held at this point while the radiance of the second (lamp 2) is set at double the radiance of lamp 1. The temperature of lamp 2 is then calculated and thereafter the radiance of lamp 1 is increased to that of lamp 2. This cycle is repeated up to the maximum operating temperature of the lamps (1700 °C) and the scale is thus established. Other evacuated lamps are calibrated up to 1700° C relative to one of these lamps. Gas filled high stability tungsten ribbon lamps are calibrated up to 2200 °C while for higher temperatures (up to 2650 °C) blackbody lamps are used.

Lamps are useful as stable transfer standard sources, but are not suitable for the calibration of many modern radiation thermometers. This is because these thermometers generally operate at longer wavelengths (e.g., 0.9 μm) and have fields of view that are typically larger than the width of a tungsten ribbon (1.5 mm or 3 mm). Recently NPL has acquired a variable temperature blackbody for the calibration of such thermometers. This device is based on the design of Groll and Neuer [6]. It has an overall temperature range of 1000 °C to 2650 °C and an aperture of 15 mm. The temperature of the blackbody is assigned using an IKE-Linearpyrometer (the LP2)[1]. This instrument is described by Schreiber, Neuer, and Wörner [7]. It is calibrated at its operating wavelengths (650 nm, 804 nm, and 906 nm) against the gold point blackbody. It can then be used to measure the temperature of the variable temperature blackbody (and other sources). Its calibration was verified at 650 nm by using it to measure the radiance temperature of calibrated standard lamps (up to 2200 °C). The temperature of these lamps as measured by the LP2, over the range 1000 °C to 2200 °C, departed by less than ±0.5 °C from their primary calibration, well within their calibration uncertainty.

2.2 The NIST Radiance Temperature Scale

The radiance scale as realized by NIST is described in detail by Mielenz et al. [8]. It is generated from the gold point, as at NPL. The NIST gold point blackbody is used to assign a temperature to a Quinn and Lee [9] tungsten ribbon cylindrical envelope lamp held at 1255.64 °C. This transfer is performed using the NIST primary photoelectric pyrometer which operates at a wavelength of 655.7 nm. The temperature scale is then transferred to a variable temperature blackbody (manufactured by Thermogage, Inc.) using the photoelectric pyrometer. The blackbody has an aperture of 25 mm and a maximum operating temperature of approximately 2700 °C. The temperature of the cavity is derived from radiance ratio measurements at 655.7 nm, using the NIST primary photoelectric pyrometer and the lamp at 1255.64 °C. This temperature is approximately eight times the spectral radiance of the gold point blackbody at 655.7 nm. As most practical radiation thermometers operate at a wavelength significantly different from 655.7 nm a correction must be applied to the radiance temperature of the variable temperature blackbody as obtained by the NIST primary photoelectric pyrometer. This is because

[1] Certain commercial equipment, instruments, or materials are identified in this paper to foster understanding. Such identification does not imply recommendation or endorsement by the National Institute of Standards and Technology or the National Physical Laboratory, nor does it imply that the materials or equipment identified are necessarily the best available for the purpose.

the spectral radiance temperature is dependent upon wavelength, emissivity (0.995 for the NIST blackbody) and thermodynamic temperature.

Since the starting point of both the NIST and the NPL scales is the freezing point of gold (ITS-90 temperature 1337.33 K) the radiance temperature scales should be identical within the calibration and measurement uncertainties.

Note that neither at NPL nor NIST is the temperature scale maintained on the variable temperature blackbody sources. Their temperatures must be determined at each point by measurement with the LP2 (at NPL) or relative to the Quinn and Lee ribbon lamp (at NIST).

3. The Intercomparison

The intercomparison was performed using a Standard Transfer Pyrometer (STP). This was a Land IR Ltd, Cyclops 52 radiation thermometer modified to meet NPL specifications. Its electronics were re-designed to improve the resolution and stability and provide a voltage output proportional to the radiance. A sensor measures the temperature of the silicon photodiode and the instrument automatically compensates for any changes from this effect. An additional lens was fitted to the front of the STP to reduce the field of view (f.o.v.) to 2.8 mm at 62 cm. The radiation thermometer operates at a wavelength of approximately 1000 nm.

The STP was calibrated at NPL using the variable temperature blackbody. A temperature was assigned to the blackbody cavity using the LP2. This was done at 906 nm but investigation showed that the temperature of the blackbody radiator was essentially the same whether it was measured at 650 nm, 804 nm, or 906 nm.

At each blackbody controller setting between eight and twelve individual readings were taken and the mean of these results was used to ascribe a temperature, T, to the radiator. The voltage output, V, of the STP for that temperature was determined using a calibrated digital voltmeter. The repeatability within each measurement set was between ± 0.2 °C; when measurements were spaced over several days and the calibration set-up was realigned, the repeatability was somewhat larger but still less than 0.35 °C.

The calibration was performed over the range 1000 °C to 2000 °C. As the STP operates at about 1000 nm and the emissivity of the blackbody is considerably greater than 0.995, a negligible uncertainty (< 0.25 °C at 2500 °C) is introduced by this transfer. Residual temperature gradients in the blackbody were accommodated by de-focusing the LP2 slightly (by moving the LP2 backwards) so that its field of view approximately matched that of the STP. Since both the LP2 and the STP were then sampling the same area of the blackbody aperture the effect of any temperature gradients were, to first order, compensated for. The measured radiance did not vary by more than the equivalent of 1 °C over the 4 mm central region of the blackbody aperture.

The results of the calibration were fitted by polynomials V vs T so that the temperature could be easily calculated from a measured STP output voltage. The entire range of the instrument was covered by separate polynomials fitted to the data for each of four overlapping subranges. These subranges were 1000 °C to 1250 °C, 1200 °C to 1475 °C, 1450 °C to 1700 °C, and 1635 °C to 2000 °C. The residuals of the fits are shown in Fig. 1. The residuals are scattered evenly and most lie within 0.3 °C of zero. The standard deviation of the residuals was used to assign a value of 0.3 °C for the expanded uncertainty of the whole of the calibration and fitting procedure. This value has been incorporated in the overall uncertainty given in the next section.

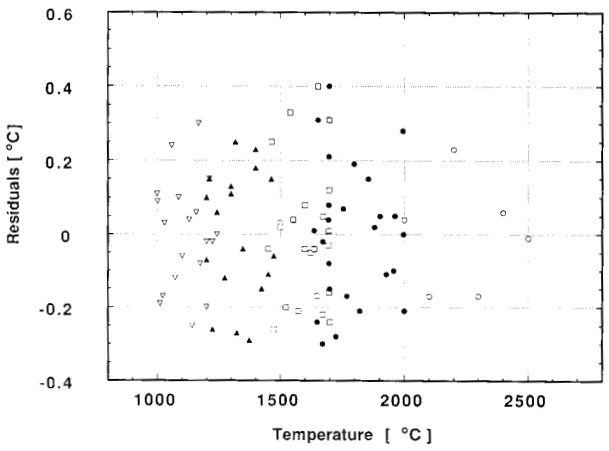

Fig. 1. The residuals, expressed in terms of temperature, for the fit of the polynomials representing the original and subsequent NPL calibration of the NPL Standard Transfer Pyrometer (STP). Different symbols represent different overlapping subranges, these are: ▽ 1000 °C to 1243 °C, ▲ 1200 °C to 1470 °C, □ 1450 °C to 1700 °C, ● 1636 °C to 2000 °C, and ○ 2000 °C to 2500 °C. The radiance temperature of the NPL blackbody source was determined through the calibration procedure described in Sec. 2.1 of the text.

At NIST the STP was recalibrated using the variable temperature blackbody source. The temperature of the blackbody was determined by the technique described in Sec. 2.2. The blackbody was then moved so that it was viewed by the STP. The STP output was then measured. This procedure was repeated at each calibration temperature, and all the temperatures were repeated at least once on a different day. Again each calibration result was the mean of several individual readings. The expanded uncertainty for these measurements also appeared to be about 0.3 °C.

While at NIST it was decided to extend the range of the intercomparison beyond 2000 °C, to 2500 °C. This was done by fitting a neutral filter of 10% transmission to the front of the STP for temperatures in excess of 2000 °C.

On return to NPL the instrument was recalibrated, including the range above 2000 °C. An extra polynomial was fitted to the data from 2000 °C to 2500 °C and the residuals of the fit can be seen in Fig. 1.

4. The Results of the Intercomparison

The results of the intercomparison are shown in Table 1 and Fig. 2. In Table 1, column 1 is the nominal intercomparison temperature in degrees Celsius. Column 2 is the difference between the NPL and the NIST calibrations of the STP. Column 3 is the expanded uncertainty that NIST ascribe to the radiance temperature of the variable temperature blackbody at 1000 nm. See Waters et al. [10] for a description of how uncertainties in this type of scale realization are determined. We have added a small contribution caused by the un-

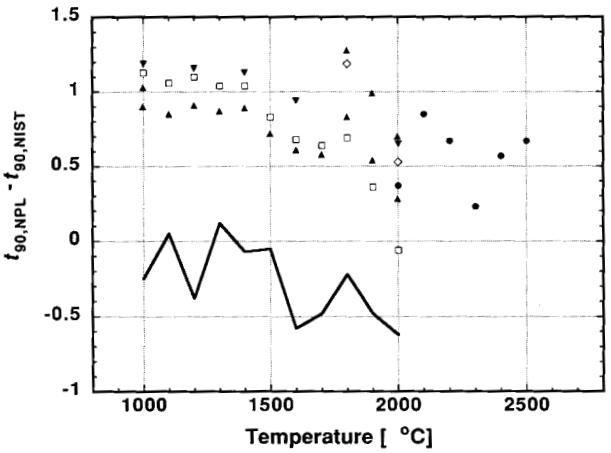

Fig. 2. Differences between the calibration of the NPL Standard Transfer Pyrometer (STP) obtained at NPL, $t_{90,NPL}$, and NIST, $t_{90,NIST}$. The radiance temperature of the NIST variable blackbody source was determined through the procedure described in Sec. 2.2 of the text. Different symbols represent different calibration runs at NIST, these are: ▲ 05 May 92, ▼ 08 May 92, ◇ 11 May 92, and □ 15 May 92. The solid circles represent the extension of the intercomparison to 2500 °C. The solid curve represents the differences between the calibration of the STP at NPL before and after the work at NIST.

Table 1. The results of the 1992 intercomparison of the NIST and NPL radiance temperature scales measured with the NPL Standard Transfer Pyrometer (STP) operating at approximately 1000 nm

Nominal temperature (°C)	$t_{90,NPL} - t_{90,NIST}$ (°C)	NIST 2σ uncertainty (°C)	NPL 2σ uncertainty (°C)	Combined 2σ uncertainty[a] (°C)
1000	+1.06	0.5	0.7	0.9
1100	+0.96	0.6	0.7	1.0
1200	+1.06	0.6	0.8	1.1
1300	+0.96	0.7	1.0	1.2
1400	+1.02	0.7	1.0	1.3
1500	+0.77	0.8	1.1	1.4
1600	+0.74	0.9	1.2	1.5
1700	+0.61	1.0	1.3	1.7
1800	+1.03	1.1	1.4	1.8
1900	+0.63	1.3	1.6	2.1
2000	+0.36	1.4	1.7	2.2
2100	+0.85	1.5	1.9	2.5
2200	+0.67	1.7	2.0	2.7
2300	+0.23	1.9	2.3	3.0
2400	+0.57	2.1	2.5	3.3
2500	+0.67	2.3	2.7	3.6

[a] Includes uncertainty in the calibration of the STP.

certainty in the effective wavelength. NIST usually also includes the uncertainty in the absolute value of the gold point temperature (see Mielenz, Saunders, and Shumaker [11] for details). But as the assigned ITS-90 value has been used in both laboratories this uncertainty has not been included. Column 4 is the expanded uncertainty of the calibration of the NPL blackbody with the LP2 as validated using the lamp (see Sec. 2.1) and column 5 gives the combined NIST and NPL uncertainties.

In the short term, the results at NPL and NIST show that the STP was repeatable to ±0.3 °C. The medium term repeatability is assessed from the difference between the NPL calibrations of the STP before and after the NIST visit. This difference is shown as the solid curve on Fig. 2. Unfortunately, because the STP developed a fault requiring repair shortly after return to NPL, only one recalibration could be performed. It is therefore important not to place too much weight on these measurements as it was not possible to repeat them. Column 5 of Table 1 gives the combined expanded uncertainty of the intercomparison between NIST and NPL, from columns 3 and 4, and includes the short term reproducibility of the STP.

5. Discussion

The NPL and the NIST infrared radiance temperature scales are in agreement to 0.1% of the temperature, the agreement improving as the temperature increases. They are, by and large, consistent with each other to within the 95% confidence intervals that are ascribed by the two laboratories.

It is surprising, however, that the largest differences occurred at the lower temperatures, close to the gold point reference temperature. To check the results at NIST the variable temperature blackbody was calibrated at 1064 °C directly against the gold point, independent of the lamp. This gave the same results as shown in Table 1.

A more likely explanation for the discrepancy lies in the use of the STP. First, its medium term repeatability could be responsible for part of the difference. Second, the f.o.v. of the STP matches neither that of the NIST primary pyrometer nor the LP2, therefore any temperature gradients were imperfectly accounted for. This could lead to an uncertainty in the calibration of the STP. As mentioned earlier, NPL de-focus the LP2 to better match the f.o.v. of the STP with the laboratory pyrometer—but effects due to imperfect matching and alignment could remain.

This intercomparison differs in some important respects from that performed by Lee et al. [1]. The main differences are that this intercomparison was detector based rather than source based—in itself something of a novelty since detectors with adequate stability and range are a comparatively recent innovation. The actual sources used in the intercomparison were blackbodies rather than lamps and the intercomparison was performed at long wavelengths, 900 nm to 1000 nm, rather than the more traditional 660 nm. Also in this instance only one artifact was exchanged. However, its prime aim was to confirm that the NIST and NPL radiance temperature scales are still in good agreement, despite the many changes that have taken place at the two laboratories, and this has been achieved, within the limits given above.

In view of the factors above, it is pleasing to note that the observed temperature differences above 1500 °C lie well within the 2 °C band allowed by the original MoU. This was found to be the case up to 2500 °C and the MoU should be extended (currently limited to 2200 °C) to reflect this new data. However below 1500 °C the MoU does not fully cover the difference observed. This is largely because, in switching to variable temperature blackbodies to provide standards of increased flexibility appropriate to modern industrial needs, both NIST and NPL have had to accommodate slight increases in the source temperature uncertainty. In the absence of a new intercomparison of lamps at 660 nm the revised MoU should relate to the present results, covering infrared wavelengths.

Finally the fact that some of the differences at lower temperatures lie outside the combined expanded uncertainties reinforces the fact that great care must be exercised when radiation thermometers are calibrated against blackbody sources. In particular, the requirements that the source aperture significantly overfills the instrument's f.o.v. and emits uniform radiance must be met to ensure that a good calibration can be performed.

6. Conclusion

These results show that the infrared temperature scales as established at NPL and NIST *are* equivalent to each other at or better than the 0.1% of the temperature. The original MoU needs some modification to take into account the larger than expected differences found at lower temperatures but it can be extended upward in range from 2200 °C to 2500 °C.

Acknowledgments

G. Machin would like to thank Bob Saunders, head of the Thermal Radiometry Group, for his contribution to this work and for his hospitality during GM's stay at NIST. He would also like to thank Brian Chu and Helen McEvoy for their help with the NPL measurements. Finally GM would like to acknowledge support from the NPL Junior Travel Award Scheme for this visit and also Land Infrared for producing the standard transfer pyrometer on a short timescale.

7. References

[1] R. D. Lee, H. J. Kostkowski, T. J. Quinn, T. R. D. Chandler, T. P. Jones, J. Tapping, and H. Kunz, Temperature its Measurement and Control in Science and Industry, Vol. 4, Pt. 1, Instrument Society of America (1972) p. 377.
[2] B. N. Taylor and C. E. Kuyatt, NIST Technical Note 1297 (1993).
[3] H. Preston-Thomas, Metrologia **27**, 3 (1990); ibid. **27**, 107 (1990).
[4] T. J. Quinn, Temperature, 2nd Edition, Academic Press, London (1990).
[5] P. B. Coates, Theory and Practice of Radiation Thermometry, Chapt. 13, D. P. DeWitt and G. D. Nutter, eds., John Wiley & Sons Inc (1988) p. 773.
[6] M. Groll and G. Neuer, Temperature its Measurement and Control in Science and Industry, Vol. 4, Pt. 1, Instrument Society of America (1972) p. 449.
[7] E. Schreiber, G. Neuer, and B. Wörner, Tempmeko 90, preprints of The 4th Symposium on temperature and thermal Measurement in industry and science, Finnish Society of Automatic Control, Helsinki (1990).
[8] K. D. Mielenz, R. D. Saunders, A. C. Parr, and J. J. Hsia, J. Res. Natl. Inst. Stand. Technol. **95**, 621 (1990).
[9] T. J. Quinn and R. D. Lee, Temperature its Measurement and Control in Science and Industry, Vol. 4, Pt. 1, Instrument Society of America (1972) p. 395.
[10] W. R. Waters, J. H. Walker, and A. T. Hattenburg, Radiance Temperature Calibrations, NBS Special Publication 250-7 (1987).
[11] K. D. Mielenz, R. D. Saunders, and J. B. Shumaker, J. Res. Natl. Inst. Stand. Technol. **95**, 49 (1990).

About the authors: *Graham Machin is team leader of the Radiation Thermometry group at NPL. Richard Rusby is head of the Temperature Standards Section at NPL. Carol Johnson is project leader for Radiation Temperature at NIST. Charles Gibson is project leader for Calibration Services at NIST and provides, radiance temperature, spectral irradiance, and spectral radiance calibrations. The National Institute of Standards and Technology is an agency of the Technology Administration, U.S. Department of Commerce.*

Volume 99, Number 6, November–December 1994
Journal of Research of the National Institute of Standards and Technology

[J. Res. Natl. Inst. Stand. Technol. 99, 737 (1994)]

Screened-Room Measurements on the NIST Spherical-Dipole Standard Radiator

Volume 99 Number 6 November–December 1994

G. Koepke and J. Randa

National Institute of Standards and Technology,
Boulder, CO 80303

We report the results of a study of measurements of radiated emissions from the NIST spherical-dipole standard radiator in several screened rooms. The study serves as a demonstration of possible applications of the standard radiator as well as an investigation of radiated-emissions measurements in screened rooms. The screened-room measurements were performed in accordance with MIL-STD-462 (1967). Large differences occurred in the field intensity measured at different laboratories and even on different days at the same laboratory. There was a systematic difference at low frequencies between the screened-room results and results obtained in a transverse electromagnetic (TEM) cell, open-area test site (OATS), and anechoic chamber. We also present the results of OATS tests confirming the temporal stability of the standard radiator and measuring the loading effect of a ground plane as a function of distance from the sphere.

Key words: MIL-STD-462; radiated emissions; screened room; spherical dipole; standard radiator.

Accepted: July 19, 1994

1. Introduction

The National Institute of Standards and Technology has recently developed a spherical-dipole standard radiator for use in electromagnetic interference and compatibility (EMI/EMC) applications. The design, construction, and operation of the device are described in Refs. [1,2], which also present results of tests in various NIST facilities—the open area test site (OATS), anechoic chamber (AC), transverse electromagnetic (TEM) cell, and mode-stirred chamber. The spherical radiator is a well controlled, well characterized source of electromagnetic radiation for the frequency range between about 5 MHz and over 1 GHz. As such, it can be used to test the ability of a laboratory to measure radiated electromagnetic emissions. That, in fact, was one of the principal motivations for the development of the standard radiator. It can also be used to compare different test methods, to test the validity of new measurement techniques, in round-robin intercomparisons among many laboratories, or as a check standard to confirm day-to-day repeatability at a single laboratory. The study reported below demonstrates several of these possible uses of the standard radiator. A preliminary account of the results is contained in Ref. [3]. The application of initial interest was in the competence testing of laboratories seeking accreditation for radiated emissions testing, but in the course of the study the standard radiator was also used as a known source to assess the basic test method, as a check standard, and as the test artifact in a multilaboratory intercomparison.

In this paper we consider radiated-emissions measurements performed on a spherical-dipole standard radiator in three different screened rooms. The original goal was to develop procedures for using the NIST spherical-dipole standard radiator in the laboratory accreditation process, particularly in the National Voluntary Laboratory Accreditation Program (NVLAP) for accrediting laboratories performing MIL-STD-462 acceptance testing. To this end, we sought and received the cooperation of three EMC test laboratories to perform MIL-STD-462 RE02 tests on the spherical radiator. The intent was to establish a baseline of performance for the radiator, against which measurements at other laboratories could be compared in order to assess their ability to perform MIL-STD-462 tests. Tests at NIST had already characterized the performance of the spherical-dipole standard radiators in test facilities simulating quasi-free-space environments (OATS, AC, TEM) and in the mode-stirred chamber, but the radiators had not been tested in screened rooms, which are the common environment for MIL-STD-462 tests.

Measurements in screened rooms have a (well-deserved) tarnished reputation. We will not examine in detail the causes of the problems of screened-room measurements, but a few comments are useful as background. Our remarks will address the case of radiated emissions, but analogous effects occur for radiated susceptibility. There are many sources of potential errors in EMI measurements inside screened rooms. Perhaps the most obvious effect is that a screened room is a conducting cavity, and thus it exhibits cavity resonances and standing waves. Consequently, the field distribution within the room generally is nonuniform, and the field intensity measured depends on the locations of the equipment under test (EUT) and the measuring antenna, as well as on the electrical size of the room. Another potential source of error is that the behavior of the receiving antenna is affected by the proximity of the conducting walls. The interactions between the antenna and its numerous images change the antenna factor, and consequently the antenna response in a given electric field depends on the antenna's location, the size of the room, and the type of antenna. A similar effect can occur for the EUT. If we think of the EUT as a transmitting antenna, its input impedance will be changed by the interaction with its images, thereby changing the ratio of terminal voltage to input current. Thus the radiated power can depend on the size of the room, the EUT's position in the room, and details of the EUT itself. (The loading effect on the standard radiator will be addressed below.) Finally, most screened-room measurements are done at low enough frequencies that the EUT and the receiving antenna are in each other's near fields.

The potential problems with screened-room measurements have been widely appreciated for some time [4–7]. Nevertheless, screened rooms are widely used in EMI/EMC. Their appeal is partly economic, partly inertial, and partly due to the fact that competing techniques are not without problems of their own. Open-area test sites admit background noise; anechoic chambers are expensive and become echoic at low frequencies; TEM cells have high-frequency cutoffs and size constraints; etc. Screened rooms are particularly prevalent in MIL-STD-462 testing [8], where their use is nearly universal. An extensive revision of MIL-STD-461/462 has recently been released, which contains (among other things) changes intended to improve screened room test methods [9]. The revised standard is labeled MIL-STD-462D. The tests described in this report were performed according to the old standard, MIL-STD-462 (1967), since the contents of the new one were not known at the time of the tests. We will discuss this below.

Over the course of a year, radiated-emissions tests were performed at the three participating EMC labs. All three screened rooms had absorber loading to some degree, and all were large enough to meet MIL-STD-462 (1967) specifications. We do not detail the actual sizes and specific configurations of the individual rooms. That information would be needed for diagnosing the cause of interlaboratory differences, for example, but for this study we are just interested in the fact that they did conform to the (old) MIL-STD requirements. (There was not enough absorber in any of the screened rooms to meet the requirements of MIL-STD-462D [9].) Each set of measurements was performed twice at each laboratory, with the setup disassembled between the two measurements, in order to evaluate the repeatability of the tests. We were thus able to address three major issues: day-to-day variations at a given laboratory, differences between results obtained at different laboratories, and differences between the screened-room results and results obtained at NIST in simulated free-space environments. The results caused us to reconsider the appropriateness of using the standard radiators in the accreditation process for MIL-STD-462 measurements (under the old standard). The differences in all three areas—day-to-day variations, interlaboratory variations, and screened-

room to free-space differences—were sufficiently large that the basic validity of the old RE02 test procedures in a screened room must be questioned. This point is addressed in the final section below. In the next section we review the general design of the spherical dipole radiator and present results of measurements at NIST facilities. In Section 3 we outline the procedures followed in the screened-room (RE02) tests on the standard radiator and present the results of those tests. Section 4 contains a discussion of the results and conclusions.

2. The Spherical-Dipole Standard Radiator

The spherical-dipole radiator is described in detail in Refs. [1,2]. For present purposes, it is sufficient to recall a few of its principal features. The radiating element is a spherical, gold-plated dipole of 10 cm diameter, the basic configuration of which is indicated in Fig. 1. The driving voltage is applied at the gap between the center posts, and the current flows up the top post to the inside top of the sphere and down the bottom post to the inside bottom of the sphere. From the poles of the inside of the sphere, the current flows on the inner surface of the sphere out to the equatorial gap, where it feeds the outer surface of the sphere. Thus, provided that the current propagates from the rf feed uniformly to all points on the equator, we have a center-fed spherical dipole, uniformly excited around its equator. The voltage at the gap of the center post is monitored continuously by a diode detector circuit, and this reading is relayed back to the control unit via optical fiber. This feature enables the operator to verify that the impressed voltage is the same from one test to another, and it also confirms that the unit is operating properly throughout a set of measurements.

The excitation waveform is fed to the sphere by an optical fiber. Inside the sphere the optical signal is converted to an electrical signal, amplified, and fed to the gap in the center post. In the tests described in this report, a single-frequency cw signal was always used. In principle, virtually any waveform could be used to drive the spherical dipole, though the radiated waveform would include the shaping effect of the sphere's frequency-dependent radiation characteristics. The pulse characteristics of the spherical dipole radiator have not yet been examined.

Detailed tests of the angular pattern and the intensity of the radiated field were reported in [1,2], and we do not reproduce them all here. One aspect of those tests which is relevant to the present study is the determination of the radiated field intensity. Although the voltage across the gap in the center post is continuously monitored, it does not enable us to directly calculate the radiated field, since the relationship between the voltage at the post gap and the voltage at the equatorial gap in the spherical shell cannot be easily calculated. Therefore the transfer function between the post gap voltage and the radiated field was determined empirically. This was done by measurements on the NIST OATS and in the AC. For a (post) gap voltage of 1 V, the

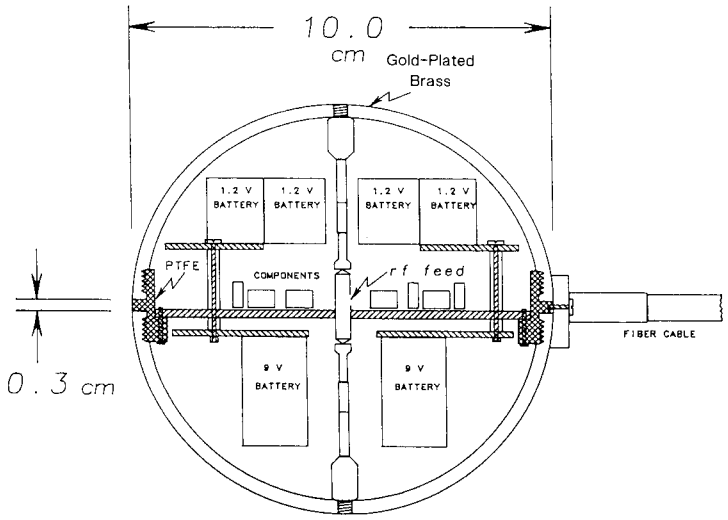

Fig. 1. Mechanical drawing of the spherical dipole radiator.

maximum field intensity was measured at some convenient distance from the sphere. The known radiation characteristics of a spherical dipole were then used to calculate the voltage at the equatorial gap. In the AC the free-space formula for the radiation pattern was used, whereas on the OATS the effect of the ground plane was taken into account. Based on those tests, a transfer function which relates the indicated post gap voltage to the radiated field intensity (in free space) was obtained. Using this measured transfer function, we can then compute the field intensity for a given indication of the gap voltage and a given position. Figure 2 plots the field as a function of frequency for a position in the equatorial plane, 1 m from the radiator. Besides the OATS and AC results, Fig. 2 also contains the results of analogous measurements in a TEM cell [1]. The results from the OATS and AC agree very well in their region of overlap (200 MHz to 1000 MHz). The TEM cell results fall below those of the OATS by about 2 dB to 4 dB (except at one anomalous point). This difference may be due to the loading effect of the TEM cell walls on the sphere, since the radiator was about 30 cm from the walls in the TEM cell measurements. The possible effects of loading are addressed below.

For virtually all standard-radiator applications, and in particular for the screened-room study reported in this paper, the radiator's repeatability is a crucial issue. We must be confident that the spherical dipole is constant if we are to use it to compare measurement results taken at different times. There is some evidence for the spherical dipole's repeatability in the agreement of AC and OATS results in Fig. 2. We have now performed a systematic test which confirms this point. Measurements of the field radiated by the spherical dipole were made on the NIST OATS on two different days, with the measurement apparatus disassembled and reassembled between the two sets of measurements. The gap voltage was maintained at (1.00 ± 0.01) V; the dipole axis was horizontal; it was about 2 m above the ground plane; and the distance from the sphere to the receiving antenna was between 7 m and 8 m in each case. The receiving antenna (a calibrated, tuned dipole) was positioned 2 m above the ground screen, provided that a usable signal was obtained at that height. For frequencies at which the 2 m height corresponded to a null of the pattern arising from interference between direct and reflected waves, the receiving height was increased until a usable signal was obtained. The measured field was converted to a field intensity at 1 m, called E_{ref}. This was done in the manner described above, except that the full expression was used for the field from the image, rather than just the ray approximation of Ref. [1]. The difference Δ between the values measured for

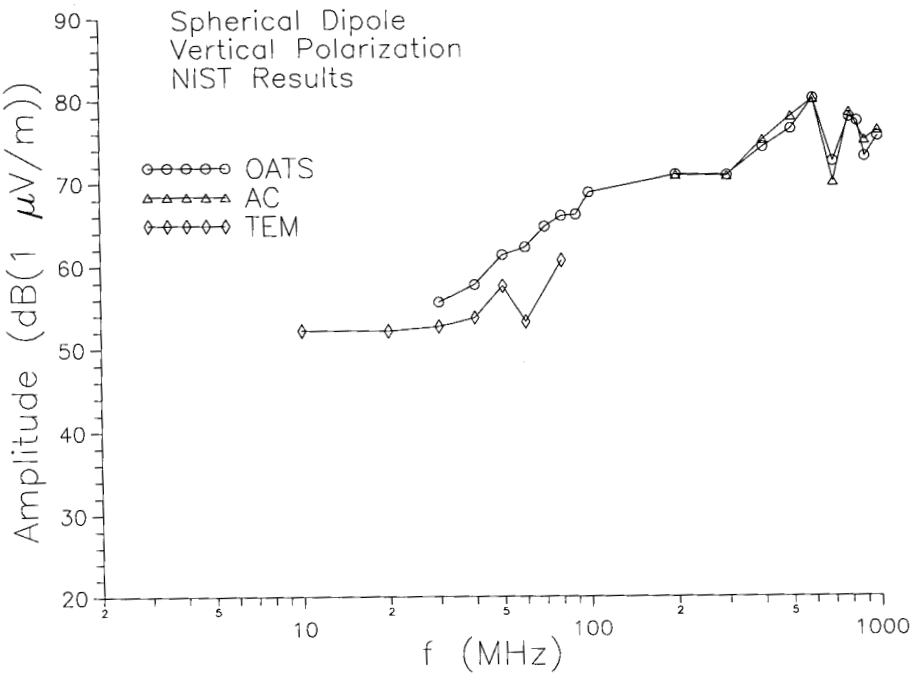

Fig. 2. Calculated field at 1 m distance using transfer function measured at NIST facilities.

E_{ref} on the two different days is plotted as a function of frequency in Fig. 3. The repeatability is very good, better than 0.55 dB at all but one measurement frequency and better than 0.1 dB at almost half the frequencies. Even at the one "bad" point (100 MHz), the difference is 0.93 dB. Such variations are consistent with what we expect from the measurement method itself; our OATS measurements have a statistical uncertainty characterized by a standard deviation of about 0.5 dB. Thus the variations in the field radiated by the spherical dipole (for a constant gap voltage) are less than or about equal to 0.5 dB, and could be significantly less.

The final aspect of the standard radiator's performance which is important to the screened-room study is the effect of loading, the sensitivity of the radiator to nearby conducting surfaces. Measurements at and above 100 MHz in the mode-stirred chamber [2] did not show evidence of a loading effect on the spherical dipole for a dipole-to-wall separation of 1 m, at least within the accuracy of the measurements, and the TEM cell results in Fig. 2 suggest that the effect is of order a few decibels for a distance of 30 cm. We have now also performed a series of measurements on the OATS for several different heights of the sphere above the ground screen. At five frequencies, from 30 MHz to 1000 MHz, the radiated field intensity was measured for four heights, h_t, ranging from 0.22 m to 2.1 m. The gap voltage was 1.00 V in all the measurements, and the measured field was converted to E_{ref}, the field at 1 m. Results are shown in Fig. 4. The uncertainty in the measurements is about 1 dB. At the lowest frequency, 30 MHz, there is a definite increase in the radiated field for $h_t < 0.5$ m. At other frequencies there is no clear evidence for an effect of loading, although something may be happening around $h_t = 0.5$ m at 1000 MHz and for $h_t < 0.5$ m at 60 MHz. For $h_t \geq 1$ m, the data do not indicate a loading effect at any frequency tested, although we cannot rule out an effect of order 1 dB-2 dB. In the screened-room measurements discussed below, the sphere was never closer to a wall than 1 m.

3. Screened-Room Measurements

3.1 Procedures

The three participating laboratories will not be identified in discussion of the results, and only aggregate data will be shown. At the time of the tests, one of the laboratories was NVLAP certified for MIL-STD-462 acceptance testing, and the other two were working toward certification. Tests were

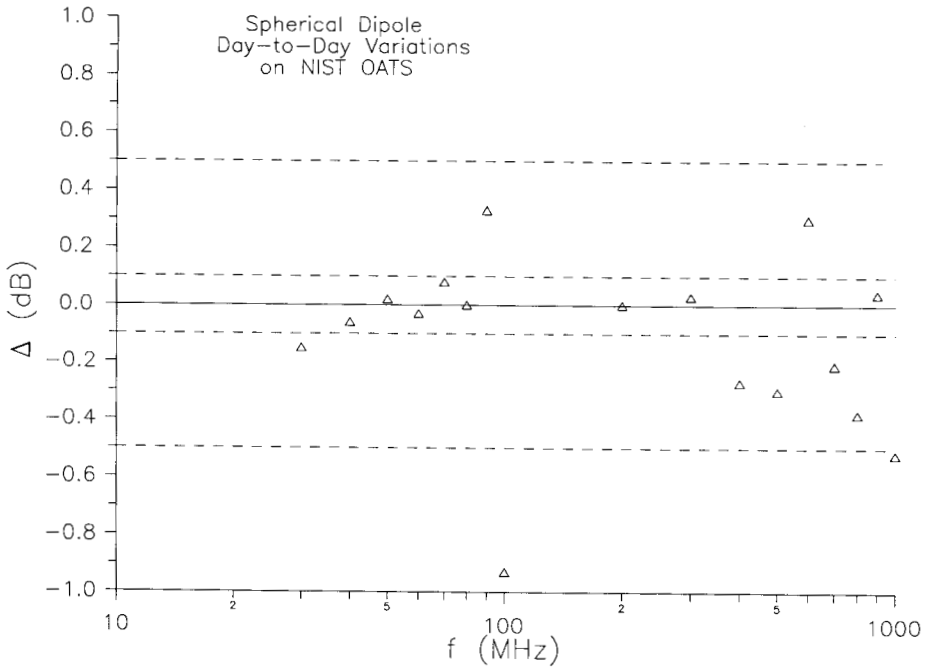

Fig. 3. Day-to-day variations in radiated emissions measurements on standard radiator on NIST OATS.

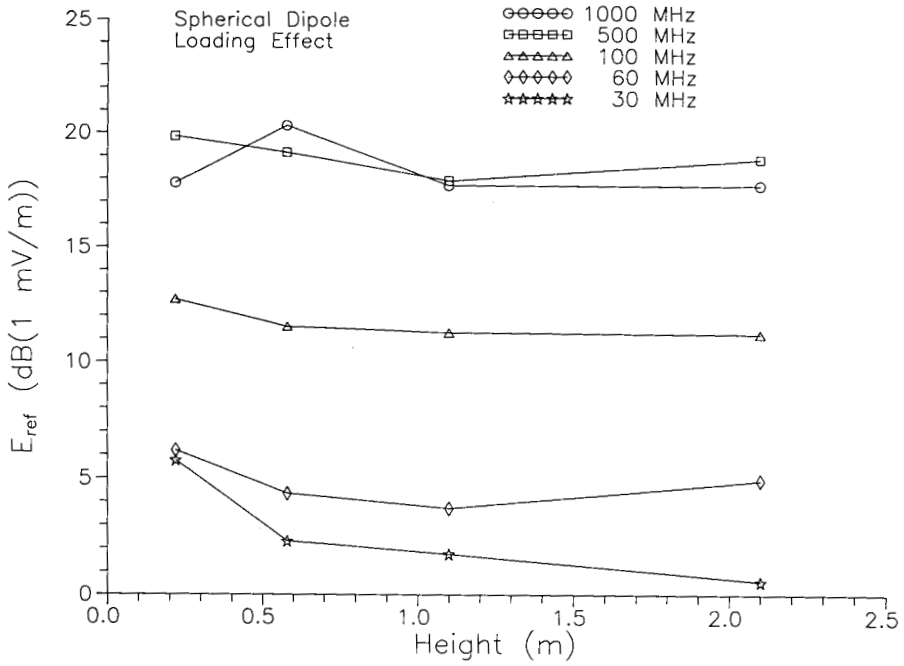

Fig. 4. Field radiated by spherical dipole as a function of height above ground plane.

performed over two days at each laboratory. The same spherical-dipole unit was used in all the tests. The intent was that the NIST dipole radiator would be treated as if it were a piece of electronic equipment submitted to the laboratory for RE02 acceptance testing. The dipole was to be treated as a piece of mobile equipment placed on a foam support out in the room. Tests were also performed on a small, battery-operated monopole radiator [3], which was tested on the bench top/ground plane. However, subsequent tests revealed possible problems with the monopole's repeatability, and so we will not present results of the monopole measurements in the screened rooms. In all the tests the radiator was oriented so that its axis was vertical. For low frequencies (below 20 MHz or 30 MHz, depending on the laboratory), the receiving antenna was a small monopole, and only the vertical component of the radiated field was measured. From 20 MHz or 30 MHz to 200 MHz, a biconical antenna was used, and vertical and horizontal components were measured separately. Above 200 MHz, all three laboratories used conical log-spiral antennas, sensitive to one circular polarization.

At 20 MHz, 30 MHz, and 200 MHz, one or more laboratories changed the receiving antenna used. At these frequencies, measurements were taken on radiated signals at frequencies at the top of the lower band and at the bottom of the upper band (e.g., 19.95 MHz and 20.05 MHz) at the laboratory changing antennas at that frequency. If a laboratory did not change antennas at that frequency, then just one measurement was taken (e.g., 20.00 MHz). For the computations in which measurements from different laboratories were paired or compared, the 20.00 MHz measurement was paired or compared with both 19.95 MHz and 20.05 MHz results.

The spherical-dipole radiator was fed with a single frequency at a time, with the frequencies chosen to correspond to those at which the radiator had been tested in NIST facilities. The engineer or technician performing the test was told the frequency, and he or she swept the receiver through a small range of frequencies around the frequency being radiated. The test frequencies for the dipole ranged from 5 MHz to 1000 MHz. The gap voltage of the dipole was maintained at the same value (1.00 V) for all the tests. Each measurement at each frequency was done twice at each laboratory, typically on successive days, but in some cases in the morning and afternoon of the same day. Between the two measurements the setup was always taken down, connections broken, etc., to insure that the two measurements were as independent as was practical. In at least one case, the positioning of antennas was intentionally altered somewhat, to simulate the variations in placement which could

occur in different tests. Thus we generally have two independent measurements at each frequency (and each polarization, where prescribed by the MIL-STD) at each of the three participating laboratories. Insofar as was possible, NIST personnel attempted not to influence the actual conduct of the tests. Some interaction did occur, of course, but we do not believe that there were any substantive effects on our general results.

3.2 Results

The collected results of the measurements on the spherical-dipole radiator at all three laboratories, for a vertically polarized receiving antenna, are shown in Fig. 5. Low-frequency (<30 MHz) results from one of the laboratories were not available because of an error in assembling an antenna. The error was discovered during the tests, but too late to repeat the measurements. Also shown in Fig. 5 are the results obtained in the NIST facilities which simulate (to differing degrees) a free-space environment. The NIST results are connected by solid lines. The single most striking feature of Fig. 5 is the large spread in the screened-room measurement results. The differences between maximum and minimum values for the radiated field strengths at different labs are as large as 25 dB to 30 dB at some frequencies, and they are of order 10 dB even at the "good" frequencies. Figure 5 also indicates that there are often large differences between the shielded room results and the results from TEM cell, OATS, and AC. Differences between the two measurements at the same frequency at the same laboratory cannot be seen in Fig. 5, but these also can be sizable.

For purposes of addressing separately the three different types of variations (day-to-day, interlaboratory, screened room to free space) it is useful to present the data in different formats. To address the question of repeatability of results at a given laboratory, we simply compute the difference, in decibels, between the two independent measurements at each frequency at that laboratory. This difference, denoted Δ, is plotted in Fig. 6 for all three laboratories. The dashed lines at ± 5 dB are included to aid the eye and facilitate discussion. As can be seen, most measurements repeated to within 5 dB, but a significant number (23%) did not, and some day-to-day variations exceeded 10 dB.

For interlaboratory variations, there are several ways in which the data might be presented. Our choice is guided by the question, "If the same measurement were made on the same device at two different laboratories, how much would the two results differ?" To answer this, we have computed at each frequency the magnitude of the difference (in

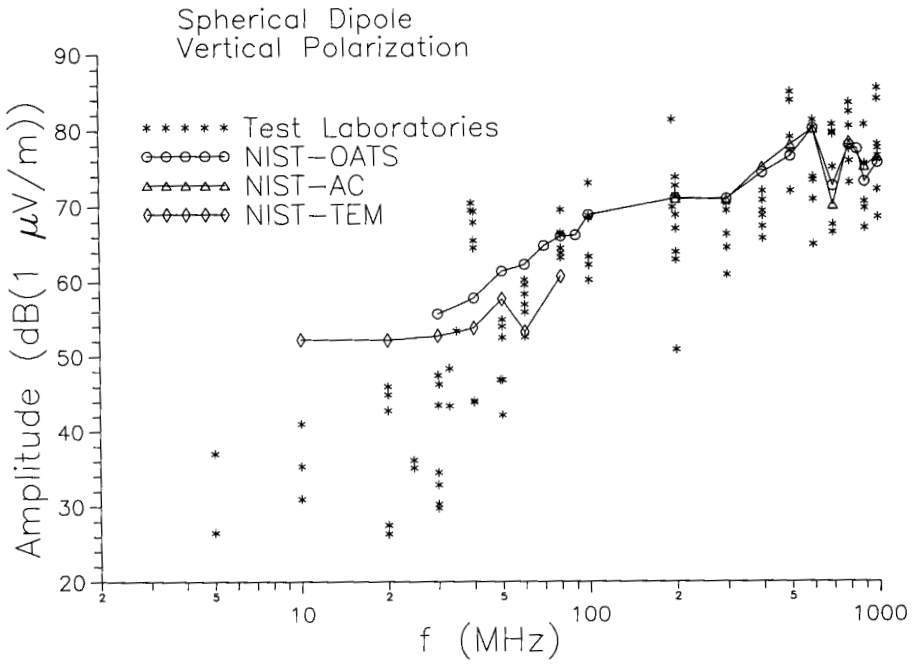

Fig. 5. Measurement results on spherical dipole standard radiator with constant gap voltage.

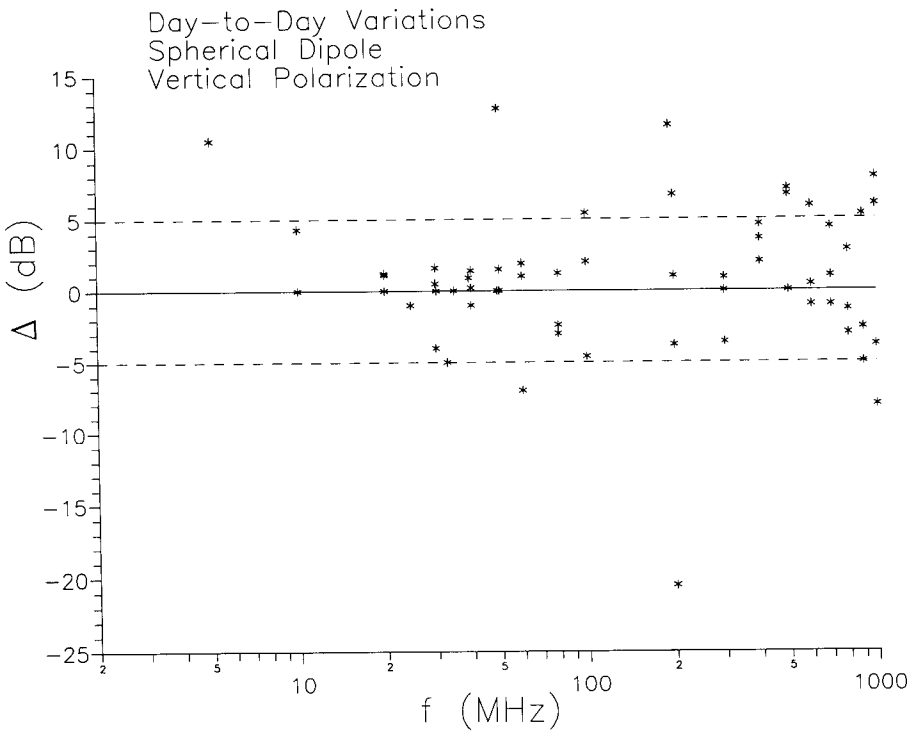

Fig. 6. Day-to-day variations in vertical polarization measurements at the same laboratory.

decibels) between each possible pair of measurements at different laboratories. Thus, at a typical frequency, where there are two measurements at each of the three laboratories, there would be 12 different pairs of measurements at different laboratories. We use D to denote the difference between two measurements at different labs. Figure 7 shows the average and sample standard deviation s,

$$s^2=\frac{1}{(N-1)}\sum_i (x_i-\bar{x})^2, \qquad (1)$$

of these differences for each measurement frequency. The statistics were done on the field strength, and the results were then converted to decibels. Results below 30 MHz are based on measurements at only two laboratories. Even above 30 MHz, the sample is not large enough for real statistical significance. Nevertheless, the results are not particularly encouraging. The *average* differences in the measurement of the same quantity at two different laboratories are over 5 dB at most frequencies and over 15 dB in some cases.

To consider differences between screened-room results and those obtained at quasi-free-space facilities, we average over the screened-room results obtained at the three EMC labs and compare to the TEM cell, OATS, and AC results at NIST. The results are shown in Fig. 8, where again the error bars correspond to the sample standard deviation. At high frequencies the screened-room results are in fair agreement with the quasi-free-space results, although the spread in the screened-room results is rather large. Below about 80 MHz the screened-room results tend to be systematically, significantly low. The one exception occurs at 40 MHz, which corresponds to a resonance frequency of two of the screened rooms and where the results in those two rooms are anomalously high, cf. Fig. 5. The other eye-catching feature of Fig. 8 is the large standard deviation just below the band edge at 200 MHz. The spread in the measurements at this point is so great that the results are essentially consistent with any result from 0 V/m ($-\infty$ dB) to the top of the bar shown on the graph.

For frequencies between 20 MHz or 30 MHz and 200 MHz, emission measurements were also made with the receiving antenna horizontally polarized. The measured amplitude are shown in Fig. 9. Unlike the results for vertical polarization, there are no results shown from NIST quasi-free-space facilities. That is because the electric field from a vertical spherical dipole in free space has no component in the ϕ direction and no horizontal

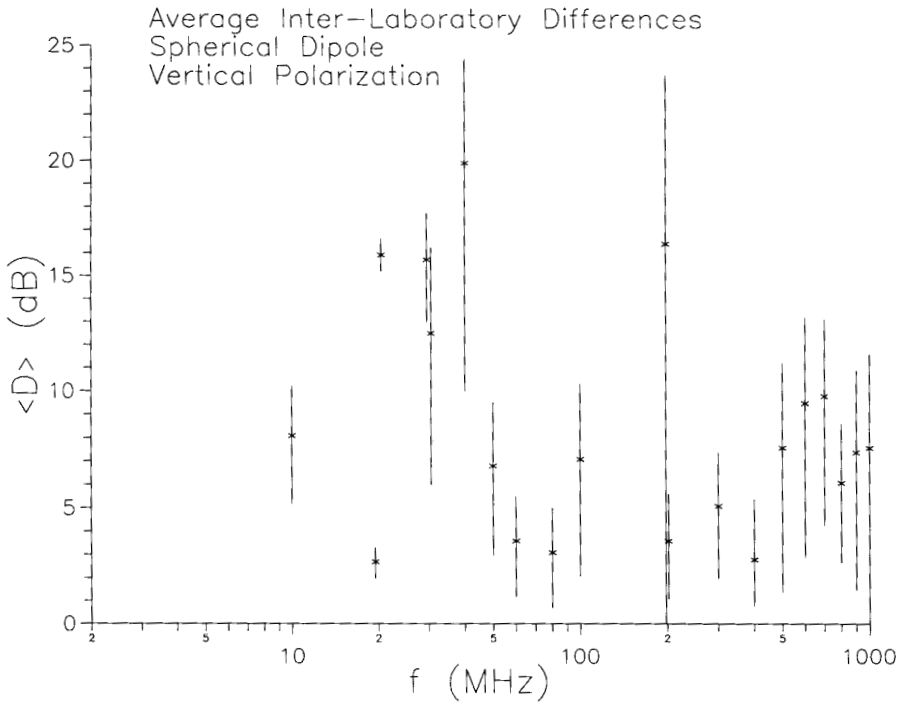

Fig. 7. Interlaboratory differences in vertical polarization emissions measurements on the spherical dipole for constant gap voltage.

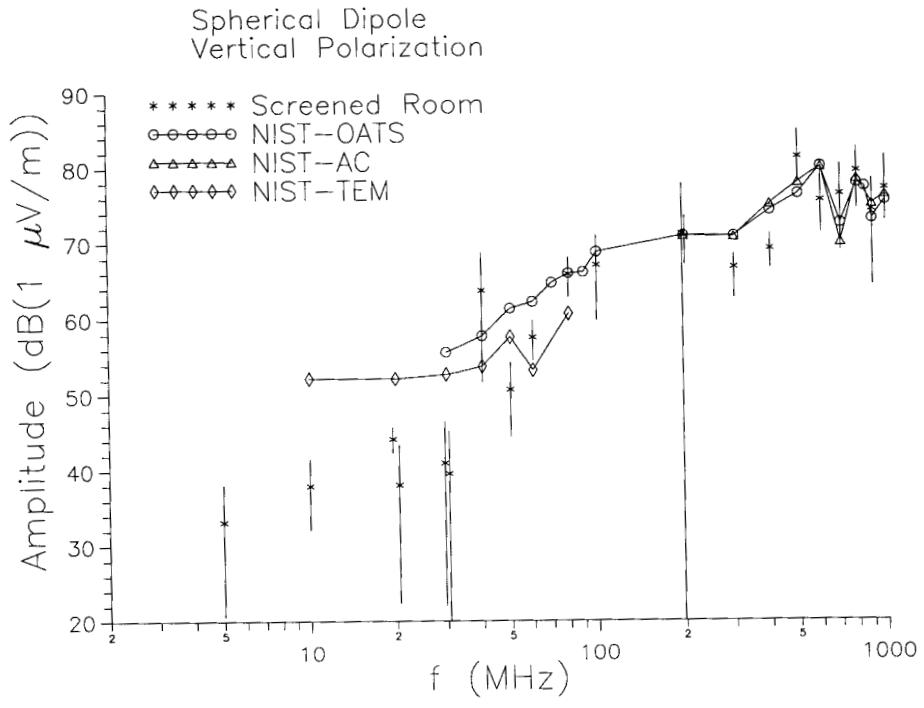

Fig. 8. Combined screened room results compared to quasi-free-space results for vertical polarization measurements on the spherical dipole.

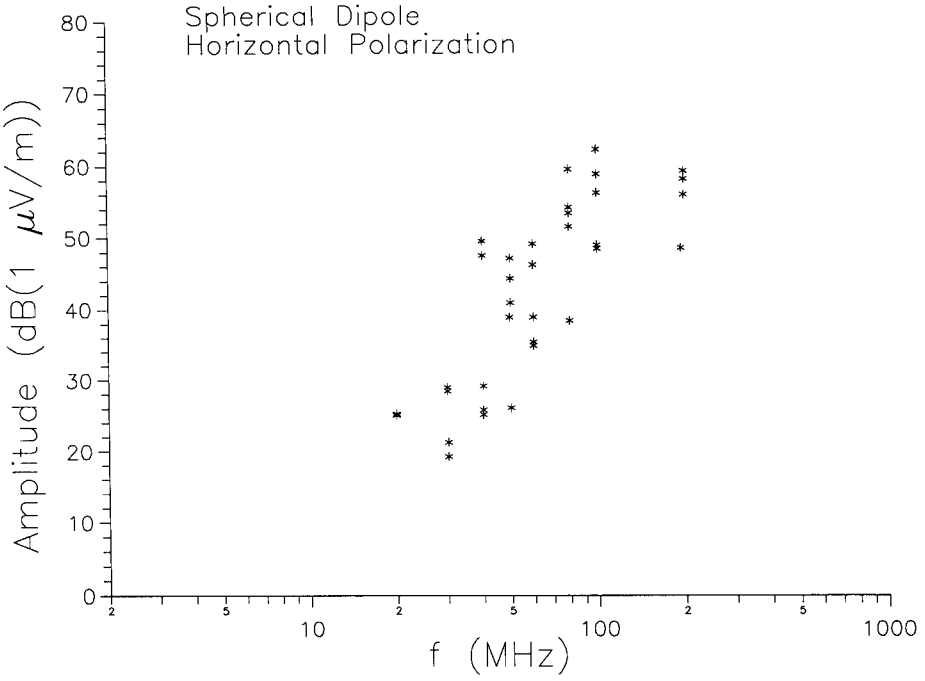

Fig. 9. Horizontal polarization emissions measurements on the spherical dipole.

component at all in the equatorial plane [10]. This was checked in a few instances in the NIST facilities, and no significant field was detected. Thus the horizontally polarized fields of Fig. 9 are an artifact of performing the measurements in a screened room.

The day-to-day and interlaboratory variations in the results for horizontal polarization can be treated in the same manner as they were for vertical polarization. The results are shown in Figs. 10 and 11. The day-to-day variations are somewhat larger than the vertical case, as are the lab-to-lab differences. The *average* interlaboratory differences are all around 10 dB, except at the 40 MHz resonance, where they are considerably more. Since the horizontally polarized fields are basically room effects, it is not surprising that there is considerable variation from room to room. Note that if the source were a horizontal dipole, then it would be the vertical fields which arose from room effects. In general, it is the cross-polarized configuration which is due to room effects.

4. Summary and Conclusions

4.1 Screened-Room Measurements

The spherical-dipole standard radiator was used to assess the repeatability of screened-room measurements and to compare screened-room radiated-emission measurements to those made in other facilities. We first address the three main types of variations discussed in the introduction. The emissions tests, performed according to MIL-STD-462 (1967), lead us to the following conclusions. (1) Day-to-day variations of about 5 dB or more occur in measurements of radiated fields of the same magnitude, frequency, and polarization. Consistent repeatability of 5 dB or less may be achievable, but probably requires considerable effort and care. (2) The average difference between measurements of radiated, vertically polarized, electric fields of the same magnitude at different laboratories was over 10 dB at several frequencies. It is about 20 dB at a resonance frequency of one of the screened rooms. For horizontal polarization (with a vertically polarized source) the average difference is consistently around 10 dB, except at the resonance frequency, where it is near 20 dB. (3) At frequencies below about 60 MHz, the screened-room results are significantly lower than the quasi-free-space results, except at the resonance frequency of the screened room. For frequencies of 80 MHz and above, the average screened-room results are usually consistent with the quasi-free-space results, albeit with large standard deviations.

What is the cause of the large variations in test results? There are three obvious suspects: variabil-

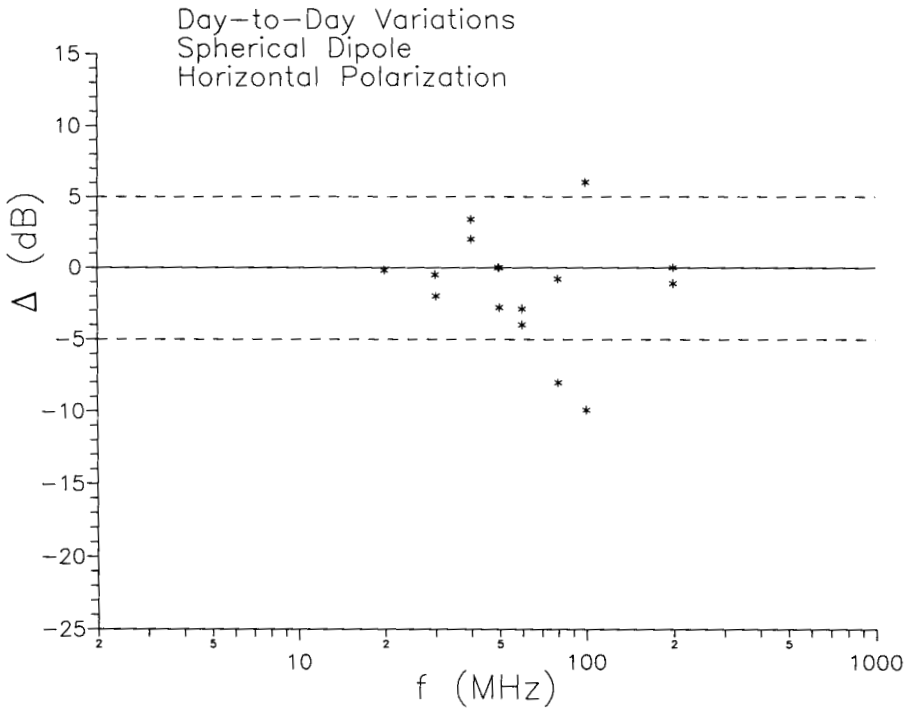

Fig. 10. Day-to-day variations in horizontal polarization measurements at the same laboratory.

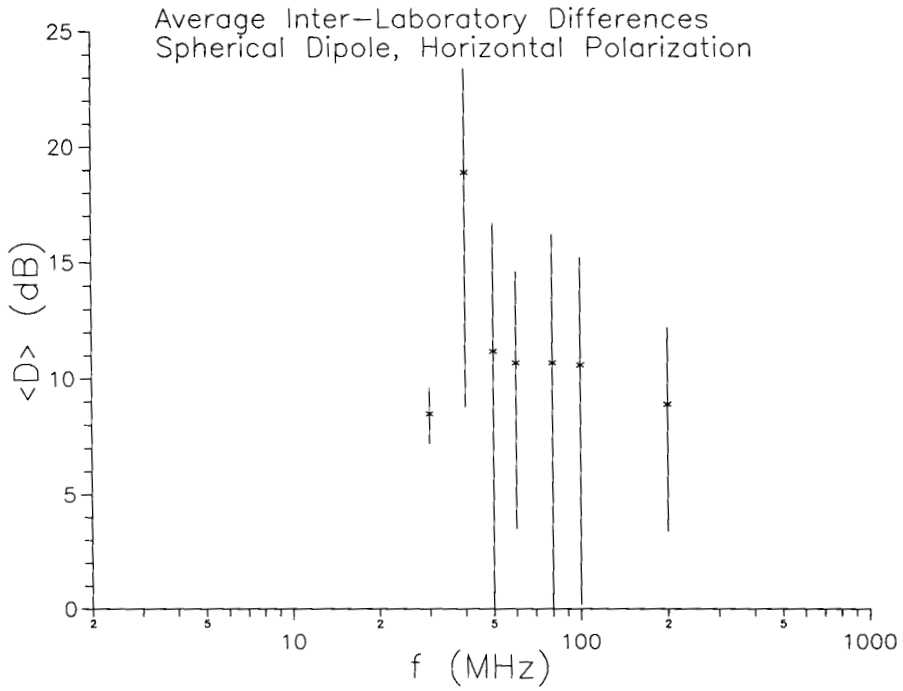

Fig. 11. Interlaboratory differences in horizontal polarization measurements on spherical dipole for constant gap voltage.

ity of the standard radiator, lack of competence of the test laboratories, and faulty test methodology (pathologies of RE02 screened-room measurements). It is very unlikely that the spherical-dipole radiator is that unstable. The gap voltage is monitored continually and is kept constant within 0.1 dB from test to test. Measurements on the NIST OATS indicated a repeatability for radiated-emission measurements of about 0.5 dB. At high frequencies there is some departure from axial symmetry in the radiated pattern [1,2], but this is only of order 3 dB to 5 dB, and it occurs only at 600 MHz and above. Furthermore, the pattern is very repeatable, even at frequencies where it is asymmetric, and in the screened-room tests the orientation of the sphere was usually the same at a given laboratory, due to positioning of the fibers running into the sphere. As for the test laboratories, in principle it is possible that they were careless or incompetent in their measurements, but we feel that this is unlikely. NIST personnel present at the tests were not trained or experienced specifically in RE02 measurement techniques and did not attempt a systematic, critical evaluation of laboratory procedures, but our impression was that laboratory personnel were in general competent and careful. As mentioned above, one of the three laboratories was NVLAP certified; and all three are large, reputable laboratories with considerable experience. Furthermore, no one laboratory stood out as having particularly bad results. Consequently, while an individual bad result could have been due to an error, we do not believe that the general pattern of variability was due to shortcomings of the laboratories or their staffs. The most likely cause of the variability of results and the deviation from free-space results appears to be the basic measurement method itself. Variations in size, shape, and loading of the screened room as well as in positioning of the source and receiving antenna within the room will lead to variations in the measured field. The existence of such effects has been known for some time and has been documented by past work at NIST [6,7] and elsewhere [4,5]. This study quantifies the magnitude of the effects in some practical measurements.

Besides the three central issues discussed above, two peripheral points which arose in this study warrant comment. The comments involve band edges. At one of the laboratories, the software and/or instrumentation were such that a peak occurring at a band edge could be missed. This problem was noted by the laboratory in question at the time of the tests. Another, more general, band edge problem is the fact that measurements in two adjoining bands do not match at the limiting frequency. In this study we found discrepancies as large as 10 dB to 20 dB at band edges. It would be desirable for the limiting frequency (at least) to be included in both bands and for techniques and calibrations to be checked until the results of the two bands agree at the limiting frequency.

In discussing the implications of our results, we emphasize that they *do not* apply to the new radiated emissions measurements as specified in [9]. The new standard incorporates modifications intended to improve various test procedures. In particular, it requires a large amount of absorber around the test setup, nearly transforming the screened room into a semianechoic chamber. The minimum acceptable performance specified for the absorber is rather modest, as it must be if anyone is to meet it; conventional absorbing materials do not perform very well at low frequencies. It is therefore not yet clear how much improvement the new standard will produce. It is clear, however, that the results of our present study do not apply to measurements in rooms meeting the new standard. They apply only to the old standard, but are significant nonetheless. For one thing, they provide a reference against which a similar study of the new standard could be compared. Such a comparison would measure how much the new standard has improved the test methods. Another consideration is that it will probably be some time before tests according to the old standard are phased out entirely. As long as the old test setup is being used, it is important that the people performing the tests—or accepting the test results—realize how accurate those results are or are not. Finally, screened rooms are used for measurements other than MIL-STD tests, and we expect the qualitative features of our study to be common to other screened-room radiated emissions measurements between 2 MHz and 1000 MHz unless special precautions are taken to mitigate the problems.

4.2 Applications of the Standard Radiator

We noted in the introduction that the spherical-dipole standard radiator has several possible applications, and this paper has impinged on a number of them. The initial purpose of this study was to develop procedures for using the NIST spherical-dipole standard radiator in the accreditation of laboratories doing MIL-STD-462 acceptance testing. The basic idea was to use the spherical dipole as a standard radiator to test whether the laboratory

could get the "correct" answer in its radiated emissions measurements. It is clear that the radiator could be used in this manner, but the goal of developing a protocol for MIL-STD-462 accreditation was not achieved. For one thing, the standard changed, and our data are not representative of results which would be obtained with the new standard. Even for the old standard, the wide disparity in the results at different labs and even at the same lab on different days led us to conclude that proficiency testing with the NIST spherical-dipole standard radiator would be pointless. Any proficiency testing would have to allow a tolerance of around 15 dB to take into account "reasonable" variations in test results. Such crude testing would not require the precision, sophistication, and concomitant expense of the spherical-dipole standard radiator.

The study does provide a good example of how the standard radiator can be used to assess the validity of a test method—by comparing results to those obtained with accepted test methods and by evaluating repeatability, both day-to-day and laboratory to laboratory. Our data constitute a clear, quantitative demonstration of the shortcomings of radiated emissions measurements in screened rooms. It would now be of great interest to perform a similar study on radiated emissions measured in conformance with the new MIL-STD. Comparison of the results of the new study to those of the old would show how much improvement the changes made.

Another application which is clearly demonstrated in the paper is use of the standard radiator by a group of laboratories in a round-robin intercomparison of radiated-emission measurements. The spherical dipole is very well suited for this purpose due to its temporal stability, its known radiation pattern, the capability of monitoring the gap voltage, and the flexibility offered in the choice of radiated frequency. As shown by the measurements of day-to-day variations, the spherical dipole can also be used by an individual laboratory as a check standard, to check that their measurement system has not changed from day to day, or to refine their measurement procedures in order to improve the repeatability of their measurements. (Commercially produced monopole radiators offer a simpler, less expensive alternative, though they are not as well characterized or as flexible.) Finally, although it was not demonstrated in this paper, we note that the standard radiator could even be incorporated into a test procedure, for example, as a standard source for the calibration of antennas.

Acknowledgments

We are grateful to the three laboratories which participated in this study and to the personnel who performed the tests at those labs. This work was funded by the Naval Air Systems Command.

5. References

[1] G. Koepke, L. Driver, K. Cavcey, K. Masterson, R. Johnk, and M. Kanda, Standard spherical dipole source, Natl. Inst. Stand. Technol. Technical Note 1351, December 1991.

[2] G. Koepke, L. Driver, K. Cavcey, K. Masterson, R. Johnk, and M. Kanda, New spherical dipole source, Proceedings of 1992 IEEE International Symposium on EMC, Anaheim, CA, August 1992, pp. 98–105.

[3] G. Koepke and J. Randa, Results of screened-room measurements on NIST standard radiators, Natl. Inst. Stand. Technol. Internal Report 5010, October 1993.

[4] J. Krstansky and R. Standley, Theory of RFI measurements in shielded enclosures, 8th Annual IEEE National Symposium on EMC, San Francisco, CA, July 1966.

[5] C. Stuckley, W. Free, and D. Robertson, Preliminary interpretation of near-field effects on measurement accuracy in shielded enclosures, 1969 IEEE EMC Symposium Record, Asbury Park, NJ, June 1969, pp. 119–127.

[6] J. E. Cruz and E. B. Larsen, Assessment of error bounds for some typical MIL-STD-461/462 types of measurements, Natl. Bur. Stand. (U.S.) Technical Note 1300, October 1986.

[7] J. E. Cruz and E. B. Larsen, Alternative techniques for some typical MIL-STD-461/462 types of measurements, Natl. Inst. Stand. Technol. Technical Note 1320, March 1989.

[8] Military Standard, Electromagnetic Interference Characteristics, Measurement of, MIL-STD-462, 31 July 1967.

[9] Military Standard, Measurement of Electromagnetic Interference Characteristics, MIL-STD-462D, 11 January 1993.

[10] S. Ramo, J. R. Whinnery, and T. Van Duzer, Fields and Waves in Communication Electronics, Sections 10.7 and 12.24, John Wiley & Sons, NY (1984).

About the authors: G. Koepke is an electrical engineer in the Electromagnetic Fields Division at NIST Boulder. J. Randa is a physicist in the Electromagnetic Fields Division. The National Institute of Standards and Technology is an agency of the Technology Administration, U.S. Department of Commerce.

Volume 99, Number 6, November–December 1994
Journal of Research of the National Institute of Standards and Technology

[J. Res. Natl. Inst. Stand. Technol. 99, 751 (1994)]

Beamcon III, a Linearity Measurement Instrument for Optical Detectors

Volume 99 Number 6 November–December 1994

Ambler Thompson

National Institute of Standards and Technology,
Gaithersburg, MD 20899-0001

and

How-More Chen[1]

Department of Electrical and Computer Engineering,
University of Alabama in Huntsville,
Huntsville, AL 35899

The design and operation of Beamcon III, the latest linearity measurement instrument using the beam addition method in the detector metrology program at the National Institute of Standards and Technology, is described. The primary improvements in this instrument are the reduction of stray radiation to extremely low levels by using three well-baffled chambers, a larger dynamic range, and an additional source entrance port. A polynomial response function is determined from the data obtained by this instrument using a least-squares method. The linearity of a silicon photodiode-amplifier detector system was determined to be within 0.054 % (2σ estimate) over nine decades of signal.

Key words: beam addition method; linearity; optical radiation detectors; silicon photodiode.

Accepted: September 2, 1994

1. Introduction

The underlying assumption in the use of most detection methods for the measurement of optical radiation is that the detector output signal is directly proportional to the input radiation flux. This proportionality is defined as linearity and conversely the departure from proportionality is defined as nonlinearity. Optical radiation detectors are typically converters of optical power (or photon flux) to measurable electrical parameters, such as current, voltage, or pulse frequency. Therefore, in radiometric applications, the linearity of a detector's signal is not only a function of the efficiency of the physical radiation detector (transducer), but also of the peripheral electronics. A well known example of this is a photomultiplier/photon-counting system where significant nonlinearity is induced at high count rates by the dead time of the pulse counter. All detector systems, consisting of detectors and peripheral electronics, are characterized by some degree of nonlinearity. The exact positions of these nonlinear regions are functions of both the detector and the accompanying electronics and should be determined experimentally for measurements of the highest accuracy. There are essentially two practical choices when confronted by nonlinear behavior of a detector system: first, to view it as a performance limit, a maximum deviation from linearity over a given range of input; second, to correct the measured signal given the known

[1] Present address: Lane 180, Kuang-Fu S. Road, #29-3(4F), Taipei, Taiwan 10553.

nonlinearity of the detector. This latter solution presupposes that the detector's nonlinearity is well characterized and should be determined with the measurement electronics that are to be routinely used with the detector.

Concern about detector linearity and the development of instruments for its measurement has a long history at the National Institute of Standards and Technology, formerly the National Bureau of Standards (NBS). Sanders [1] reported in 1972 the results of photocell linearity measurements using a multi-aperture design. Also in 1972, Mielenz and Eckerle [2] utilized a double-aperture method to characterize the NBS Reference Spectrophotometer. In 1984 Saunders and Shumaker [3] reported measurements using an automated radiometric linearity tester. This instrument was called a beamconjoiner.

Based on this initial work, we now report on our latest generation of beamconjoiner technology, Beamcon III. This instrument was specifically designed to characterize radiometric detectors, particularly at low flux levels approaching the noise equivalent power (NEP) of the detector. To facilitate low level measurements, this instrument has three well-baffled chambers to reduce the stray radiation to extremely low levels. Other improvements are additional filters to give a larger dynamic range and a second source entrance port for a laser source or for source mixing. The data analysis algorithm of Beamcon III calculates the responsivity of the detector system assuming a polynomial relationship between the input flux and the output signal from the detector system. Beamcon III will serve as an automated instrument for routine detector linearity characterization and for determining the linearity of NIST's monochromator-based systems (e.g., spectroradiometers and spectrophotometers).

2. Description of Beamcon III and its Operation

A schematic diagram illustrating the technique of beamconjoining is shown in Fig. 1. The input beam from the source is split into two optical paths by the first beamsplitter BS1 and variably attenuated by filters on either wheel W1 or W3. After reflection off mirrors M1 and M2, the two beams are combined by beamsplitting BS2 and attenuated again by a third filter on wheel W2 before falling on the detector. All filters are metallized neutral density filters with quartz substrates, and the filter

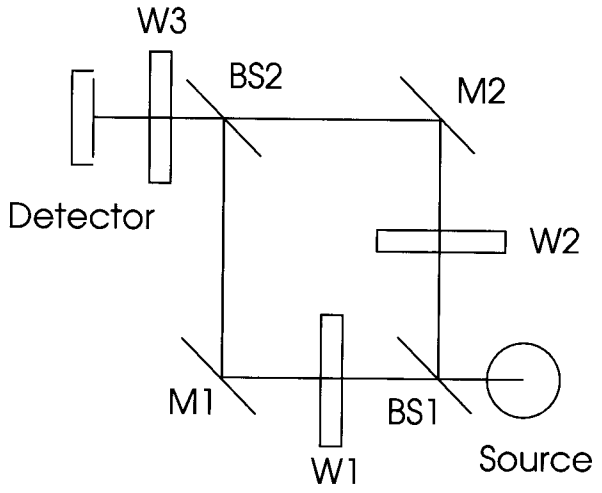

Fig. 1. Schematic optical diagram of Beamcon III showing the primary optical elements. BS: beam splitter; W: filter wheel; and M: mirror.

wheels are tilted to preclude interreflection between filters. In addition the beamsplitters are wedged to prevent etaloning.

A complete schematic diagram of Beamcon III, including all ports, optics, and chambers, is shown in Fig. 2. Beamcon III provides four basic advantages over the previous technology: 1) each chamber is optically isolated from the next chamber except for a 3 inch diameter throughput port, thereby reducing scattered radiation; 2) there are two source input ports for both laser and broadband sources either singly or concurrently for

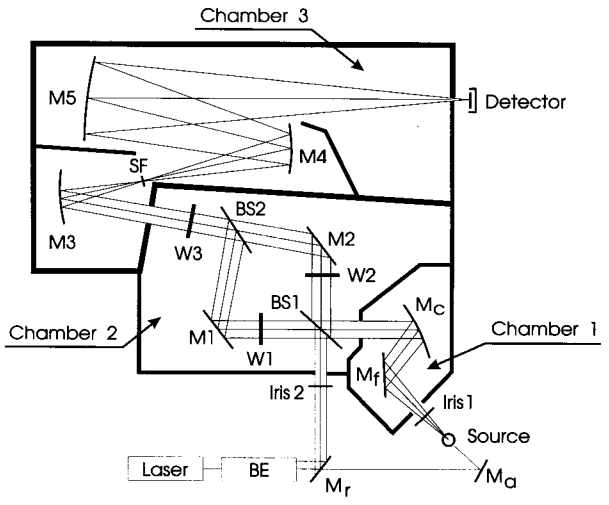

Fig. 2. System layout of Beamcon III. Chamber 1 collimates the beam from the source. Chamber 2 splits the beam into two paths and recombines it. Chamber 3 has a spatial filter SF to eliminate stray light and focuses the beam onto the detector.

source mixing; 3) a steel base plate allows for magnetic mounting of additional optical components; 4) an external translation stage on the broadband input port can vary the numerical aperture and collimate the source beam. A microcomputer controls the positions of the filter wheels and records the signal from the detector.

An incoherent light source (Source, Fig. 2), either a quartz halogen or arc lamp, is placed on a translation stage in front of the input port to Chamber 1. The input power of the source beam is varied either by changing the aperture of the iris diaphragm (Iris 1) or by translating the Source, or both. The input beam in Chamber 1 is folded by a flat mirror (M_f) and collimated by a concave spherical mirror (M_c), which projects the beam through the input port of Chamber 2. For narrowband operation with an incoherent light source, an interference filter can be placed at the input port of Chamber 2. The first beamsplitter (BS1) yields two separate beams which are independently attenuated by two filter wheels (W1) or (W3). These filter wheels contain four neutral density filters with differing optical densities. The two beams are folded by mirrors (M1) or (M2) and recombined into a single beam by beamsplitter (BS2). This beam is further attenuated by passing through a third filter wheel (W2) containing five different neutral density filters. The beam then passes into Chamber 3, which contains a set of concave mirrors (M3 and M4). A spatial filter (SF) at the focal point between the two mirrors filters out scattered and diffracted light, resulting in a uniform output field at the detector. A concave mirror (M5) focuses the beam onto the detector. Translational shifting of M5 controls the image plane of the instrument and varies the irradiance at the detector. The detector is generally overfilled to prevent artifacts due to different cut-off edges in the optical path (optical stop variation) and to the local nonuniformity of the detector. In addition environmental parameters such as humidity and temperature are constantly monitored at the detector. A monochromator can also be attached at the exit port to select a wavelength for narrowband operation.

Beamcon III has a second input port into Chamber 2, which can be used singly or in concert with the beam from Chamber 1. Generally the input port of Chamber 2 is used for sources such as He-Ne or Ar^+ lasers. A beam expander BE is used to minimize scattering losses and filter transmittance nonuniformity. The laser can also be used to align both optical paths by removing the reflecting mirror (M_r) and inserting the mirror (M_a) to guide the laser beam through the center of the lamp filament and of every optical element. The mixed source method has not been attempted as yet, but is planned in future studies, as it has advantages for studying differential spectral detector nonlinearities [4].

Stepping motors control the filter wheel positions, each with 400 steps/revolution. A tolerable error is one step, therefore the error in filter position is 0.9°. The space between two filters on each wheel acts as a shutter position for a dark signal measurement. Thus, the total number of filter combinations is 150, and a full 150 measurements is called a pass. Of these, 30 are dark signal measurements: 5 when both W1 and W3 are shuttered and 25 when W2 is shuttered. The remaining 120 filter combinations, yielding 120 response signal measurements, are randomized in each pass to prevent hysteresis. The dark signal/filter combinations are randomized and inserted after every five measurements. Each dark signal is used to correct the succeeding five response signal measurements. Generally, five passes are taken and averaged to reduce the random error and to collect information about possible source, filter, and detector drift. The maximum throughput is 7 % at a wavelength of 632.8 nm, and the total attenuation factor is about 3000 against a light source.

The output beam is partially vertically polarized for an unpolarized source since each tilted surface preferentially reflects the vertical component of the incident beam. The ratio of the polarization in the vertical direction to that in the horizontal direction is 1.17. Thus, it is critical to keep the polarization direction of a source (e.g., laser) constant in order to eliminate this polarization preference.

3. Polynomial Response Function Fitting

The principle of operation of Beamcon III is the beam addition method, in which different filter wheel combinations result in different fluxes at the detector. This method assumes that the flux from the source remains constant during all measurements and that the output flux at the detector is the sum of the two fluxes along the two different paths.

The final flux ϕ at the detector is the sum of the fluxes ϕ_1 and ϕ_2 from the two paths. Indexing the fluxes by the filter combination,

$$\phi(i,j,k) = \phi_1(i,k) + \phi_2(j,k), \tag{1}$$

where i equals 0 to 4 designates the filter on wheel W1, j equals 0 to 4 the filter on W3, and k equals 0 to 5 the filter on W2. In each case, an index value of 0 corresponds to an opaque, shuttered position. For a single path, there are 30 possible filter combinations. Of these, no flux is transmitted for 10 combinations. Thus, each path has 20 filter combinations that result in a response signal.

Since the detector is assumed to be nearly linear, it is appropriate and convenient to assume an n-th order polynomial response function for the detector [3], so that

$$\phi(i,j,k)=r_0+r_1 s(i,j,k)+r_2 s^2(i,j,k)+\ldots+r_n s^n(i,j,k), \quad (2)$$

where $s(i,j,k)$ is the measured response signal, corrected by the dark signal and indexed by the filter combination, and r_0, r_1, r_2, ..., r_n are the response function coefficients. The coefficient r_1 is set equal to one, both because the detector is assumed to be nearly linear and to normalize the flux to the same units as the signal.

Combining Eqs. (1) and (2), with $r_1=1$, yields

$$\phi_1(i,k)+\phi_2(j,k)=r_0+s(i,j,k)+r_2 s^2(i,j,k)+\ldots+r_n s^n(i,j,k). \quad (3)$$

There are 120 expressions of the form of Eq. (3) from the 120 distinct response signals measured in each pass, with $40+n$ unknown variables from the 20 filter combinations along each path and the n response function coefficients. The fluxes of shuttered filter combinations are set equal to zero. These 120 expressions are solved using the linear least-squares technique to determine the values of the unknowns. While the values of the polynomial response function coefficients are the primary goal of the measurements, the values of the fluxes are useful for monitoring the stability of the filters.

Solving for both the fluxes along the paths and the response function coefficients provides two ways in which to determine the total flux at the detector, using Eqs. (1) and (2), and therefore serves to verify the results. A measurement run yields 120 residuals between the total fluxes calculated in these two ways. If there is a slope in a time-ordered plot of these residuals, then either dark signal or source intensity variations likely exist. Also, the standard deviation of these residuals indicates the noise level present during the measurement, either from the source, filters, or detector. For most detectors, a second-order polynomial accurately fits the data. However, if the detector is highly nonlinear, the power of the polynomial is increased until the residuals are normally distributed about zero. If the response function coefficients remain unreasonable, then either a polynomial is not an appropriate fitting function or the detector and its associated electronics are not functioning properly.

The algorithm for determining the $40+n$ unknown variables from a complete measurement was extensively tested using synthetic data sets with known response function coefficients for second-order polynomials. It was also tested using synthetic data sets corresponding to two cases of nonlinear behavior, suprarespondsivity and saturation at high flux levels [5]. The algorithm was successful in fitting these two behaviors with a third- and a sixth-order polynomial, respectively.

4. Linearity Measurement of a Silicon Photodiode

Beamcon III was used to determine the linearity of a silicon photodiode-amplifier detector system designed and constructed at NIST for multi-decade performance and described previously [6]. The linearity was determined for amplifier gains from 10^4 to 10^{10}. The broadband source was a 1000 W tungsten-halogen lamp operated at a constant current of 7.6 A. In order to cover the entire signal range of the detector system without changing the spectral distribution of the source, the flux from the lamp was varied either by changing the numerical aperture of Iris 1 in Fig. 2 or by placing neutral density filters in Chamber 1, or both.

The relative responsivity of a detector system indicates deviations from linearity. Once the response function coefficients have been determined, the total normalized flux for a given signal is given by the response function [the right-hand-side of Eq. (3)]. If the detector system is linear, the total normalized flux is simply the signal. Therefore, the relative responsivity at a given signal is the response function divided by the signal. The results from one measurement of the linearity of the detector system at a gain of 10^6 is shown is Fig. 3, where the relative responsivity is plotted as a function of signal. The response function was a second-order polynomial with coefficients $r_0=-5.53\times10^{-9}$ and $r_2=-1.56\times10^{-5}$. Over the three decades of signal measured at this gain, the detector system is linear to within 0.027 % (2σ estimate).

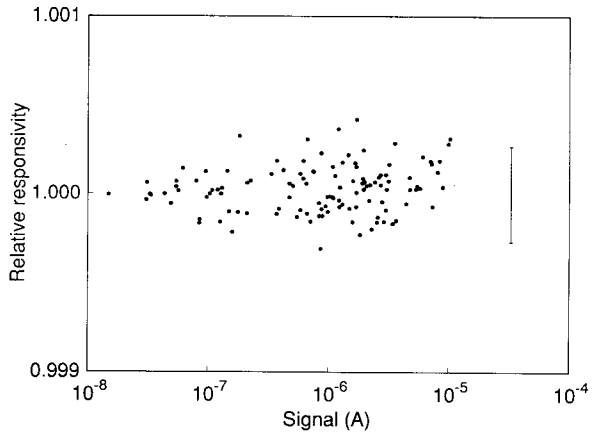

Fig. 3. Relative responsivity as a function of signal for a silicon diode-amplifier detector system at a gain of 10^6. The error bar indicates the 2σ estimated uncertainty of the relative responsivity.

The maximum signal for the detector system, determined by the source and throughput of Beamcon III, was about 10^{-3} A. At a bandwidth of 0.67 Hz, the NEP of the detector system resulted in a minimum measurable signal of about 10^{-12} A. In order to characterize the detector system between these limits, linearity measurements were performed at all seven amplifier gain ranges. A second-order polynomial response function was calculated for each range, and the relative responsivity over nine decades of signal is shown in Fig. 4. The detector system is linear to within 0.054 % (2σ estimate) over the entire range, and to within 0.209 % (2σ estimate) for currents less than 10^{-11} A. Thus, Beamcon III was able to determine the linearity of this detector system for signals approaching its NEP.

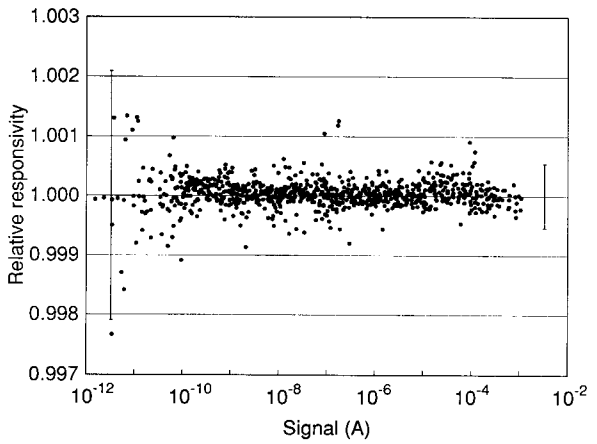

Fig. 4. Relative responsivity as a function of signal for a silicon diode-amplifier detector system over its entire signal range of nine decades. The error bars indicate the estimated 2σ uncertainty of the relative responsivity for signals less than 10^{11} A (on the left) and over the entire range of signal (on the right).

5. Conclusions

The design and operation of our latest generation of beamconjoining technology, Beamcon III, was detailed. Using this instrument, the linearity of a silicon photodiode-amplifier detector system was determined over nine decades of signal, approaching its NEP at the smallest signals. Beamcon III will permit both routine calibration of detector systems and research into detector-amplifier effects on nonlinearity. Future studies on the linearity of solid state detector-amplifier systems, photomultiplier photon-counting systems, and multichannel detectors (i.e., diode arrays and charge coupled devices) are planned, as well as on the capabilities of Beamcon III for source mixing.

Acknowledgments

The authors gratefully acknowledge helpful discussions with Bob Saunders and George Eppeldauer.

6. References

[1] C. L. Sanders, Accurate Measurements of and Corrections for Nonlinearities in Radiometers, J. Res. Natl. Bur. Stand. (U.S.) **76A**, 437–453 (1972).
[2] K. D. Mielenz and K. L. Eckerle, Spectrophotometer Linearity Testing Using the Double-Aperture Method, Appl. Opt. **11**, 2294–2303 (1972).
[3] R. D. Saunders and J. B. Shumaker, Automated Radiometric Linearity Tester, Appl. Opt. **23**, 3504–3506 (1984).
[4] J. Metzdorf, W. Moller, T. Wittchen, and D. Hunerhoff, Principle and Application of Differential Spectroradiometry, Metrologia **28**, 247–250 (1991).
[5] W. Budde, Multidecade Linearity Measurements on Si Photodiodes, Appl. Opt. **18**, 1555–1558 (1979).
[6] G. Eppeldauer and J. E. Hardis, Fourteen-Decade Photocurrent Measurements with Large-area Silicon Photodiodes at Room Temperature, Appl. Opt. **30**, 3091–3099 (1991).

About the authors: Ambler Thompson is a member of the Radiometric Physics Division of the NIST Physics Laboratory. How-More Chen was a guest researcher at NIST and this linearity work was done in partial completion of a Master of Science degree from the University of Alabama in Huntsville. The National Institute of Standards and Technology is an agency of the Technology Administration, U.S. Department of Commerce.

Volume 99, Number 6, November–December 1994
Journal of Research of the National Institute of Standards and Technology

[J. Res. Natl. Inst. Stand. Technol. 99, 757 (1994)]

Spectroscopic Study of Quantized Breakdown Voltage States of the Quantum Hall Effect

Volume 99 Number 6 November–December 1994

C. F. Lavine, M. E. Cage, and R. E. Elmquist

National Institute of Standards and Technology,
Gaithersburg, MD 20899-0001

Quantized breakdown voltage states are observed in a second, wide, high-quality GaAs/AlGaAs sample made from another wafer, demonstrating that quantization of the longitudinal voltage drop along the sample is a general feature of the quantum Hall effect in the breakdown regime. The voltage states are interpreted in a simple energy conservation model as occurring when electrons are excited to higher Landau levels and then return to the original level. A spectroscopic study of these dissipative voltage states reveals how well they are quantized. The statistical variations of the quantized voltages increase linearly with quantum number.

Key words: breakdown of dissipationless state; histograms; quantum Hall effect; quantized voltage states; two-dimensional electron gas; spectra.

Accepted: July 26, 1994

1. Introduction

In the integer quantum Hall effect [1] the Hall resistance R_H of the ith plateau of a fully quantized two-dimensional electron gas (2DEG) assumes the values $R_H(i)=h/(e^2i)$, where h is the Planck constant, e is the elementary charge, and i is an integer. The current flow within the 2DEG is nearly dissipationless in the Hall plateau regions of high-quality devices, and the longitudinal voltage drop V_x along the sample is very small. At high currents, however, energy dissipation can suddenly appear in these devices [2,3], and V_x can become quite large. This is the breakdown regime of the quantum Hall effect. The dissipative breakdown voltage V_x can be detected by measuring voltage differences between potential probes placed on either side of the device in the direction of current flow.

Bliek et al. [4] proposed the existence of a new quantum effect to explain the breakdown structures in their curves of V_x versus magnetic field for samples with narrow constrictions. Cage et al. [5] observed distinct quantized V_x states in wide samples. Cage then found that the quantization of these states was a function of magnetic field [6] and current [7]. In this paper we present quantized breakdown voltage data for a second wide sample made from another wafer to give further evidence that there indeed is a new quantum effect. We then investigate how well these breakdown voltages are quantized using a number of experimental techniques.

2. Sample

The sample is a GaAs/$Al_xGa_{1-x}As$ heterostructure grown by molecular beam epitaxy at AT&T Bell Laboratories,[1] with $x=0.29$. It is designated as

[1] Certain commercial equipment, instruments, or materials are identified in this paper to foster understanding. Such identification does not imply recommendation or endorsement by the National Institute of Standards and Technology, nor does it imply that the materials or equipment identified are necessarily the best available for the purpose.

GaAs(8), has a zero magnetic field mobility of 100 000 $cm^2/(V \cdot s)$ at 4.2 K, and exhibits excellent integral quantum Hall effect properties. This sample and the AT&T GaAs(7) sample used in the previous breakdown experiments [3,5–8] have been used as the United States resistance standard. The inset of Fig. 1 shows the sample geometry. It is 4.6 mm long and 0.4 mm wide. The two outer Hall potential probe pairs are displaced from the central pair by ±1 mm. The magnetic field is perpendicular to the sample; its direction is such that probes 2, 4, and 6 are near the potential of the source S, which is grounded. Probes 1, 3, and 5 are near the drain potential D. The dissipative voltages V_x for this paper were measured between potential probe pair 4 and 6, hereafter denoted as $V_x(4,6) \equiv V_x(4) - V_x(6)$.

3. Longitudinal Voltage Versus Magnetic Field

Figure 1 shows two sweeps of $V_x(4,6)$ versus the magnetic field B for the $i = 2$ (12,906.4 Ω) quantized Hall resistance plateau at a temperature of 0.33 K and a current I of +220 μA, where positive current corresponds to electrons entering the source and exiting the drain. This current is approaching the 227 μA critical current value above which, in this magnetic field region, V_x is non-zero for these particular potential probes.

Figure 2 shows fourteen sweeps of $V_x(4,6)$ versus B over the dashed region of Fig. 1 at the +220 μA current. The data clearly show discrete, well-defined voltage states, with switching between states. Individual sweeps are not identified in the figure because the magnetic field values at which the states switch have no correlation with sweep number.

We next demonstrate that the discrete voltage states of Fig. 2 are equally separated, and that this separation is a function of magnetic field. This is done by drawing a family of seventeen shaded curves through the data in Fig. 2. The curves have equal voltage separations at each value of magnetic field. The voltage separations are, however, allowed to vary with B in order to obtain smooth curves that fit the data. We have argued in Refs. [6,7] that this behavior suggests quantization.

The lowest shaded curve was constrained to be at 0.0 mV everywhere except on the high field side, where a small background voltage was added to provide the best fits as a function of B; this deviation from zero voltage presumably arises from some other dissipative mechanism. The 17 shaded curves, which correspond to a $V_x = 0.0$ mV ground state in the lowest occupied Landau level and 16 excited states, are labeled in brackets as quantum numbers 0 through 16. Deviations of the data from the equally-spaced shaded curves do occur, but the overall trend is clear.

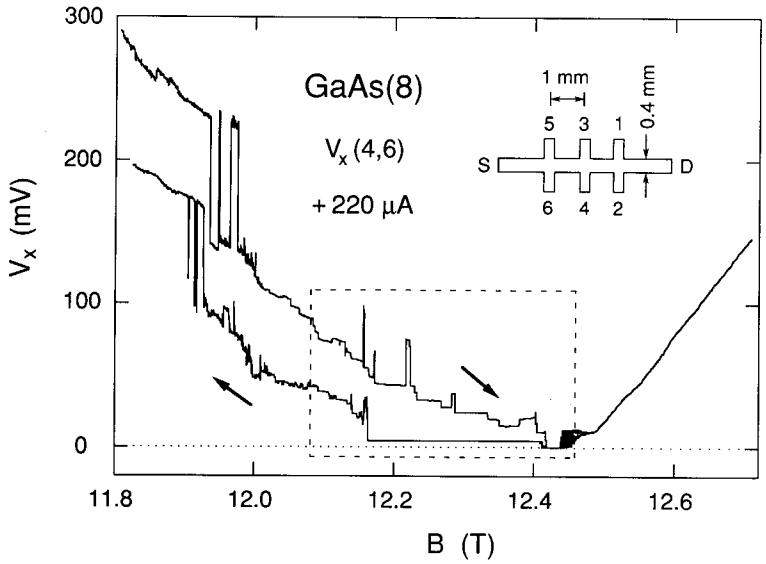

Fig. 1. Two sweeps of $V_x(4,6)$ versus B for the $i = 2$ plateau at +220 μA and 0.33 K. Arrows indicate the sweep directions. The inset displays the sample geometry.

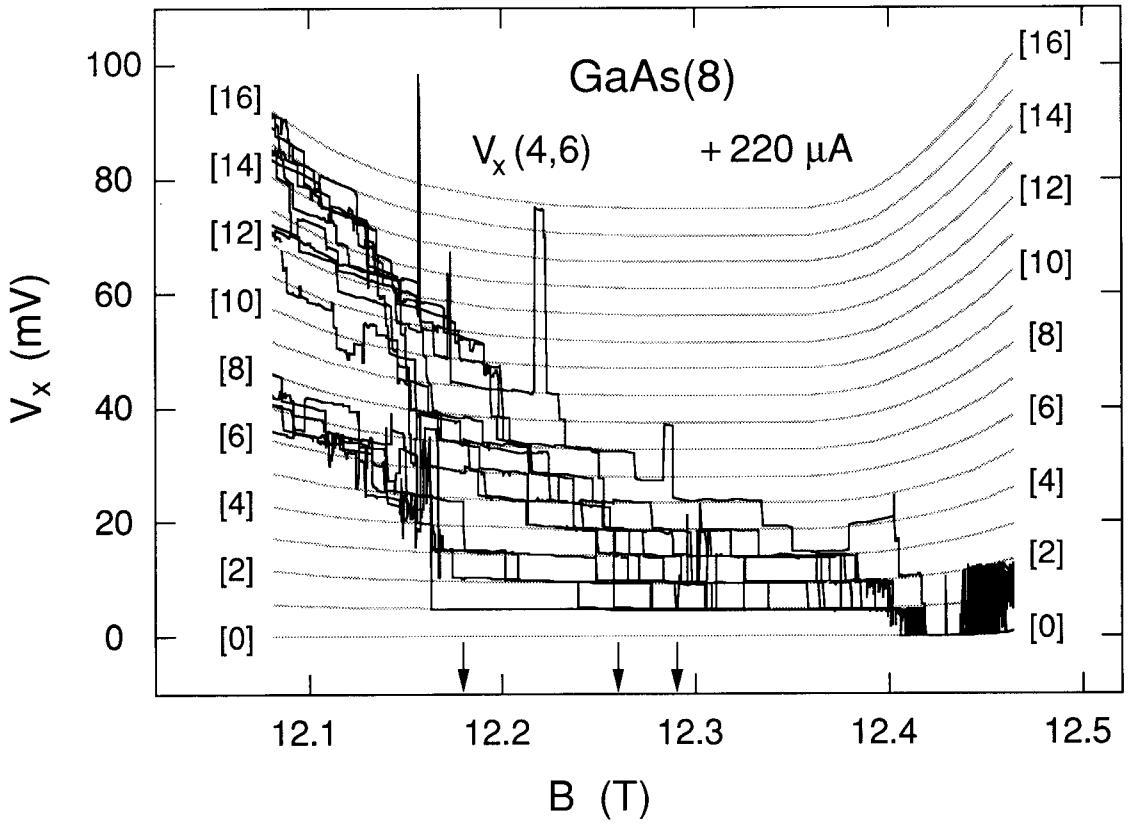

Fig. 2. Fourteen sweeps of $V_x(4,6)$ versus B at +220 μA, plus a family of 17 shaded curves fitted to these data. The shaded curves were generated with an accuracy of ~1 % and a resolution of ~0.1 %. Voltage quantization numbers are shown in brackets. The vertical arrows indicate magnetic field values of 12.18 T, 12.26 T, and 12.29 T, at which the data shown in Figs. 3–5, and 7–10 were obtained.

The breakdown activity shown in Fig. 2 is confined to the region between, but not including, the Hall probe pairs 3,4 and 5,6 of Fig. 1. This was demonstrated by measuring the voltages of both Hall probe pairs at this current. The V_H versus B curves of the two Hall probe pairs also had quantized structures, but they occurred over different magnetic field regions than V_x. In addition, the V_x signals were the same on both sides of the sample for probe pairs 3,5 and 4,6.

4. Histograms

Cage et al. [8] and Hein et al. [9] have shown that the V_x signal can sometimes be time-averages of two or more discrete dc voltage levels in which only one level is occupied at a time, but where switching occurs between the levels. Therefore, histograms were made to ensure that the signals in Fig. 2 are not time-averages of several levels. Each histogram consists of 16 000 measurements of the V_x signal in a 2.4 s sampling period. They are snapshots in time of the dissipative states and are selected to convey the maximum information. Figure 3(a) shows the time-dependence of one such sampling period at 12.26 T; Fig. 3(b) shows the associated histogram. Figure 4 shows another representative histogram at 12.29 T. No histograms yielded any voltage states other than the ones which appear in the shaded curves of Fig. 2.

The histogram peaks are much sharper in Fig. 4 than in Fig. 3, which suggests that the peak widths increase with quantum number. This is investigated in Fig. 5 by plotting the full-width-at-half-maximums (FWHM) of all the prominent histogram peaks observed versus the peak centroids $\overline{V_x}$. The plot is linear with voltage. If the peak widths are a measure of the lifetimes of the excited states, then the lifetimes decrease with increasing quantum number.

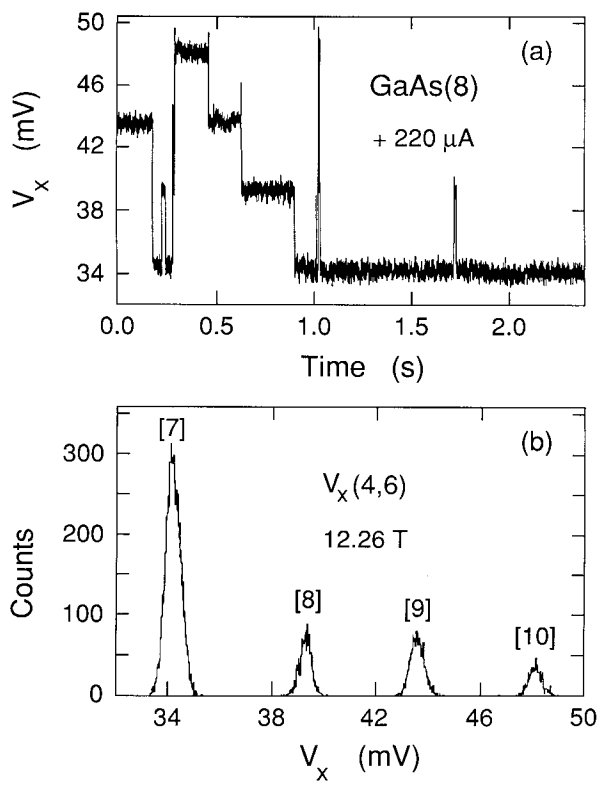

Fig. 3. Time sequence of V_x and its histogram at 12.26 T. The numbers in brackets are quantum numbers obtained from Fig. 2.

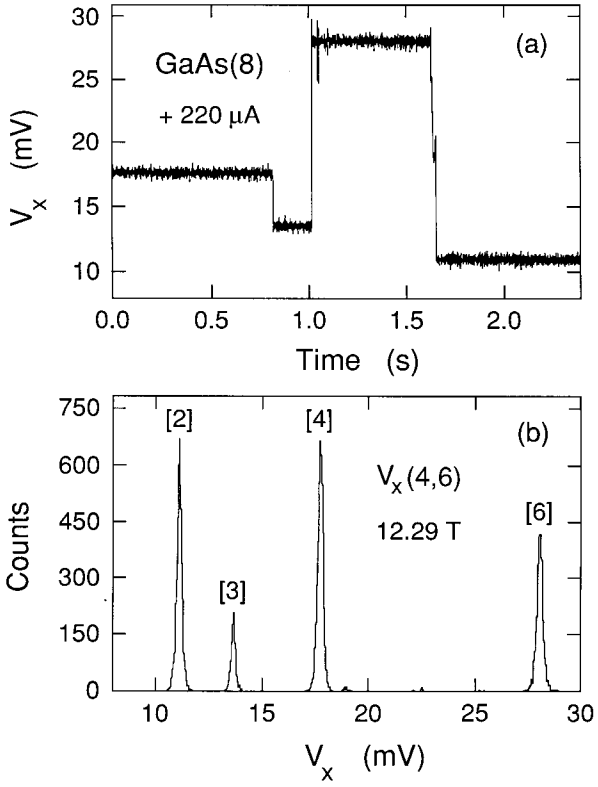

Fig. 4. Time sequence of V_x and its histogram at 12.29 T. The numbers in brackets are quantum numbers obtained from Fig. 2.

5. Simple Model

Many explanations have been proposed [10–17] for the complicated nonlinear breakdown phenomenona. In order to avoid controversy about which explanation is appropriate, we use a simple model [6] based on energy conservation arguments to interpret the voltage quantization displayed in Fig. 2. The breakdown region between the Hall probe pairs 3,4 and 5,6 is treated as a black box. The dissipation is assumed to arise from transitions in which electrons from the originally full Landau levels are excited to states in higher Landau levels and then return to the lower Landau levels. The electrical energy loss per carrier for M Landau level transitions is $M\hbar\omega_c$, where $\omega_c = eB/m^*$ is the cyclotron angular frequency and m^* is the reduced mass of the electron (0.068 times the free electron mass in GaAs). The power loss is IV_x. If (a) the ground state involves several filled Landau levels, (b) only electrons in the highest-filled Landau level make transitions, and (c) electrons of both spin sublevels of a Landau level undergo transitions,

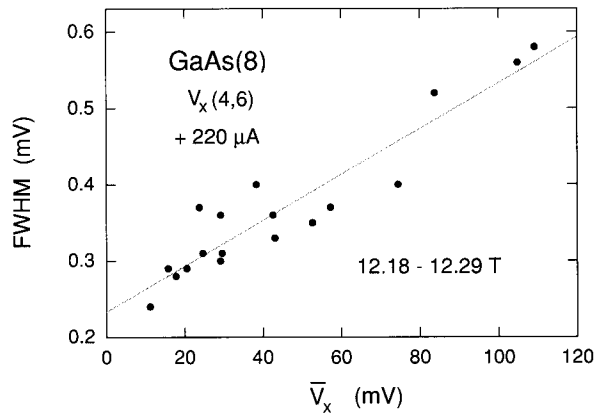

Fig. 5. The full-width-at-half-maximums (FWHM) of the histogram peaks that were large enough to obtain adequate measurements. They are plotted versus the histogram peak centroids. The shaded line is a linear least-squares fit to the data.

then $IV_x = r(2/i)M\hbar\omega_c$, where r is the total transition rate and i is the Hall plateau number. Thus

$$fM = \left(\frac{re}{I}\right)M = \left(\frac{i}{2}\right)\left(\frac{m^*}{\hbar}\right)\left(\frac{V_x}{B}\right), \qquad (1)$$

where f is the ratio of the transition rate r within the breakdown region to the rate I/e that electrons transit the device; f can also be interpreted as the fraction of conducting electrons that undergo transitions.

We associate the quantized values of M with the numbers in brackets for the shaded curves in Fig. 2. I, V_x, and B are measured quantities, and i, m^*, and $\hbar$ are constants. Therefore, f and r can be determined from the V_x versus B plots and Eq. (1) because M is known.

Figure 6 shows the variation of the voltage quantization V_x/M over the magnetic field range of Fig. 2. This quantization is model-independent, except for assigning the quantum numbers M to the shaded curves. V_x/M varies within the range 4.68 mV to 6.30 mV. The fractions f (expressed as a percentage) of electrons that make the transitions in the shaded curves of Fig. 2 were calculated using Eq. (1), and are also shown in Fig. 6; f varies between 22.4 % and 29.8 %, corresponding to transition rates between 3.1×10^{14}/s and 4.1×10^{14}/s. The large numbers of electrons involved in these transitions imply a collective effect.

6. Spectra

The voltage states are clearly quantized, but how *well* are they quantized? Voltage spectra would be useful to address this question. Histograms are not themselves spectra because the areas under the peaks do not correspond to the excitation probabilities. Many histograms must be accumulated to obtain a spectrum. This is very time-consuming. Therefore, we devised another method to obtain voltage spectra by momentarily pushing the sample current to 390 μA at a fixed magnetic field and then reducing it back to 220 μA. This procedure induced the dissipative dc voltage states that were then recorded.

Three voltage spectra are shown in Fig. 7. Spectra 1 and 2 correspond closely to the V_x versus B sweeps in Fig. 2, but the pulsed current induced much higher states in spectrum 3 then observed in Fig. 2. This is due to a bifurcation effect in which a second range of states can be excited, as was observed in GaAs(7) [6,7]. Figure 8 plots the centroid or mean value $\bar{V}_x$ of each peak of the three spectra in Fig. 7 versus the quantum number M. The

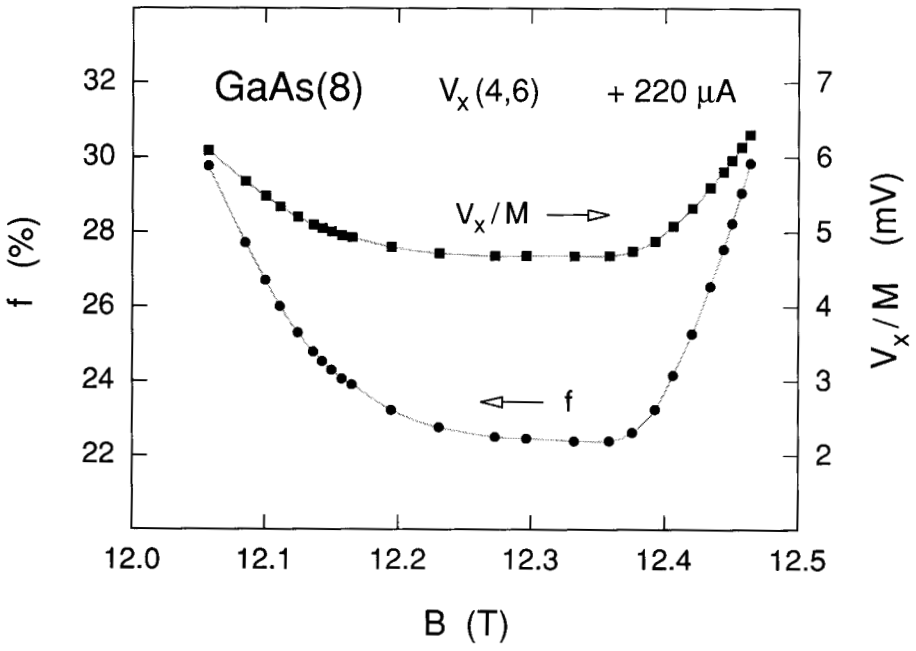

Fig. 6. The voltage quantization V_x/M and the fractions f (expressed as a percentage) of electrons making the Landau level transitions for the seventeen shaded curves shown in Fig. 2 at +220 μA. See Eq. (1) for the definition of f.

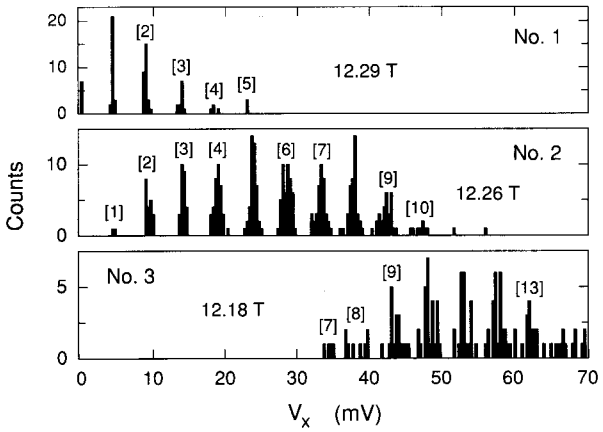

Fig. 7. Three voltage spectra taken at the B values indicated by the arrows in Fig. 2. The numbers in brackets are the M values.

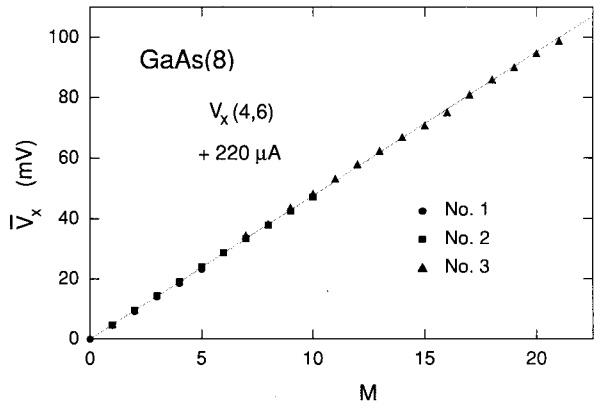

Fig. 8. Average value $\overline{V}_x$ of each voltage peak of the three spectra in Fig. 7 versus the quantum number M, plus a shaded linear least-squares fit to the data.

shaded line is a least-squares fit to the data. The fit provides an average value of the dissipation voltage per quantum level, $\overline{V}_x/M$, of 4.76 mV, and a corresponding average f value of 22.9 %.

The linear fit in Fig. 8 is excellent, but we know from the family of shaded curves in Fig. 2 that the values of $\overline{V}_x/M$ and f vary with B. Therefore, $\overline{V}_x/M$ is plotted versus M in Fig. 9 for the three spectra in Fig. 7. The f values, corresponding to the horizontal dashed lines representing the weighted means of $\overline{V}_x/M$, are within 0.5 % of those obtained from the shaded curves of Fig. 2. The two shaded lines in Fig. 9 are weighed least-squares fits to spectra 2 and 3; they suggest a tendency for the voltage quantization to decrease with increasing M values at a constant B. This decrease provides a cautionary note about the degree of quantization, and also about the assumptions in the simple black box model that the values of f and r remain constant for increasing M at constant B. However, this apparent quantization decrease with increasing M is a small effect, and it does not seriously affect interpretation of the data—as evidenced by the fit in figure 8.

Another measure of the degree of quantization is the sharpness of the spectra peaks. This is explored in Fig. 10. The standard deviations of those peaks of the spectra in Fig. 7 that contain at least eighteen counts are plotted versus the peak centroids. There is a linear increase in peak width with quantum number, perhaps due to a decrease in lifetimes for higher-lying excited states, just as there was for the histograms. The statistical fluctuations of the voltage quantization increase linearly with increasing quantum number.

7. Conclusions

Quantized dissipative voltage states clearly exist in the breakdown regime of the quantum Hall effect. This quantization is interpreted in a simple model as occurring when electrons make transitions from a lower Landau level to a higher level and then return to the lower level. The large V_x signals imply a high transition rate and a collective effect. Voltage quantization suggests that individual electrons either make a single transition, or a fixed number of multiple transitions, because varying numbers of transitions would result in a continuum of V_x values rather than voltage quantization.

The data presented here are very striking, with sharp vertical features in V_x versus B plots, switching between states, and sufficient variations between sweeps to generate families of shaded curves, detailed histograms, and sharp spectra, and thereby to unambiguously determine values of the quantum number M. The voltage quantization is not perfect. It may decrease slightly with increasing quantum number, and its statistical variation increases linearly with quantum number. Still, the degree of quantization is quite surprising.

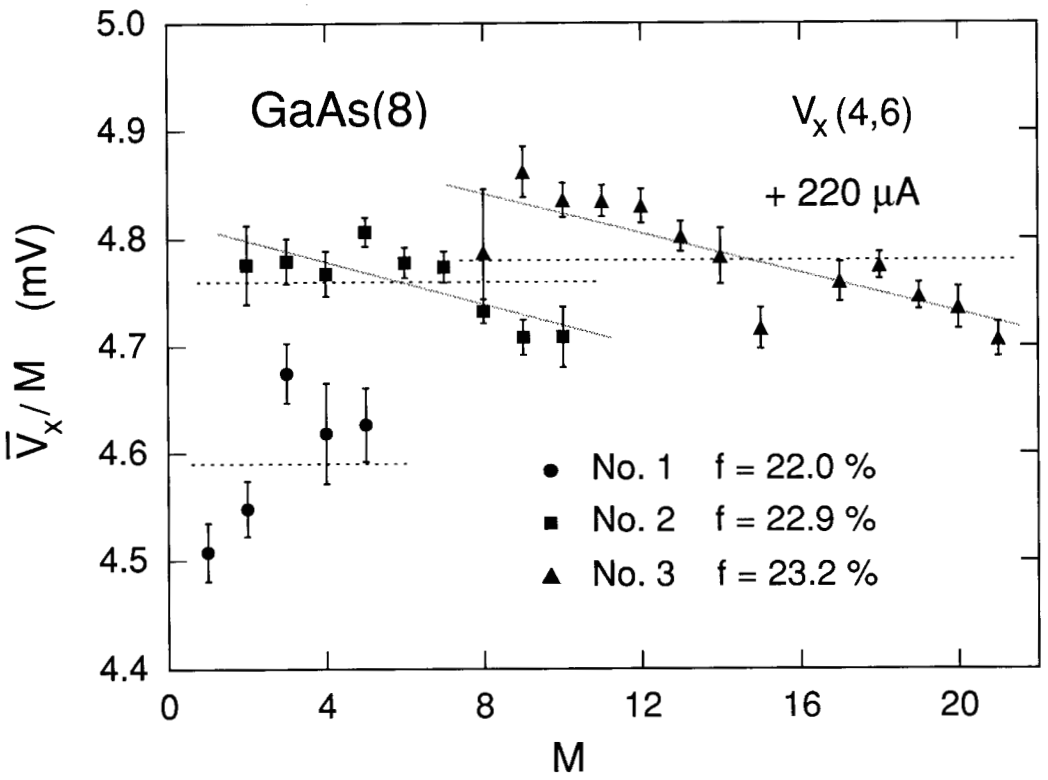

Fig. 9. Mean values of $\overline{V}_x/M$ for the three spectra in Fig. 7 plotted versus M. Only peaks with at least seven counts are included for spectra 2 and 3. The error bars represent one-standard-deviation uncertainties. There is more scatter in the values for spectrum 1 because $\overline{V}_x$ is divided by smaller values of M. Horizontal dashed lines are weighted averages of $\overline{V}_x/M$; corresponding f values are also displayed. The two shaded lines are least-squares fits that were weighted by the measurement uncertainties.

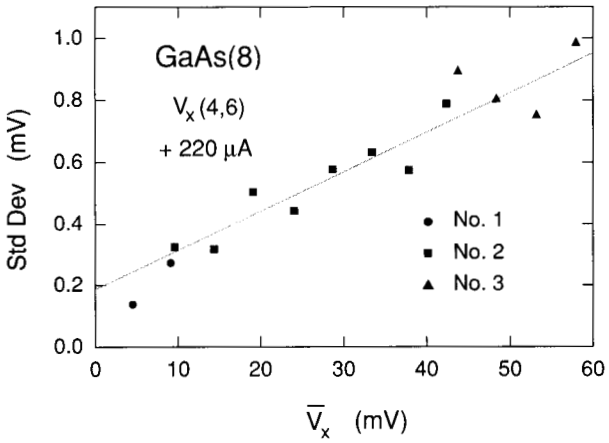

Fig. 10. Standard deviations of those peaks of the spectra in Fig. 7 that contain at least eighteen counts plotted versus the peak centroids, plus a linear least-squares fit to the data.

Acknowledgments

The authors thank A. C. Gossard (now at the University of California at Santa Barbara) who made the MBE-grown GaAs/AlGaAs heterostructure at AT&T Bell Laboratories, D. C. Tsui of Princeton University who defined the device geometry and made ohmic contacts to the 2DEG, and M. D. Stiles, K. C. Lee, R. F. Dziuba, and E. R. Williams for their discussions and comments. This work was supported in part by the Calibration Coordination Group of the Department of Defense.

8. References

[1] K. von Klitzing, G. Dorda, and M. Pepper, Phys. Rev. Lett. **45**, 494 (1980); The Quantum Hall Effect, R. E. Prange and S. M. Girvin, eds., Springer-Verlag, New York (1987).
[2] G. Ebert, K. von Klitzing, K. Ploog, and G. Weimann, J. Phys. C **16**, 5441 (1983).
[3] M. E. Cage, R. F. Dziuba, B. F. Field, E. R. Williams, S. M. Girvin, A. C. Gossard, D. C. Tsui, and R. J. Wagner, Phys. Rev. Lett. **51**, 1374 (1983).
[4] L. Bliek, G. Hein, V. Kose, J. Niemeyer, G. Weimann, and W. Schlapp, Proc. Int. Conf. on the Application of High Magnetic Fields in Semiconductor Phys. **71**, G. Landwehr, ed., Springer-Verlag, Berlin (1987) p. 113.
[5] M. E. Cage, G. Marullo Reedtz, D. Y. Yu, and C. T. Van Degrift, Semicond. Sci. Technol. **5**, 351 (1990).
[6] M. E. Cage, Semicond. Sci. Technol. **7**, 1119 (1992).
[7] M. E. Cage, J. Res. Natl. Inst. Stand. Technol. **98**, 361 (1993).
[8] M. E. Cage, D. Y. Yu, and G. Marullo Reedtz, J. Res. Natl. Inst. Stand. Technol. **95**, 93 (1990).
[9] G. Hein, P. Schneider, L. Schweitzer, F. J. Ahlers, L. Bliek, H. Nickel, R. Losch, and W. Schlapp, Surf. Sci. **263**, 293 (1992).
[10] S. Komiyama, T. Takamasu, S. Hiyamizu, and S. Sasa, Solid State Commun. **54**, 479 (1985); Surf. Sci. **170**, 193 (1986).
[11] A. S. Sachrajda, D. Landheer, R. Boulet, and T. Moore, Phys. Rev. B **39**, 10460 (1989).
[12] O. Heinonen, P. L. Taylor, and S. M. Girvin, Phys. Rev. **30**, 3016 (1984).
[13] L. Eaves and F. W. Sheard, Semicond. Sci. Technol. **1**, 346 (1986).
[14] D. C. Tsui, G. J. Dolan, and A. C. Gossard, Bull. Am. Phys. Soc. **28**, 365 (1983).
[15] V. L. Pokrovsky, L. P. Pryadko, and A. L. Talapov, Sov. Phys. JETP **68**, 376 (1989); J. Phys.: Condens. Matter **2**, 1583 (1990).
[16] J. R. Kirtley, Z. Schlesinger, T. N. Theis, F. P. Milliken, S. L. Wright, and L. F. Palamateer, Phys. Rev. B **34**, 5414 (1986).
[17] A. J. Kent, D. J. McKitterick, L. J. Challis, P. Hawker, C. J. Mellor, and M. Henini, Phys. Rev. Lett. **69**, 1684 (1992).

About the authors: *Charles F. Lavine is a professor of physics at St. John's University, Collegeville, Minnesota, and was a guest researcher at NIST. Marvin E. Cage and Randolph E. Elmquist are physicists in the Electricity Division at NIST. The National Institute of Standards and Technology is an agency of the Technology Administration, U.S. Department of Commerce.*

Volume 99, Number 6, November–December 1994
Journal of Research of the National Institute of Standards and Technology

[J. Res. Natl. Inst. Stand. Technol. 99, 765 (1994)]

Conference Report

WORKSHOP ON CRITICAL ISSUES IN AIR ULTRAVIOLET METROLOGY Gaithersburg, MD May 26–27, 1994

Report prepared by

Ambler Thompson

Radiometric Physics Division,
National Institute of Standards and Technology,
Gaithersburg, MD 20899-0001

and

Mitchell K. Hobish

5606 Rockspring Road,
Baltimore, MD 21209

1. Introduction

Several national programs and a variety of industrial applications today require the use or monitoring of ultraviolet (UV) radiation. The need for high accuracy radiometry in this region of the electromagnetic spectrum is becoming increasingly urgent. In response to this need, NIST's Radiometric Physics Division organized a Workshop on Critical Issues in Air Ultraviolet Metrology. This workshop was held at NIST/Gaithersburg on May 26 and 27, 1994, immediately following the 1994 Council for Optical Radiation Measurements (CORM) meeting at NIST. The workshop was attended by more than 120 registered participants from industry, federal agencies, and academe. The goals of this workshop were to identify the needs of the UV measurement communities for standards and instrumentation necessary for absolute measurements of irradiance and radiance, compile a list of specific recommendations to improve the nation's UV measurement capabilities, and determine NIST's role in supporting these efforts. The Workshop was cosponsored by the Radiometric Physics Division of the National Institute of Standards and Technology, the Office of Research and Development of the Environmental Protection Agency, the Office of Polar Programs of the National Science Foundation, the National Renewable Energy Laboratory UV Monitoring and Assessment Program Panel, and the Cooperative State Research Service of the United States Department of Agriculture.

The complete ultraviolet spectral wavelength region is from 10 nm to 400 nm. Ultraviolet radiation is identified in working wavelength regions on both physical biological bases. The UV wavelength region designations on a physical basis are: the near UV (300 nm to 400 nm), the middle UV (200 nm to 300 nm), the far UV (100 nm to 200 nm) and the extreme UV (10 nm to 100 nm). The air UV region, or the UV region which air transmits is generally considered to be from 200 nm to 400 nm. Below 200 nm air is strongly absorbing and is termed the vacuum UV. The biological UV wavelength regions as defined by the Commission International De L'Eclairage (CIE) are: the UV-A (315 nm to 400 nm), the UV-B (280 nm to 315 nm), and the UV-C (100 nm to 280 nm). There is some confusion in the literature about the wavelength demarcation between the UV-A and UV-B regions, since the CIE has defined the demarcation as 315 nm and the more traditional breakpoint was 320 nm.

The workshop was organized to be tutorial in nature, showing the fundamental derivation of the UV measurement chain from basic physical radiometric standards, and the transfer of the radiometric measurement chain to specific applications, with attention to error propagation and uncertainty analysis. Due to the short duration and tutorial nature of the workshop, every important UV application could not be addressed. Because of the programmatic interests of the cosponsoring agencies, the second day of the workshop specifically showcased the radiometric needs for long-term solar UV monitoring and for medical and biological UV researchers. These application areas are of topical interest due to concerns over the increasing depletion of the stratospheric ozone layer.

The invited speakers were instructed to indicate the economic, social, or environmental importance of UV measurement applications, uncertainty requirements, problems in utilizing existing standards, and anything else important to the UV metrology communities. The workshop was organized into four oral presentation sessions, with four invited papers per session. The titles for the sessions were:

I. Ultraviolet Radiometric Standards

II. Radiometric Instrumentation, Calibration, and Measurement Uncertainty

III. Measurement Requirements of Solar Ultraviolet Monitoring and Ozone Depletion

IV. Quantitation of Ultraviolet Biological Effects and Hazard Evaluations

An open forum discussion took place at the end of each session, during which details of that session's presentations were discussed, and related issues raised.

Each of the sessions will be described below. The concerns raised at each individual session forum have been collated into a section on crosscutting issues, presented as a separate section, followed by a statement of workshop conclusions and directions for future work.

2. Opening Remarks

The workshop was opened by Dr. Katharine Gebbie, the Director of the NIST Physics Laboratory, who welcomed the attendees and provided background for the workshop by first describing the role of the National Bureau of Standards (NBS) from its inception in 1901 through to the Omnibus Trade and Competitiveness Act of 1988, as a result of which NBS became the National Institute of Standards and Technology (NIST) with broad new responsibilities. To further focus the Workshop, Dr. Gebbie described NIST's Mission Statement generally, and the thrust of the Physics Laboratory specifically, with particular emphasis on UV metrology. Dr. Gebbie then discussed the Advanced Technology Program (ATP) in terms of its mission, strategy, and competitions, which are designed to increase the interactions between industry and government in (for the present) five focused areas: tools for DNA diagnostics, information infrastructure for health care, manufacturing composite structures, component-based software, and computer-integrated manufacturing for electronics.

A detailed introduction to the Radiometric Physics Division was then provided by Dr. Albert C. Parr, Chief of the NIST Radiometric Physics Division. Dr. Parr described the Division's three primary goals: development, improvement, and maintenance of national standards and measurement techniques for radiation thermometry, spectroradiometry, photometry, and spectrophotometry; the dissemination of these standards; and the conduct of fundamental and applied research to support future measurement services. Dr. Parr provided an organizational overview of the Division, and then presented some details of the Division's capabilities by describing the High Accuracy Cryogenic Radiometer, the Radiometric Calibration Chain, the Detector Comparator Facility, and the filter radiometer program. Dr. Parr closed with a discussion of the Division's Calibration and Reference Material Programs, describing detector calibration, source calibration, and reflectance and transmittance capabilities. He noted that the Division is building the capability to perform material characterization in the infrared out to 25 μm in wavelength.

3. Session I: Ultraviolet Radiometric Standards

The first session was chaired by Mr. William E. Schneider from Optronic Laboratories, Inc. Dr. Donald Heath, from Research Support Instruments, Inc. presented the first of the tutorial talks, *Introduction to the Ultraviolet Spectral Region*. The

approach was at first historical, referring to the work of Melvill (1752), Herschel (1800), Ritter (1801), Young (1802), Wollaston (1802), Fraunhofer (1814, 1823), Becquerel (1840), Kirchoff (1859), Angstrom (1868), Rowland (1887), Balmer (1885), Kayser, Runge, Rydberg (all 1890), Abbott (1923–1952), and Kiepenheuer (1930s). Dr. Heath also covered the phenomenological definitions of the UV regions: the air ultraviolet (200 nm to 400 nm), UV-A (315 nm or 320 nm to 400 nm), UV-B (280 nm to 315 nm or 320 nm), UV-C (200 nm to 280 nm). There is still not a consensus about the wavelength demarcation between the UV-A and UV-B regions Dr. Heath noted that the first measurements on extraterrestrial solar UV spectra were carried out by the Naval Research Laboratory in 1946 using spectrographs flown on captured V2 rockets. They observed that at 210 nm the solar irradiance was lower than expected from the Sun's visible and UV blackbody temperatures; further into the UV, the solar emission exceeded that expected from the blackbody curve. Dr. Heath went on to describe solar ultraviolet radiation, and begin a detailed discussion of the solar spectrum. He opened up the topic of the effects of ozone (and its depletion) on UV levels measured at the Earth's surface, thereby demonstrating the need for accurate UV data. To support the acquisition of these data, Dr. Heath opened a discussion on techniques for the calibration of UV spectroradiometric instruments, and provided some specific recommendations for radiometric calibration of UV surface radiation monitoring instruments.

The *Importance of Ultraviolet Measurements and Proposed Improvements to NIST's Synchrotron Ultraviolet Radiation Facility (SURF II)* was the focus of the presentation made by NIST's Dr. Robert Madden. Following the openings provided by Dr. Heath, Dr. Madden discussed the importance of high-accuracy radiometry by describing the needs of both national programs and industry in such measurements, with specific emphasis on the role of high-accuracy measurements in assessing the biological effects of UV-B radiation to human health directly, via skin carcinomas and melanomas, and the effects on food supplies, including both crops and ocean algae. Dr. Madden showed an action spectrum of the carcinogenic effectiveness of ultraviolet light, and data on the Antarctic ozone hole, emphasizing the need for measurements from instruments both above and below the ozone layer to monitor the incident and transmitted solar radiation, respectively. In support of the acquisition of high-accuracy data, NIST is making improvements to its SURF II, the characteristics of which are predictable from fundamental physics, and which will provide a continuum of radiation throughout the air and vacuum UV spectral regions. These improvements will fine-tune the electron orbital geometry in the storage ring, increase the energy of the stored electrons, and directly determine the radiant flux from the storage ring with a cryogenic radiometer. These improvements should achieve a radiometric uncertainty of less than 0.5 % in the absolute value of flux, and 0.1 % in its relative spectral distribution. The improvements should also extend NIST's capabilities by providing spectral coverage to 2.4 nm, and should permit the determination of black body temperatures independent of gas thermometry.

The necessity for good, application-level UV measurements was addressed by Dr. Christopher L. Cromer, from NIST, in his presentation on *Ultraviolet Detector Metrology and Filter Radiometry*. Dr. Cromer first addressed the operational aspects of UV measurements with a description of the construction and workings of a typical UV meter. He stated that all too frequently, users employ such meters unmindful that the spectral range is generally not well defined. He demonstrated that large errors can be incurred either during calibration or through improper use. These errors could be due to the meter's out-of-band rejection, nonlinearity, or non-cosine response. The calibration of the instrument and its use is dependent upon the spectrum of the calibration source and its similarity to the spectrum of the optical radiation to be measured. In addition, the relation of the sensor's real response function to the ideal response function or desired action spectrum must be addressed. Dr. Cromer went on to describe source-based and detector-based calibration, NIST's capabilities for UV detector metrology, and then suggested strategies for proper and effective calibration of UV meters.

The topic of proper calibration and suitability of standards for a given application was addressed by Mr. Robert D. Saunders, also of NIST, who presented material on *Choosing the Proper Standards for the Radiometric Application*. Mr. Saunders began by describing the parameters that need consideration, and, for the first time in the Workshop, addressed the need for portability and ease-of-use for standards and instruments. After describing the roles of primary, secondary, and working standards, Mr. Saunders went on to discuss the advantages and disadvantages of primary physical standards such as cryogenic radiometers, blackbod-

ies, trap detectors, synchrotron radiation, parametric down conversion, and hydrogen arcs. A similar discussion of secondary and working standards followed, including 1000 watt quartz halogen tungsten lamps, D_2 lamps, argon mini-arcs, tungsten strip lamps, and filtered detectors. Mr. Saunders then provided a look at the status of UV measurements, including the spectral irradiance intercomparison, and an ongoing air UV intercomparison, and showed how international irradiance scales compare with the NIST scale based on the international irradiance intercomparison performed in 1990.

4. Session II: Radiometric Instrumentation, Calibration, and Measurement Uncertainty

After a break for lunch, Session II was convened, with Dr. Theodore W. Cannon, from the National Renewable Energy Laboratory, as Chair. Dr. Cannon introduced Dr. Henry Kostkowski, of Spectroradiometry Consulting, who gave an excellent presentation on *Measurement Errors and Their Control in UV Spectroradiometry*. Dr. Kostkowski addressed the simple measurement equation, and showed how and under what conditions it could be employed. Discussion of the ideal responsivity function and actual responsivity (R) functions followed, with some guidelines on elimination of errors due to changing responsivity with direction and position through use of an averaging sphere, or the use of roughened quartz surfaces, which provide less attenuation. Things get more complicated when R changes with direction, requiring the use of a correction term in the measurement equation. Other errors are incurred (and must be corrected for) when R varies with polarization, the magnitude of the flux (nonlinearity), spectral scattering, distortion, drift, hysteresis, and wavelength instability. Dr. Kostkowski provided the group with some guidelines for choosing a UV spectroradiometer for high signal-to-noise ratios, and showed how the state-of-the-art could reduce uncertainties for solar terrestrial measurement at 295 nm by almost a factor of three. Dr. Kostkowski closed his talk with a nine-point plan for reliable spectroradiometry.

The need for calibration standards between laboratories was addressed in a presentation on the *NCSL: UV Radiometer Round-robin*, by Dr. L. Kasturi Rangan, of Lockheed Missile and Space Co., Inc. Dr. Rangan described a round-robin measurement program for UV irradiance among metrology standards laboratories under the auspices of the National Council of Standards Laboratories (NCSL). Fifteen laboratories—including NIST, the three primary standards laboratories of the DoD, and several aerospace companies—are participating. The circumstances which prompted this round-robin were discussed, as were the scope and status of the activity. Dr. Rangan presented information on the end-use of the UV sources measured by the calibrated meters, along with the manufacturers and models of those instruments. Further details for the instrumentation were provided, including the number of units calibrated by each laboratory per year, wavelength and bandwidth requirements, and irradiance levels. Five sources are to be used in the round robin along with several other optical components. Details on the UV round-robin parameters were presented, and a chart showing the uncertainty for each laboratory was shown. The circulating unit is now being calibrated at NIST and the estimated time for completion of the round-robin is on the order of 1 year.

Further information on *Spectral Ultraviolet Measurements and Utilization of Standards* was presented by Mr. William E. Schneider, of Optronic Laboratories, Inc. Mr. Schneider addressed instrumentation, standards, calibration, and measurement of optical radiation, and described the essential components of an automated spectroradiometric measurement system. Across his presentation were issues addressing the effects of wavelength accuracy and precision, linearity, slit function, stray light, scanning speed, cosine response, temperature dependence, and system calibration on the overall performance of the measurement system, with emphasis on the problems unique to measuring solar spectra in the ultraviolet. He described the construction and operational details of single and double monochromators of the Czerny-Turner variety, and showed a schematic diagram of a portable double monochromator spectroradiometer. After a discussion of general detector specifications, Mr. Schneider discussed signal detection systems, and proceeded to discuss various input optics, including none at all, cosine receptors, imaging optics, and fiber optics, with particular emphasis on an improved design for an integrating sphere. A short discussion of automatic data reduction systems followed, with a warning that operational details of these sometimes industry-standard components must be taken into account, as such a system is as much a part of the calibration and measurement chain as are

standards and sources. Mr. Schneider then addressed calibration standards, particularly mercury arcs for wavelength standardization, and tungsten and deuterium lamps for spectral irradiance response standards. He then discussed the utility of plug-in irradiance standards, and ended with discussion of an automated spectroradiometer configured for measuring spectral irradiance.

The last of the formal presentations for Session II was by Mr. Daryl R. Myers, from the National Renewable Energy Laboratory, who discussed *The Uncertainty Challenge in Solar Terrestrial Ultraviolet Radiometry*. Mr. Myers reemphasized the importance of accurate and reproducible solar terrestrial ultraviolet metrology data, and so addressed his remarks to the problems associated with the calibration and measurement of solar terrestrial ultraviolet radiation between 280 nm and 400 nm. Using a standardized approach to uncertainty analysis, the sources and magnitudes of uncertainty in broadband and spectral UV radiometry were discussed, with examples of typical, currently available instrumentation, calibration sources, and techniques. Mr. Myers discussed the concept of acceptable uncertainty, and went on to describe in detail several sources of uncertainty, noting strongly the need to determine sources of uncertainty for all components in a measurement chain, making distinctions between random fluctuations which are reducible by increasing sample size, and systematic effects, some of which may be calibrated out by proper utilization of standards. Both types must be quantified and combined to yield total uncertainty for a measurement. Of great importance to the overall process is accurate reporting of uncertainties, so that workers in the discipline area may assess the validity of a measurement, given the real-world constraints of instrumentation.

A poster session was held at the Gaithersburg Hilton Thursday evening following the first day's sessions. Some 15 posters were presented, representing several aspects of manufacturers' progress and concerns in the production of measurement instrumentation, characterization and calibration of various instruments and networks, new mathematical corrections for radiometer data, and more. The poster session was well-attended, and resulted in significant, in-depth discussion among the participants.

5. Session III: Measurement Requirements of Solar Ultraviolet Monitoring and Ozone Depletion

The second day of the Workshop opened with Dr. C. Rocky Booth, of Biospheric Instruments, Inc., as Chair. The second day's topics addressed specifics of applied measurements by researchers in the fields of solar UV monitoring, particularly as it applied to ozone monitoring and the biological effects of UV-B.

Dr. Booth introduced Mr. Ernest Hilsenrath, of NASA Goddard Space Flight Center, who discussed *Ultraviolet Calibration Requirements for Satellite Detection of Ozone, Solar Irradiance, and UV-B Trends*. Mr. Hilsenrath noted that the amount and spectral range of UV radiation reaching the Earth's surface is a function of solar zenith angle, clouds, atmospheric turbidity, and the column amount of ozone. Changes in ozone, as a controlling factor for surface UV, becomes important only over the long term. To measure these long-term trends, NASA and NOAA have embarked on a program to monitor ozone and solar irradiance from space using the backscatter ultraviolet (BUV) technique. The program began in 1978 with Nimbus-7 SBUV/TOMS instruments. A national plan for ozone monitoring carries these measurements into the twenty-first century. These measurements will require accurate prelaunch calibration, careful monitoring, and precise on-orbit characterization. Corrections for albedo changes must be taken into account, but absolute accuracy relies on NIST's standards to yield a calibration precision of 1 % at the 1σ level. The uncertainty in an ozone measurement for 1 % calibration error varies, depending on the altitude. Mr. Hilsenrath concluded by noting that pre-launch activities require that absolute irradiance calibrations meet this uncertainty requirement and that absolute radiance calibrations based on BRDF and standard lamps are a problem. The problem of calibrations of multiple instruments is currently being studied and the requirement for post-launch instrument characterization to the 1 % level over long time periods is a major challenge.

Continuing the theme of global and regional UV level monitoring, Dr. C. Rocky Booth discussed *Calibration Aspects of the United States National Science Foundation's UV Monitoring Network for Polar Regions*. This program, instituted in 1988, places a network of high spectral resolution (0.7 nm) UV spectroradiometers in locations around the globe, including Antarctica, Argentina, Alaska, and San

Diego. These instruments are designed to be run in fully automated mode, and to provide continuous operation, 24 hours a day. The system is optimized for operation in the UV and visible spectral regions up to 600 nm. A vacuum-formed Teflon® diffuser serves as an all-weather irradiance collector, and is heated to discourage ice and snow buildup. Provision is made for automatic wavelength and responsivity calibration 2–4 times daily. The instruments are comprised of two major subassemblies. The first includes the irradiance collector, monochromator, PMT and internal calibration sources. These components are mounted in a weather-proof enclosure, designed for mounting in the roof of existing structures. The second subassembly consists of power supplies, temperature controllers, electronic interfaces, and a personal computer. This group of components is usually mounted on a lab bench, away from the vagaries of weather. Dr. Booth described the details of calibration and characterization generally, and proceeded to discuss the data obtained by the network, which are available annually on CD-ROM, and will be made available over the Internet.

Dr. Brian Gardiner, of the British Antarctic Survey, commented on his being the only non-U.S. representative at this Workshop, and then proceeded to discuss *European Community Solar UV Spectroradiometer Intercomparisons: Review and Recommendations*. These intercomparisons were performed to improve the accuracy and reliability of solar ultraviolet spectral irradiance measurements in Europe. Over 3 annual campaigns, 14 different types of UV spectroradiometers have been studied. Each intercomparison campaign consisted of a variable number of instruments making simultaneous spectral measurements of the solar irradiance at one site over a range of observing conditions. These activities have resulted in improvements in instrument design, operational procedures, and increased the skill of the participants. The intercomparisons demonstrated that the best instruments show good agreement in their absolute irradiance calibration (although all instruments run into difficulties at the shortest UV wavelengths), but that there is still room for improvement in calibration techniques and procedures. These intercomparisons have also demonstrated the ability of workers to make plausible but still erroneous measurements. Based on laboratory measurements of slit functions and angular responses, the main areas of uncertainty in the irradiance measurements are scattered light in the calibration lamp room, accuracy of transfer lamp calibrations, temporal drift in the irradiance calibration of an instrument during the course of the day, and the effect of imperfect cosine and azimuth responses. Design and operational parameters for the better spectroradiometers include the use of double monochromator scanning spectrometers providing a spectral bandpass of 1.0 nm or less, and capable of making measurements every 0.5 nm in the range 280 nm to at least 420 nm.

Continuing the discussion of global-scale monitoring of UV levels, Dr. Betsy Weatherhead, of the Cooperative Institute for Research on Environmental Sciences/NOAA, opened her talk on *Ultraviolet Indexes and UV Monitoring Around the World* with a discussion of the need for such monitoring, and then provided a brief overview of UV instrumentation and an historical view of UV monitoring. This was followed by material on the purposes and outstanding problems of UV monitoring. She presented information on the locations of UV measurement stations around the world, and showed the near-exponential growth in numbers of spectral and broadband instrument stations from 1987 to the present. The difficulties in providing long-term, accurate, calibrated data sets are manifold, requiring calibration, documentation, careful analysis, and appropriate instrument placement and maintenance. These activities require large-scale coordination across organizational and national boundaries. Of particular importance is the need to communicate the results of such measurement campaigns to the public-at-large; this task is being addressed by the creation of UV indices. After presenting material on the definition of UV indices and their purposes, i.e., education of the public as to the effect of changing UV levels on their day-to-day activities and long-term health, Dr. Weatherhead went on to discuss the distinction between indices based on computer models and those based on measurements, discussing the advantages and disadvantages of both approaches. Real-world difficulties in generating such indices were discussed, including the differences between indices generated in different countries utilizing different criteria and parameters. Ultimately, representatives of the atmospheric, health, and educational communities must come together to define workable indices whose metrics will be usable regardless of geographical location.

6. Session IV: Quantitation of Ultraviolet Biological Effects and Hazard Evaluation

Session IV began when Dr. Martyn Caldwell, of Utah State University, was introduced by the session's Chair, Dr. Edward DeFabo, of George Washington University Medical Center. Dr. Caldwell opened the discussion of biological effects of UV radiation by addressing *Ultraviolet Radiation Measurement Requirements in Terrestrial Plant Experiments*.

Understanding the mechanisms whereby biological systems are affected by environmental insults is not as clear-cut as understanding physical mechanisms of instrumentation response. To provide the best data in plant experiments both direct beam and diffuse ambient solar spectral measurements are required, as are spectral measurements of filtered solar radiation. Determining the action spectra of biological responses is necessary in order to determine what biomolecules are being affected by the incident radiation. Often, these spectra represent only a small portion of the incoming radiation spectral distribution. In most cases, action spectra for a given biological effect are different than for other effects. For example, the UV action spectra for the photoinhibition of the photosynthetic Hill reaction is significantly different from the action spectra for inhibition of ATPase, and action spectra for general DNA damage in stationary phase cells differs from induction of single strand breaks in DNA. As a result, care must be taken to fully define the spectral regions of incident UV radiation that are responsible for specific effects. To support this analysis, several different needs for UV measurements in plant experiments are necessary: spectral measurement of ambient solar radiation to establish benchmarks with solar radiation transfer models used to characterize baseline levels of UV-B radiation; spectral measurements of radiation used in experiments (from lamps, filtered solar radiation, etc.); continuous broadband measurements throughout the duration of experiments of ambient solar UV-B, UV-A, and visible radiation; and specialized measurements in some experiments, e.g., spectral irradiance within plant canopies. UV-B dosimeters have a significant role to play here, for continuous monitoring of solar and lamp radiation, routine checking of lamps and filter aging, and to check the spatial distribution of radiation fields. Other dosimeters may be used to monitor visible radiation, and for UV-A monitoring.

Continuing the discussion of biological responses to UV radiation, Dr. Robert M. Sayre, of Rapid Precision Testing Laboratories, discussed *UV Measurements in Photobiology and Photomedicine*. Ultraviolet sources are used for a variety of biologically related purposes, ranging from the treatment of disease conditions (such as psoriasis and atopic dermatitis), cosmetic uses (such as indoor tanning), drug phototherapy, efficacy testing of sunscreens and drug products, photostability testing of products and packaging, and as surgical and examination lamps. While some of these uses have had standards for measurement and usage developed, other photobiological uses are less well-defined, and are usually dependent upon specific action or response spectra. For sources covered by regulatory requirements, spectroradiometric measurements are required, and must be interpreted relative to a specific risk spectrum. Dr. Sayre discussed regulations, the nature of sources, and measurement requirements to support these uses. He made a strong case for long-term and ongoing monitoring of sources such as are used in tanning beds, as dosage is dependent on flux, which is known to vary with time. Further, Dr. Sayre amply demonstrated that many of the sources currently in use for photomedicine and photobiology and which are touted as providing reasonable representation of solar UV spectra do not, in fact, mimic those spectra with adequate fidelity. Specifically, Dr. Sayre concluded that specific standards for a given spectrum must be established, and that each source must be measured to insure that it meets that standard. Further, merely specifying a filter type is inadequate, as manufacturers' specifications often ignore out-of-band transmission. Sources must be described by spectroradiometric techniques; vague descriptions that a specific lamp was filtered with a specific filter are not adequate. Procedures must be developed for measuring sources, and these procedures must be standardized. Even in cases where laboratory measurement procedures have been standardized, it must be recognized that in-the-field use is not always congruent with laboratory procedures. Dr. Sayre asserted that educational programs must be established to train scientists in proper techniques for characterizing their sources, and to educate journal editors that sources are not generic.

Dr. Edward C. DeFabo, of the Laboratory of Photoimmunology and Photobiology at The George Washington University, carried some of the topics addressed by Dr. Sayre further in his presentation on *Skin Cancer, Immune Suppression, and*

UVB Radiation: Issues in Measurement. UV-B has been specifically linked to skin cancer formation, and is also associated with local and systemic immunosuppression in mammals, although the mechanisms are not fully understood. The operational requirements of dealing with living, moving organisms provided significant challenges for dosage determination. To develop the action spectrum for immune suppression, Dr. DeFabo and his colleagues developed an optical dispersion system that could provide an area of exposure large enough to irradiate the dorsal surface of three mice at once, and to produce radiation with waveband resolution narrow enough (~2.5 nm) to allow for sufficient wavelength discrimination. This system was used to determine the absorption characteristics of the photoreceptor mediating immune suppression. In order to determine UV dosage, broadband and spectroradiometric measurements were utilized. Frequent calibration was required to accurately determine the absolute dose-response for immune suppression. The care taken in these studies allowed Dr. DeFabo and his colleagues to identify a unique photoreceptor on mammalian skin: a deamination product of histidine, an amino acid common to many proteins. This photoreceptor is commonly found in human skin, and may play a critical role in skin cancer development. The UV immune suppression phenomena have grave implications for susceptibility to contagious diseases and parasites due to the expected increase in solar ultraviolet irradiance projected to result from ozone depletion.

The question of correlating skin cancer occurrence with UV radiation dose was addressed by Dr. Martin A. Weinstock, of the Dermatoepidemiology Unit at Brown University. Dr. Weinstock discussed the *Epidemiological Correlations of Skin Cancer with Ultraviolet Exposure*, and described some of the adverse effects of sun exposure on human health. Specifically, Dr. Weinstock described malignant melanoma (MM), squamous cell carcinoma (SCC), and basal cell carcinoma (BCC). All three have been linked to sun exposure, although the nature of that linkage varies. An action spectrum has been determined for SCC, but not for the other types of cancer. Dr. Weinstock stated that precise geographic measurements of UV may assist in determining the other action spectra, and that these results will have significant implications for understanding the role of sunscreens, shade, and simple avoidance in the prevention of skin cancer. Dr. Weinstock emphasized that epidemiologists must distinguish between cultural shifts in behavior, e.g., clothing styles, and changes in environmental conditions, e.g., ozone depletion, in assessing skin cancer incidence trends.

7. Cross-Cutting Issues

Several themes kept arising throughout the presentations and during the discussions following each session. There was consensus that high-accuracy UV metrology was necessary to allow researchers to answer questions about biological effects of UV radiation and to monitor long-term environmental trends in such UV-related phenomena as ozone levels. To support this level of metrology, careful characterization of sources, filters, and instrumentation, as well as instrument intercomparison campaigns are required. It is not enough to say merely that a given source/instrument/filter combination was used, but rather calibration data must be provided in all reports. For a full understanding of the phenomena described above, the state-of-the-art in metrology must be extended well into the UV-C region. Common instrumentation needs included portability, ease-of-use, standardization of procedures, and improvement of integrating spheres.

The role of the various players in UV metrology was discussed at length, focusing most specifically on the national capabilities provided by NIST. With the increasing demand for high-accuracy radiometry, there is increased need for the secondary standards laboratories to provide for the transfer of NIST's scales to the level of users' needs. These secondary standards laboratories are private sector as well as governmental. A discussion of increasing use of secondary standards laboratories led to the conclusion that much, if not most, of the work of calibration and characterization needed for solar radiometry must be provided by NIST, EPA, NIH, NSF, DoE and other such groups, perhaps in the formation of core facilities for use by researchers in many communities and disciplines, thereby obviating the strong potential for duplication of effort.

Throughout the discussions ran the theme of education—of users, manufacturers, funding agency representatives, journal editors, and the general public. Users must be able to fully define their metrology requirements, matching required fluxes, accuracy, and precision with the instrumentation and sources needed to obtain suitable measurements. Users must also become better versed in the operational requirements of UV experimentation, and understand the relative uncertainties associ-

ated with each link in the measurement chain. Indeed, reports of experiments must include the calibrations described above, and a complete error and uncertainty analysis that includes all contributing factors, both qualitative and quantitative. Manufacturers must be educated about the needs of their end-user communities, including portability requirements, ease-of-use, and requirements for complete characterization of their instruments and sources to allow end-users to do top-quality experiments and measurements. Funding agency representatives must fully understand that when a researcher requests funds for an instrument of a given degree of precision and accuracy, that a less-expensive, less-accurate replacement will not suffice; research must be results-driven, not cost-driven. Journal editors must understand that full characterization of measurement chains is a *sine qua non* for publication of experimental and metrological results, for without such characterization it is almost impossible for other researchers to fully understand the measurements being presented, or to duplicate the work being reported. Finally, the public-at-large must understand that UV metrology can and will have increasing effects on their lives, as we struggle to understand how this energetic region of the electromagnetic spectrum affects biological systems.

8. Conclusions and Future Directions

In support of some of the issues raised during this Workshop, NIST has the ability to achieve accurate radiometric transfer from basic physical standards (primary standards) to detector or source secondary standards within their stated uncertainty. The use of these standards at their stated level of uncertainty requires that others understand the source under test, the standard, and the measurement instrumentation with a level of detail and proficiency approaching that of NIST's scientists. Improvements in radiometric standards alone, uncoupled from a concomitant improvement in understanding of measurement instrumentation will not improve the accuracy of the nation's measurement activities, as demonstrated by the results of the instrument intercomparisons and round-robins such as were reported on during this Workshop. The disagreement in measurements of a common source using a common standard are all-too-frequently inconsistent within the combined measurement uncertainty; therefore, improvements in the accuracy of the standards must be coupled to defining protocols and procedures for instrument intercomparisons and characterizations. There must be a strong educational component to the transfer of the radiometric measurement scales to applications. For important national programs and state-of-the-art-radiometry, NIST's direct involvement may be necessary, but improvements can also be made through interactions with instrument manufacturers, secondary standards laboratories and measurement standardization organizations (i.e., Council for Optical Radiation Measurements (CORM), American Society for Testing and Materials (ASTM), and CIE).

The Workshop participants felt that this workshop was well organized and well run, and that it had already made a difference in the way many of them looked at their particular piece of the measurement puzzle. While industrial applications of UV radiometry were not represented in the body of the workshop presentations, there was strong representation by the industrial radiometry community in those who attended, which was an advantage provided by scheduling the workshop in proximity to the CORM94 meeting. A workshop to specifically target industrial applications of radiometry and photometry is being planned, as such input is required for the overall process of understanding the metrologic requirements of the radiometric community at large.

The material presented at this workshop will be collated and integrated into an Executive Summary, which will be published as a NIST Interagency Report by September 1994. The Workshop Proceedings will be published as a NIST Special Publication early in 1995.

Acknowledgments

This workshop could not have been held without the professional contributions of the workshop steering committee, presenters, and participants, and the financial contributions of the workshop cosponsors. Encouragement and financial support from NIST to hold the workshop were provided by Mr. Robert Saunders and Dr. Albert Parr of the Radiometric Physics Division. Special thanks to Ms. Dawn Russell and Ms. Sally Bruce of the Radiometric Physics Division for their invaluable assistance in planning this workshop. We gratefully acknowledge the support of the NIST Conference Facilities personnel for logistically organizing the meeting and seeing that it ran smoothly.

Volume 99, Number 6, November–December 1994
Journal of Research of the National Institute of Standards and Technology

[J. Res. Natl. Inst. Stand. Technol. 99, 775 (1994)]

Conference Report

DATA ADMINISTRATION MANAGEMENT ASSOCIATION SYMPOSIUM Gaithersburg, MD May 17–18, 1994

Report prepared by

Judith Newton

Information Systems Engineering Division,
Computer Systems Laboratory,
National Institute of Standards and Technology,
Gaithersburg, MD 20899-0001

1. Introduction

Along with capital and human resources, an organization's data represents one of its fundamental assets. Data administration (DA) attempts the effective planning, organization, and management of an enterprise's data resource, with the intention of empowering the organization to achieve its mission and goals.

Achieving enterprise integration, and developing the supporting information technology infrastructure, is a critical need for organizations. Yet despite substantial attention by business managers, technologists, and vendors of tools and methodologies, there are few obvious solutions or guidance on how to accomplish this.

The Data Administration Management Association (DAMA) is the professional organization for data administrators. An international board oversees a loose federation of local chapters in the United States, Canada, Australia, and Europe. The National Capital Region Chapter (NCR DAMA) has monthly meetings from September through April, as well as a Symposium in May.

NCR DAMA held its seventh annual Symposium at NIST on May 17-18, 1994. The theme this year was *Enterprise Integration in the Turbulent 90s*. Attended by over 200 Federal and private industry data administrators, the Symposium was cosponsored by NIST and NCR DAMA.

The Symposium emphasized the practices, technologies, activities, initiatives and ideas that deliver clearly visible value to the users, or "customers" of data administration. In addition to presentations by nationally recognized experts and practitioners, it included breakout dialog sessions and panel discussions. Topics ranged from the keynote speech on the National Information Infrastructure to the latest implementation of the Information Resource Dictionary System (IRDS) standard. New this year was a Vendor Exhibit Area, where the latest tools for implementing the practices of Data Administration could been seen.

2. Speakers

The keynote speaker was Arati Prabhakar, Director of NIST, describing the government's role in the National Information Infrastructure.

Mary "Bunny" Smith provided a personalized perspective of information systems design for new, very small businesses. Spreadsheets are invaluable both for planning and cost accounting. One can not start to model one's business too soon, even if it occurs on the kitchen table.

Dr. Mike Mestrovitch, DoD, discussed transforming the enterprise through Enterprise Integration, and what transformation is planned for DoD. It will involve changing every aspect of the organization to meet new circumstances and expectations. It is a way of using information as a strategic asset to manage the enterprise far more effectively and efficiently. It bridges functional and technical boundaries to increase flexibility and to focus all available capabilities on mission results. The process includes: establishing a vision for the future; creating a sense of urgency about the vision; redefining the business processes; redefining resource capabilities; creating a new work environment; re-creating management systems and structures; and building an information and technology architecture to empower the organization to execute.

The last speaker, John Zachman of Zachman International, presented his Information Architecture concept together with his personal view of the future of manufacturing and technology. We must change from Custom-design-and-build and Provide-from-stock to Assemble-to-order processes. He issued a challenge for everyone in the audience to rise to meet "The New Realities of the Information Age."

3. Concurrent Sessions

A series of concurrent sessions focused on various managerial and technical aspects of enterprise integration. Several sessions addressed the National Performance Review. Others considered data modeling, EDI, and open systems.

4. Panels

The following panel discussions were presented:

- Repository, A Missing Link in Enterprise Integration, Carla von Bernewitz, DoD, moderator;
- Using IDEF in Conjunction with Information Engineering, Vince Cordovano, James Martin Consulting, moderator;
- Standards for Data Administration, Judith J. Newton, NIST, moderator;
- GOV-SIG: Stepping Stone to Public Sector Integration, Pam Piper, DoD, and Tom Kurihara, NIST, moderators;
- Linking IRM Initiatives to Strategic Planning, Stephanie Wietecha, FC Business Systems, moderator;
- Reengineering a Data Management Program, Patricia Simes, SRA, moderator.

5. Proceedings

The proceedings of this, the Third, the Fifth, and the Sixth Symposia were distributed at the event. The Proceedings of the First,[1] Second,[2] and Fourth[3] Symposia were published by NIST and copies are still available. The Eighth Annual Symposium will be held May 16-17, 1995.

[1] Judith J. Newton, and Frankie E. Spielman, eds., Data Administration: Management and Practice, Proceedings of the First DAMA Symposium, NIST Special Publication 500-159, National Institute of Standards and Technology, Gaithersburg, MD, October 1988.

[2] Judith J. Newton, and Frankie E. Spielman, eds., Data Administration: Standards and Techniques, Proceedings of the Second Annual DAMA Symposium, NISTIR 90-4292, National Institute of Standards and Technology, Gaithersburg, MD, April 1990

[3] Judith J. Newton, Mary Lou Melley, and Holly Higgins, eds., Managing Data: From Vision to Reality, Proceedings of the Fourth Annual DAMA Symposium, NISTIR 4843, National Institute of Standards and Technology, Gaithersburg, MD, May 1992.

Volume 99, Number 6, November–December 1994
Journal of Research of the National Institute of Standards and Technology

[J. Res. Natl. Inst. Stand. Technol. 99, 777 (1994)]

Conference Report

NORTH AMERICAN INTEGRATED SERVICES DIGITAL NETWORK (ISDN) USERS' FORUM (NIUF) Gaithersburg, MD June 21–24, 1994

Report prepared by

Elizabeth B. Lennon

Computer Systems Laboratory,
National Institute of Standards and Technology,
Gaithersburg, MD 20899-0001

1. Introduction

The Computer Systems Laboratory (CSL), National Institute of Standards and Technology (NIST), hosted the twenty-first North American ISDN Users' Forum (NIUF) at its Gaithersburg, Maryland, site on June 21-24, 1994. About 175 users, implementors, and service providers of ISDN technology attended the meeting. CSL collaborated with industry in 1988 to establish the NIUF to ensure that emerging ISDN applications meet the needs of users. A Cooperative Research and Development Agreement (CRADA) with industry was established in 1991 to govern the management of the forum; as of June 1994, the CRADA had 32 signatories from industry and academia. CSL serves as chair of the forum and hosts the NIUF Secretariat. NIUF membership is open to all interested users, product providers, and service providers; meetings are held three times a year at various locations throughout North America.

2. The Development of ISDN Standards

International standards for ISDN support global communications for the exchange of voice, data, and image information among users, independent of any manufacturer, service provider, or implementation technology. ISDN standards are developed by the International Telecommunication Union - Telecommunication Standardization Sector (ITU-T) and in North America in particular, by the Exchange Carriers Standards Association (ECSA) accredited standards committee, T1, under the umbrella of the American National Standards Institute (ANSI).

ISDN standards provide a broad variety of options and parameters to meet many potential needs and applications. To ensure interoperability and terminal portability within the ISDN network and its attendant equipment, a uniform subset of options and parameters must be selected for implementation. Each application usually requires only a subset of total functionality available in the standards; for ISDN products and services to work together in a multivendor environment, common sets of options must be selected.

To cope with this proliferation of choices and to provide interoperable products and services which meet the needs of users, the standards specification process has been augmented to develop application profiles, implementation agreements, and conformance criteria. The NIUF addresses all of these areas.

3. NIUF Objectives and Structure

The NIUF seeks to achieve three principal goals:

- To promote an ISDN forum committed to providing users the opportunity to influence developing ISDN technology to reflect their needs;
- To identify ISDN applications, develop implementation requirements, and facilitate their timely, harmonized, and interoperable introduction; and
- To solicit user, product provider, and service provider participation in the process.

The actual work of the NIUF is accomplished in two workshops: the ISDN User's Workshop (IUW) and the ISDN Implementor's Workshop (IIW). The IUW produces application requirements which describe potential applications of ISDN and the features which may be needed. The IIW develops application profiles, implementation agreements, and conformance criteria which provide the detailed technical decisions necessary to implement an application requirement in an interoperable manner. The NIUF Executive Steering Committee coordinates the activities of the two workshops.

4. NIUF Achievements

Since its inception in 1988, the NIUF has achieved the following:

- 42 applications for development of application profiles are in process;
- application profiles have been completed for 17 applications;
- 15 implementation agreements have been completed; and
- 12 conformance tests have been completed.

CSL established the NIST Special Publication 823 series, Integrated Services Digital Network Technology Publications, to publish the approved implementation agreements, conformance tests, and other NIUF documents. To date five documents have been published. Copies of these documents are available for sale by the Government Printing Office, (202) 512-1800 or the National Technical Information Service, (703) 487-4650.

4. Highlights of June 1994 NIUF

A special one-day National Information Infrastructure (NII) Seminar focused on "Clarifying the Vision of the Information Highway." Dr. Arati Prabhakar, NIST Director, presented the keynote address on the NII Task Force. Other presentations covered High-Performance Computing and Communications; information technology applications such as education, libraries, healthcare, and the environment; and NII application projects at NIST including the NIST NII Agent and the Advanced Technology Program (ATP) Focused Program on Information Infrastructure for Healthcare.

Tutorials presented at the June meeting included an overview of the NIUF for new users and implementors; a session on point-to-point protocol over ISDN; and a general survey of the ISDN wiring and powering work program.

Highlights from the Executive Steering Committee standing groups included an update on the new NII Working Group (NIIWG) and its agenda for meeting the needs and challenges for NII applications. The group's charter states that the NIIWG will focus on "the requirements of efficient access to the information infrastructure, the use of standards, interoperability and the development of suitable ISDN technologies to support the NII." The NIIWG Applications Committee and the NIIWG Architecture Committee created charters and established future projects. The NIIWG Applications Committee will re-categorize existing NIUF ISDN application profiles into appropriate NII application categories, such as healthcare. The NIIWG Architecture Committee plans to develop an ISDN portion of the NII model. The Versions—Capability and Analysis Planning meeting consisted of a presentation by a representative from Bell Atlantic on the content and schedule for National ISDN-3 specifications.

IUW working group highlights included the following: the IUW General Users' Meeting revamped and prioritized NIUF applications, which will now be categorized as complete, inactive, or open/ongoing. The IUW and the IIW will jointly draft a letter to regional user groups to ask for assistance in championing applications within the NIUF. The Government Services Group has established a "Government" newsletter to promote local, state, federal, and international government ISDN success stories. The Private Industries Group addressed the "road blocks" that face industry organizations in the deployment of ISDN.

At the Mass Market Industries Group, speakers from MFS Datanet, AT&T Global Business Communications Systems, and IBM shared their experiences with various ISDN applications. The Enterprise Network Data Interconnectivity Family demonstrated remote local-area-network (LAN) access for ISDN devices using a single B channel between seven vendors for bridging and routing, a milestone event. The Ad Hoc Group on the Simplification of ISDN Ordering, Provisioning, and Installation approved as working group stable two packages, P and Q, which were an outgrowth of ISDN Solutions '94.

The IIW enjoyed a successful week. To maximize the effectiveness of its resources and expertise, the IIW reorganized into the following functional groups: Application Profile Team, Technical Working Group, Application Analysis, ISDN Conformance Testing, and ISDN CPE (Customer Premises Equipment) and Software Working Group.

IIW working groups reported the following activities: the Call Management Profile Team discussed open applications and determined that there are no profiles to be written at this time. At its first meeting, the Multimedia Applications and Networking Profile Team and Family announced it will focus on the development of application profiles and implementation agreements surrounding the definition, service description, network and interoperability requirements for providing end-to-end ISDN-based multimedia services. The Security and Network Management Technical Working Group and Profile Team established the foundation for contributions to NII security. The ICOT ACT 23 Working Group reviewed Basic Rate (BRI) and Primary Rate (PRI) protocol implementation conformance statements (PICS) and finalized these documents.

The ISDN CPE and Software Working Group is collecting information on ISDN-based products for inclusion in its third edition of the "Catalog of National ISDN Solutions for Selected NIUF Applications," to be published in February 1995. Previous editions of the catalog have been distributed to thousands of end users, systems integrators, service providers, and product manufacturers and distributors.

The PBX Issues Subcommittee defined and categorized issues as they relate to PRI users and implementors, with a view toward providing technical and business solutions for these requests. These issues will be used for input to the ongoing national ISDN process. The ISDN Powering and Wiring Group received Plenary approval for certain sections of their current ISDN Powering and Wiring Guidelines (Residence and Small Businesses). Future work might include a pamphlet for ISDN Wiring and a possible new document on ISDN Wiring and Powering for High-Rise and Apartment Buildings. The CPE Compatibilities and Capabilities Profile Team heard a presentation on processing for CPE-to-CPE application interoperability between heterogeneous systems.

The closing Plenary approved three new documents and announced two documents as working group stable. Also approved were six working group charters: National Information Infrastructure Working Group (NIIWG); NIIWG–Applications Committee; NIIWG–Architecture Committee; ISDN Security Family; Multimedia Applications and Networking Profile Team and Family; and Private Industries.

5. For More Information

For more information about the NIUF and its publications or to obtain conference proceedings, contact the NIUF Secretariat: Sara Caswell, Computer Systems Laboratory, National Institute of Standards and Technology, Building 223, Room B364, Gaithersburg, MD 20899-0001; telephone (301) 975-2937 or fax (301) 926-9675.

Volume 99, Number 6, November–December 1994
Journal of Research of the National Institute of Standards and Technology

[J. Res. Natl. Inst. Stand. Technol. 99, 781 (1994)]

Conference Report

COMPASS '94, NINTH ANNUAL CONFERENCE ON COMPUTER ASSURANCE Gaithersburg, MD June 27–July 1, 1994

Report prepared by

Laura M. Ippolito,
Dolores R. Wallace, and
Elizabeth B. Lennon

Computer Systems Laboratory,
National Institute of Standards and Technology,
Gaithersburg, MD 20899-0001

1. Introduction

Cosponsored by the IEEE Aerospace and Electronics Systems Society and the IEEE National Capital Area Council, COMPASS is an organization which advances the theory and practice of building computer assurance into critical systems. NIST's Computer Systems Laboratory hosted the Ninth Annual Conference on Computer Assurance (COMPASS '94) on June 27-July 1, 1994, and served as cosponsors with the following industry and government organizations: Arca Systems, Inc.; Booz-Allen & Hamilton; CSA (Control Systems Analysis, Inc.); Kaman Sciences Corporation; Logicon, Inc.; National Institute of Standards and Technology; Naval Research Laboratory; Naval Surface Warfare Center; Systems Safety Society; Trusted Information Systems; TRW Systems Division; and the U.S. General Accounting Office. COMPASS '94 attracted more than 150 participants from government, industry, academia, and foreign countries such as Canada, England, Japan, Germany, Scotland, Korea, and Sweden. This year's focus was on the use and assessment of formal methods and on alternatives to formal verification in the critical areas of safety, reliability, fault tolerance, concurrency and real time, and security.

2. Tutorials

COMPASS '94 featured two full-day tutorials and two half-day tutorials. In the first full-day tutorial, John McDermid (University of York) and Christopher Locke (York Software Engineering Limited) discussed "Formal Software Development Using Z." The general characteristics of formal methods for software development were addressed, examples of using the Z Formal Method were given, and a demonstration of the tool CADiZ (Computer Aided Design in Z) was performed.

Hans-Ludwig Hausen (German National Research Center for Computer Science) gave the second full-day tutorial on "Software System Evaluation and Certification." This tutorial focused on the methods and tools for the evaluation and assessment of software products and processes. Particular emphasis was given to identifying and selecting software characteristics and metrics and the handling of evaluation methods and tools.

The first half-day tutorial on "Software Hazard Analysis" was given by Nancy Leveson (University of Washington). This tutorial presented information on techniques used to construct safe and correct process-control software. A system engineering approach was described, where the

software hazard analysis is conducted to ensure requirements specifications are consistent with system safety constraints. Some examples of the formal techniques used on the Traffic Alert and Collision Avoidance System (TCAS) II project were also provided.

Marvin Schaefer (Arca Systems, Inc.) conducted the final, half-day tutorial on "Trusted DBMS Considerations and Issues." He addressed issues connected with building trusted DBMS's, and presented current state of the art and trends. Major risks and problems were also discussed.

3. General Conference

The first full day of the conference opened with welcoming remarks by H. O. Lubbes and Jan Filsinger, COMPASS '94 General Co-Chairs, and John McLean, COMPASS '94 Program Chair. This was the first year that COMPASS included a tools fair. Nine vendors exhibited fifteen tools: Risk Watch (Expert Systems Software, Inc.); AeSOP and Aries (The Aerospace Corporation); EVES (ORA – Ottawa); AdaWise, Penelope, Romulus, and Larch-Ada (ORA – Ithaca), McCabe Toolset (McCabe & Associates); ModeChart Toolset (NRL); Centurion (SRS Technologies); RDD-100 (Ascent Logic Corporation); Boundary Flow Covert Channel Analysis (CTA, Inc.); INTERLOCKS (CSA); and FDR Tool (formal systems ltd).

Jerry O. Tuttle, VADM USN (RET.), delivered the keynote address on the importance of computer systems in the present-day world. The dependence on critical systems demands that the systems are built with safety and security assurances. Tuttle noted the explosion in information and ever-increasing need to build secure systems not only in military systems but also in industry. He noted that "opportunity is often disguised as unsolvable problems." He noted that this challenge to improve technology to make systems safe and secure should be accepted.

4. Safety I

The first paper of the conference, "Experience Applying the CoRE Method to the Lockheed C-130J Software Requirements," was presented by Stuart Faulk, Lisa Finneran, and James Kirby (SPC), and James Sutton (Time Plus). It described the CoRE class model, a descendant of the Ward/Mellor Structured Analysis method, and its application to the C130J project.

Stephen S. Cha (The Aerospace Corporation) discussed "AeSOP: An Interactive Failure Mode Analysis Tool." His presentation included a demonstration of the AeSOP tool to assist in fault tree analysis using petri-nets.

"A Development of Hazard Analysis to Aid Software Design" was presented by John McDermid and D. J. Pumfrey (University of York). This talk described the application of the technique of HAZOP (Hazard and Operability Studies), adapted from the chemical industry, to hazard analysis.

5. Use and Assessment of Formal Methods

David Guaspari (ORA) began this session with a paper on "Formal Methods in the Design of Ada 9x." He related experiences of using a mathematical model for verifying the design of the Language Precision Team that is revising Ada 9x language.

A "Case Study: Applying Formal Methods to the Traffic Alert and Collision Avoidance System (TCAS) II" was detailed by Joan J. Britt (MITRE). She described the TCAS II System Requirements Specification written in RSML (Requirements State Machine Language), illustrating how formal methods have been applied to this safety critical system. Britt noted improvements in quality assurance in three areas: product review, process and personnel certification, and functional testing. She also proposed improvements that can develop RSML into a methodology.

"Formal Methods and Dependability Assessment" was presented by V. Stavridou, S. Liu, and B. Dutertre (University of London). The fact that formal methods are used increasingly for system development was discussed. Their potential advantages for dependability assurance have been recognized. However, no measurable evidence exists that supports or refutes the efficacy of formal methods.

6. Alternatives to Formal Verification

This session featured two papers. "Using Formal Methods To Derive Test Frames In Category-Partition Testing" was presented by Paul Ammann and Jeff Offutt (George Mason University). "Application Of An Informal Program Verification Method To Ada" was presented by Bruce Wieand (IBM) and William E. Howden (University of California). Both presentations dealt with verification; however, they covered activities that apply to

different stages in the software life-cycle. The first paper discussed mechanization of requirements test suite derivation while the second proposed enhancements to code inspection process.

Offutt presented an extension of category partitioning, a specification-based testing method to mechanize construction of test specifications. An application of this method was shown using an example study of a simple file system. The authors believe that this formalization of the notion of a test specification fills the large gap between the functional specifications and the actual test cases. Further, this formality allows mechanization of test specifications so that the tester can focus on only the aspects of testing that demand engineering judgment. The method can be employed early in the life-cycle of the project, and the products from this step (coverage metric and the test specification) are useful in determining when to stop testing. The experimenters concluded that the method is relatively inexpensive and feasible.

Wieand presented the QDA (Quick Defect Analysis) informal program verification method as an aid to code inspection. Previous work in QDA has shown this method to be effective for assembly language programs. The current prototype is an application of QDA to Ada. The method essentially verifies all assumptions by associating objects and their properties. Any unconfirmed hypothesis triggers an investigation probably leading to a program fault or an error in assumption. This experiment has proved that the method (with appropriate enhancements) is applicable to a high-level language.

7. Fault Tolerance

"Centurion Software Fault Tolerance Design and Analysis Tool" by G. Steve Wakefield (SRS), Roger Dziegiel (USAF Rome Laboratory), and Laura L. Pullum (Quality Research Associates) described Centurion, a computer-aided software fault tolerance design and analysis tool. This tool may be used to evaluate software and the associated computer and communications hardware.

Cristian Constantinescu (Duke University) presented "Estimation of Coverage Probabilities for Dependability Validation of Fault-Tolerant Computing System." Coverage probability is estimated by statistically processing information collected through physical or simulated fault injection. The statistical experiments are carried out in a three-dimensional fault space that accounts for system inputs, fault injection times, and fault locations. The proposed solution technique is tested against the data generated by a program that mimics a fault environment.

"Formal Verification of an Interactive Consistency Algorithm for the Draper FTP Architecture Under a Hybrid Fault Model" is the subject of a paper by Patrick Lincoln and John Rushby (SRI International). A hybrid fault model as opposed to the classical Byzantine model was presented to be used on an asymmetric architecture. Although this scheme reduces the number of processors needed to withstand a given number of faults, this extended fault model and the asymmetric architecture complicate the arguments for correctness.

8. Concurrency and Real-Time Systems

Inhye Kang and Insup Lee (University of Pennsylvania) presented a paper on "State Minimization for Concurrent System Analysis Based on State Space Exploration." They discussed a method to compress similar states in the reachable state space during concurrent system analysis.

"Compositional Model Checking of Ada Tasking Programs" by Jeffrey Fischer (Verdix) and Richard Gerber (University of Maryland) discussed another method of state space compression by analyzing a subsection of the state space first and reducing it to a smaller graph.

Azer Bestavros (Boston University) presented "An Ounce of Prevention is Worth a Pound of Cure: Towards Physically-Correct Specifications of Embedded Real-Time Systems." This presentation covered CLEOPATRA, a methodology that prevents system specification that have certain physically impossible specifications (timing, infinite capacity, etc.).

9. Panel: Software Testability for Critical Systems

The four members of the panel were Jeff Voas (Reliable Software Technologies Corporation), Dick Hamlet (Portland State University), William E. Howden (University of California at La Jolla), and Keith Miller (Sangamon State University). Jeff Voas talked about testability, testing and critical software assessment. Complexity measures and coverage criteria are only two classes of measures in the class of testability metrics. Software testability is a metric that analyzes the code itself in a "white-box" fashion. Testability measurement plan will decrease development costs and will not in any way slow down progress.

In Dick Hamlet's absence, Keith Miller presented Hamlet's views on software reliability. He discussed software reliability that is inherently dependent on the very nature of software. One cannot measure software reliability with efforts made in development. Instead, we ought to seek the relationship between defect-detection methods employed during the development and the quality of these methods. W. E. Howden's presented views on testability, failure rates, detectability, trustability and reliability.

Keith W. Miller discussed testability, including its theoretical aspects, its practical implementation, and its application to reliability estimation. He described the complementary advantages and disadvantages of random testing and testability analysis. Finally, he explained how a fully automated system, such as PISCES, can make testability analysis possible without any oracle for correctness.

10. Hardware Verification

The first paper of the session was "A Formal Model of Several Fundamental VHDL Concepts" by David M. Goldschlag (NRL). This presentation began with a brief introduction to VHDL. The key concepts of VHDL, concurrency, real time, and event driven simulation, were discussed and Goldschlag proposed an extension to VHDL: nondeterministic behavioral specification, both in timing and in functions. Questions involved other approaches to formalizing VHDL (which are, according to Goldschlag, operational) and the advisability of adding features to VHDL. Goldschlag responded that his intent was not to affect the language, but to explore VHDL as an interesting programming language in its own right.

The next paper was "Experiences Formally Verifying a Network Component" by Paul Curzon (University of Cambridge), reporting on the verification of a small component of a network. This is a real, fabricated component that is in use, but was designed with no thought for formal verification. Curzon gave a summary of the application, which is a packet (communications) switch, and discussed the seven-week verification process.

11. Safety II

"Evaluating Software for Safety Systems in Nuclear Power Plants" by J. Dennis Lawrence, Warren L. Persons, and G. Gary Preckshot (Lawrence Livermore National Laboratory), and John Gallagher (U.S. Nuclear Regulatory Commission [NRC]) described some of the work done by the NRC in investigating methods for evaluating software in nuclear power plants. The NRC conducted a workshop with technical experts and investigated practices used by industry in developing safety-critical software.

Amer Saeed, Rogerio de Lemos, and Tom Anderson (University of Newcastle) presented "An Approach for the Risk Analysis of Safety Specifications." This talk dealt with the risk analysis of the results of the requirements phase for software. The aim is to locate and remove faults introduced in the requirements phase. The methodology for risk analysis focuses on the analysis of the safety requirements. It consists of a framework with phases of analysis, a graph that depicts the relationship between the safety specifications, a set of formal techniques for the issues to be analyzed, and a set of procedures for the risk analysis of the safety specifications.

"Causality as a Means for the Expression of Requirements for Safety Critical Systems" was presented by Andrew Coombes, John McDermid, and Philip Morris (University of York). This talk described a method for the development of requirements for software, in particular, software for safety-critical applications. The method described uses formal methods as the underlying principal and involves modeling three main components: the environment into which the system is embedded; the fundamental requirements or system goals; and the derived requirements, which result by considering how to satisfy the fundamental requirements in the specific environment. An example was given of modeling the fuel management system for a fighter aircraft. The modeling technique is described as "work in progress," with more research needed. Future work includes developing tools, performing case studies, developing concrete syntax and semantics, and using causal logic to animate the specifications.

12. Security

"Covert Channels Here to Stay?" by Ira S. Moskowitz and Myong H. Kang (NRL) covered a new metric, the small message criterion, for use in the analysis of reducing the threat of covert channels without crippling performance.

Charles N. Payne, Andrew P. Moore, and David M. Mihelcic (Naval Research Laboratory [NRL]) submitted "An Experience Modeling Critical Requirements" which discussed NRL's experience and lessons learned in designing a Selective Bypass Device (SBD) application.

"On Measurement of Operational Security" by Sarah Brocklehurst and Bev Littlewood (City University), and Tomas Olovsson and Erland Jonsson (Chalmers University of Technology) covered the results of an experiment in operation security using college students to break into a computer system.

13. Evening Event

The COMPASS '94 banquet speaker, Professor Brian Randell of the University of Newcastle upon Tyne, summed up COMPASS this way:

> COMPASS is filling a need that no other conference is attempting. COMPASS recognizes that problems in security may be shared by software safety and system safety, and vice versa. In both cases, reliability is the goal to be achieved. COMPASS looks at formal proofs, testing, and fault tolerance methods as complementary instead of rival approaches. Most of all, COMPASS is bringing together software and hardware communities, and security and safety communities from industry, government and academia.
>
> Together, these communities may make great gains in solving the problems of providing computer assurance in complex systems, such as aerospace systems, medical devices, military weapons, and transportation.

14. COMPASS '95

COMPASS '95 will be held June 26-30, 1995, at NIST in Gaithersburg, Maryland. The deadline for papers submitted for COMPASS '95 is January 14, 1995. For information about COMPASS '95 or how to obtain proceedings of COMPASS '94, contact Dolores Wallace, Computer Systems Laboratory, National Institute of Standards and Technology, Building 225, Room B266, Gaithersburg, MD 20899-0001; telephone (301) 975-3340 or fax (301) 926-3696.

Acknowledgments

The authors wish to acknowledge the following people for their contributions to this article: Joseph Poole, NIST; Wayne Salamon, NIST; James Graham, NIST; Uma Satyen, The MITRE Corporation; and David Barton, Intermetrics Corporation.